FINITE DEFORMATIONS IN ELASTIC-PLASTIC MEDIA SUBJECTED TO IMPULSIVE LOADINGS BY THE FINITE ELEMENT METHOD

by

JOSEPH HEIFETZ

A dissertation submitted to the Graduate Faculty in Engineering in partial fulfillment of the requirements for the degree of Doctor of Philosophy, The City University of New York.

1971

This manuscript has been read and accepted for the Graduate Faculty in Engineering in satisfaction of the dissertation requirements for the degree of Doctor of Philosophy.

7 December 1971 — date

Carl J Costantino — Chairman of Examining Committee

Dec 7, 1971 — date

Jacques E. Benveniste — Executive Officer

(Chairman)

David H. Cheng, Civil Engineering
Carl J. Costantino, Civil Engineering
Norman C. Jen, Civil Engineering
Ming L. Pei, Civil Engineering
Richard G. Stoneham, Mathematics

Supervisory Committee

The City University of New York

TABLE OF CONTENTS

Figures

Figures (cont'd)

ACKNOWLEDGEMENTS

I wish to express my sincere gratitude to Professor Costantino for his excellent guidance during the course of this thesis investigation. I also am indebted to Professors Pei and Benveniste for their sincere interest and very helpful advice during the critical phases of my work.

In addition I wish to thank Mr. David Pollack for his able assistance in systems debugging and Mrs. Phyllis Wentworth for her patient and careful typing.

Finally I owe my deepest gratitude to my wife Rose, who encouraged me and endured during the years of my travail.

ABSTRACT

FINITE DEFORMATIONS IN ELASTIC-PLASTIC MEDIA SUBJECTED TO IMPULSIVE LOADINGS BY THE FINITE ELEMENT METHOD

by

JOSEPH HEIFETZ

Advisor: Professor C.J. Costantino

In this thesis the kinematics of large deformations are considered together with the effects of non-linear (or plastic) material behavior on the dynamic response of structures. The elastic-plastic incremental stress-strain law is written in terms of frame indifferent quantities and applied to materials undergoing large deformations due to impulsive loadings.

The finite element method is developed by first writing expressions for the incremental strain, stress and rotation of an element and then applying these expressions to the equations of motion written in incremental form. The resulting equations of motion are developed for triangular and quadrilateral elements for both planar and axi-symmetric configurations. Expressions for the equilibrium of each node in the system are then obtained as a set of second order differential equations. The numerical integration procedure used for the solution of these equations is

discussed in terms of relative error and stability.

Results obtained to verify the validity of the method are shown for a cylindrical bar, a circular plate a spherical shell and a ring reinforced cylindircal tube. These results are shown to compare favorably with known solutions and data. In addition, results are shown for a flat, circular plate impinging on a rigid, parabolic die and for an ogive nosed projectile impinging on a flat rigid surface.

CHAPTER I

Introduction

In recent years a broad interest in problems associated with the explosive forming of metals and the high impulse loading of plates and shells has appeared in the technical literature. In these problems, highly ductile metals are subjected to the impulsive pressure of explosives and deform permanently, either by free movement or by impinging upon dies. The resulting deformations are large and the dominant material properties during the finite phase of deformation are generally in the strain hardened, plastically yielded range. Because of the complexity of such problems, the analytic solutions available require the introduction of many simplications such as the use of total deformation laws to describe elastic-plastic behavior, symmetry to reduce the dimensionality of the problem and proportional loading with monotonically increasing stress states.

Any satisfactory treatment of a general two dimensional problem* in large deformations involving a general loading pattern, must consider the effects of unloading in various parts of the continuum due both to

---

*Note: Axially symmetric problems are herein considered as two-dimensional.

the finite duration of the applied loadings and to wave reflections at boundaries. Furthermore, the constitutive laws governing large deformations must agree with physical observation in both the finite and infinitesmal straining range and satisfy requirements of frame indifference.

In dealing with complex problems of this sort, great flexibility may be achieved by a numerical formulation, particularly if the method used is the finite element method. The method lends itself to a simplified formulation of boundary conditions, even for highly irregular boundaries, while element sizes may be readily changed to facilitate investigation of local regions within a continuum. As of now, there appears to be no published examples of finite element methods that can be used to solve problems in the finite deformation of dynamically loaded elastic-plastic media in axial symmetry, plane stress or plane strain.

The objective of this thesis has been to develop a finite element technique that may be used for the solution of two dimensional problems in which solid bodies having non-linear material properties are subjected to dynamic loadings and large deformations.

The solution capability of the method developed herein will be demonstrated by comparing the numerical results of this method, for elastic-plastic materials, with several available analytic solutions and one experimental result. In addition to these, results will be presented for several other problems of interest in elasto-plasticity, for which solutions have not as yet appeared in the literature. These problems consist of circular plates, shells and solids subjected to impulsive loads.

CHAPTER II

State of the Art

Hudson[32] made perhaps one of the earliest analyses of the permanent deformation of thin circular diaphragms subjected to impulsive loads uniformly distributed on the diaphragm surface. He assumed an annular plastic bending wave traveling radially inwards while the portion of the diaphragm inside the bending wave remained perfectly flat. The material was considered to be ideally rigid plastic and deformation theory of plasticity was assumed. Subsequent analyses of thin membranes subjected to impulsive loads were made by Munday and Newitt[36] and Boyd[58], all assuming deformation theories and neglecting elastic effects. Wang[37] derived an expression for the permanent deflection of a simply supported circular plate subjected to a blast load by using plate bending analysis of a rigid plastic material and by ignoring the effects of membrane stresses. Florence[26] conducted experiments on simply supported circular plates and concluded that the membrane stresses added considerably to the plate strength when deflections exceeded one fifth of the plate radius. Jones[34,55] used deformation theory to derive expressions for the

permanent deflection of rigid plastic plates subjected to impulsive loads. His analysis included the effects of both membrane and bending stress. Baker[25] derived expressions for the motion of a linear strain hardening elastic-plastic thin spherical shell subjected to a uniformly distributed internal triangular pulse. He based his analysis on deformation theory using the Mises yield criterion and considered wall thinning effects. Masaki[33] derived expressions for the permanent deformation of a thin cylinder with ring reinforcements at two locations and a uniformly distributed outward radial impulse. He used incremental theory for a rigid plastic Mises material and based his analysis on kinematic assumptions. He concluded that the final shape of the cylinder profile can be spherical, conical or trapezoidal, depending on the particular values of geometric and loading parameters.

Work on high velocity impact and projectile penetration represents another area of interest in dynamic finite deformations. Zaid and Paul[57] proposed a kinematic mechanism to model high speed projectile penetrations of thin flat plates. In this model, it is assumed that inertial effects

predominate over the material strength of the plate. Thus, during projectile penetration, the plate material follows the contour of the projectile as if it were a 'limp rag'. The work of Taylor[59], Wiffen[60], Raftopoulos and Davids[44] and others were intended to deduce the mechanical properties of materials at high strain rates.

In addition to the above list of analytic solutions and experiments in dynamic large deformations, a number of numerical codes have been developed over the past ten years. The finite difference 'Tensor' code by Maenchen and Sachs[34] solved two dimensional problems in cylindical symmetry involving transient stresses in elastic-plastic media. The code was formulated in material (Lagrangian) coordinates using incremental elastic plastic stress-strain laws and a numerical integration scheme to solve the equations of motion. An artificial viscosity term was added to the equations of motion to dampen spurious oscillations in stress occurring at shock fronts. The code was developed to investigate underground explosion phenomena, but published results were for elastic and plastic spheres subjected to internal radial impulse loads. Wilkins

'Hemp' code[40] has many features of the 'Tensor' code above but differs in that it may deal with material properties in the high kilobar range (such as may occur with contact explosives). The code also provides for the sliding of different materials with respect to each other at boundaries. Leech et al.[38] developed a finite difference shell program, 'Petros I' to find the permanent deformation of thin elastic-plastic cylinders subjected to dynamic loading. In none of the above codes was any consideration given to the frame indifferent expression for stress rate, although all of these codes used incremental plasticity theory.

Finite element approaches to large deformations in non-linear media have been published for static problems. Oden and Sato's[41] development was for a non-linear elastic (Mooney-Rivlin) membrane for which all strains, etc. were referred to an initial coordinate system. Hibbitt et al.[43] described a method of formulating a finite element approach to problems in large deformations for elastic-plastic media. They stressed the necessity of using incremental methods in solving the equations of motion; i.e. by treating the equations as piece-wise linear over small intervals. They also

noted the importance of using the frame indifferent Jaumann 'flux' in place of true stress increments in the constitutive equations. In addition to the above, are Becker's[42] finite element solutions for rubber membranes and Turner's[48] and Martin's[99] developments for problems in stability.

Finite element solutions to two dimensional wave problems in small deformations have been obtained using lumped nodal masses. Costantino's developments[46,47] used the Newmark method for elastic and plastic media. Artificial 'correction' forces were introduced into the equations of motion to account for the effects of the non-linear components of strain. Fu's[45] development applied the de Vogelaere integration method to general linear media with damping.

There appears to be no published finite element development for transient stress problems in two dimensional elastic-plastic media including large deformations. In particular, there is no published analysis for the permanent deformation of plates impinging upon rigid dies after being subjected to uniform impulsive loads. This thesis, therefore, is directed towards filling the aforementioned void in the technical literature.

CHAPTER III

Kinematics

The kinematics of large deformations presented herein is considered in two parts; i.e. total and incremental deformation. The terms of incremental deformation are to be used in the constitutive equations, whereas the total deformation terms represent a state of current strain and are found from purely kinematic considerations.

3.1 Notation

For this section the following notation will apply

Subscripts and Superscripts

Greek, lower case; position vectors and coordinates in an initial or reference configuration

Roman, lower case; position vectors and coordinates in a current or spatial configuration

The position vector will also be designated as:

X_α, X^α if referred to an initial configuration

x_i, x^i if referred to a current configuration

Whenever indicial notation is used, the convention of summation over repeated indices applies with the understanding that $(\ ),_j$ is the covariant derivative of the quantity in parentheses with respect to x^j;

3.2 Strain Displacement Relationships

The mapping of points from an initial to a current configuration may be expressed as;

$$x^i = g^i_\alpha X^\alpha + u^i \tag{3.1}$$

where u^i is a displacement vector and g^i_α is the shifter that transforms the position vector from the initial to a current coordinate reference frame.

Since the mapping is one to one and invertible, the following functional relationships hold;

$$x^i = x^i(X^\alpha) \tag{3.2a}$$

$$X^\alpha = X^\alpha(x^i) \tag{3.2b}$$

$$dx^i = x^i_{,\alpha}\, dX^\alpha \tag{3.2c}$$

$$dX^\alpha = X^\alpha_{,i}\, dx^i \tag{3.2d}$$

$$x^i_{,\alpha} X^\alpha_{,j} = \delta^i_j \tag{3.2e}$$

Furthermore;

$$dx^i = (g^i_\alpha + u^i_{,\alpha})\,dX^\alpha \tag{3.3}$$

Hence, from (3.2c) and (3.3);

$$x^i_{,\alpha} = g^i_\alpha + u^i_{,\alpha} \tag{3.4}$$

which is called the 'deformation gradient'.

The lengths of differential line elements in a deformed and initial configuration are given by;

$$ds^2 = g_{ij}\,dx^i dx^j \tag{3.5a}$$

$$dS^2 = g_{\alpha\beta}\,dX^\alpha dX^\beta \tag{3.5b}$$

The difference of these quantities is therefore a measure of deformation and is given by;

$$ds^2 - dS^2 = (g_{ij}\,x^i_{,\alpha}\,x^j_{,\beta} - g_{\alpha\beta})\,dX^\alpha dX^\beta \tag{3.6}$$

where g_{ij} and $g_{\alpha\beta}$ are the metric tensors of the current and initial coordinate systems respectively. Thus, the Langrangian strain tensor may be defined as;

$$\epsilon_{\alpha\beta} = \tfrac{1}{2}(g_{ij}\,x^i_{,\alpha}\,x^j_{,\beta} - g_{\alpha\beta}) \tag{3.7}$$

Expanded expressions for $x^i_{,\alpha}$, $\epsilon_{\alpha\gamma}$ and the jacobian of transformation J are shown in Appendix D for the plane strain, plane stress and axi-symmetric cases.

According to Cauchy's polar decomposition theorem[2] transformations of the type given by (3.4) are made up of a pure rotation and a pure deformation. If $\underset{\sim}{F} = x^i_{,\alpha}$, then;

$$\underset{\sim}{F} = \underset{\sim}{R}\,\underset{\sim}{U} = \underset{\sim}{V}\,\underset{\sim}{R} \tag{3.8}$$

where $\underset{\sim}{R}$ is an orthogonal matrix such that $\underset{\sim\sim}{R}\underset{\sim\sim}{R}^T = \underset{\sim\sim}{R}^T\underset{\sim\sim}{R} = \underset{\sim}{I}$ (the identity matrix)

$\underset{\sim}{U}$ is a symmetric matrix such that $\underset{\sim}{U}^T = \underset{\sim}{U}$ and

$\underset{\sim}{V} = \underset{\sim\sim\sim}{R}\underset{\sim}{U}\underset{\sim\sim}{R}^T$ is a symmetric matrix

Note, that if $\underset{\sim}{U}$ is considered to be the pure deformation of a body referred to its initial, undeformed configuration, then $\underset{\sim}{V}$ is the pure deformation referred to its deformed state. Then according to (3.8), the deformation gradient $\underset{\sim}{F}$ is composed of a pure deformation followed by a rigid body rotation, if the deformation tensor $\underset{\sim}{U}$ is used; or a rigid body rotation followed by a pure deformation if the tensor $\underset{\sim}{V}$ is used.

The material derivative of $\underset{\sim}{F}(t)$ leads to the introduction of two more terms; i.e. the 'stretching' and the 'observer's spin' (or simply the 'spin'). For;

$$\dot{\underset{\sim}{F}}(t) = \frac{D}{Dt}(x^i_{,\alpha}) = (\dot{x}^i)_{,\alpha} = V^i_{,\alpha} \qquad (3.9a)$$

or

$$\dot{\underset{\sim}{F}}(t) = V^i_{,k}\, x^k_{,\alpha} \qquad (3.9b)$$

Then define; $G_{ks} = g_{ki} V^{,i}_{s} = V_{k,s}$ (3.10)

and note that every tensor can be decomposed into a symmetric and anti-symmetric tensor;

$$G_{ks} = \tfrac{1}{2}(V_{k,s} + V_{s,k}) + \tfrac{1}{2}(V_{k,s} - V_{s,k}) \qquad (3.11)$$

Then we define the terms;

$$D_{ks} = \tfrac{1}{2}(V_{k,s} + V_{s,k}) \qquad (3.12a)$$

and

$$W_{sk} = \tfrac{1}{2}(V_{k,s} - V_{s,k}) \qquad (3.12b)$$

These terms are subject to physical interpretation; i.e. the material derivative of the term $(ds)^2$ leads to;

$$\begin{aligned}
\frac{D}{Dt}(ds^2) &= \frac{D}{Dt}(g_{ij}\, dx^i dx^j) \\
&= g_{ij}\left(\frac{D}{Dt}(x^i_{,\alpha}\, dx^\alpha)dx^j + \frac{D}{Dt}(x^j_{,\gamma}\, dx^\gamma)dx^i\right) \\
&= g_{ij}\left(V^i_{,k}\, x^k_{,\alpha}\, dx^\alpha dx^j + V^j_{,k}\, x^k_{,\gamma}\, dx^\gamma dx^i\right) \\
&= g_{ij}\left(V^i_{,k}\, dx^k dx^j + V^j_{,k}\, dx^i dx^j\right) \\
&= V_{j,k}\, dx^k dx^j + V_{i,k}\, dx^i dx^k
\end{aligned}$$

Since k is a dummy index, let k = i in the first term above and k = j in the second term above, then;

$$\frac{D}{Dt}(ds^2) = (v_{j,i} + v_{i,j})\,dx^i dx^j = 2\,D_{ij}\,dx^i dx^j \qquad (3.13)$$

Now (3.13) may be written as;

$$\frac{1}{ds}\,\frac{D}{Dt}(ds) = D_{ij}\,n^i n^j \qquad (3.14)$$

where $n^i = \frac{dx^i}{ds}$; $n^j = \frac{dx^j}{ds}$ are unit vectors in the x^i and x^j directions.

Now if $n^{(1)} = \begin{Bmatrix} 1 \\ 0 \\ 0 \end{Bmatrix}$ is a principal direction of D_{ij} then;

$$D_{(1)} = \frac{ds}{ds}\,n^{(1)} n^{(1)} \qquad (3.15)$$

and it is seen that stretching is an instantaneous rate of change of stretch at a spatial point in a continuum.

The spin can now be shown to be the instantaneous rate of angular change of the principal axes of the stretching[1].

Let $D_{(n)}$ = the principal values of D_{ij}

Then $\left| D_1^k - D_{(n)}\,\delta_1^k \right| = 0$

Consider the material derivatives of $n^k = \frac{dx^k}{ds}$ tangent to coordinate axes;

$$\dot{n}^k = \frac{1}{ds}\frac{D}{Dt}(dx^k) - \frac{1}{ds^2}dx^k\frac{D}{Dt}(ds)$$

Now $\frac{D}{Dt}(dx^k) = V^k_i dx^i$ and along a principal direction;

$$D_{(n)} = \frac{1}{ds}\frac{D}{Dt}(ds)$$

Hence, for principal directions;

$$\begin{aligned}\dot{n}^k &= \frac{1}{ds}(V^k_{,i}dx^i - D_{(n)}\delta^k_i dx^i)\\ &= (V^k_{,i} - D_{(n)}\delta^k_i)n^i\\ &= (D^k_i + W^k_i - D_{(n)}\delta^k_i)n^i \qquad (3.16)\end{aligned}$$

where n^1 lies along a principal direction of D_{ij}.

But $\left(D^k_i - D_{(n)}\ \delta^k_i\right) n^i = 0$. Therefore;

$$\dot{n}^k = W^k_i n^i \qquad (3.17)$$

and since (3.17) is the time rate of change of a unit vector referred to spatial coordinates, W^k_i must be a rotational tensor; i.e. one that does not change the length of n^i.

CHAPTER IV

Frame Indifferent Quantities and Their Use in Constitutive Equations

4.1 Frame Indifferent Quantities

Let the rigid body motion of an observer's reference frame be given by;[2]

$$\underset{\sim}{X}^* = \underset{\sim}{C}(t^*) + \underset{\sim}{Q}(t^*)\ (\underset{\sim}{X}-\underset{\sim}{X}_o) \tag{4.1a}$$

$$t^* = t - a \tag{4.1b}$$

where $\underset{\sim}{Q}(t^*)$ is a time dependent, orthogonal transformation matrix, $\underset{\sim}{C}(t^*)$ is a position vector locating a point in space at time t^*, and 'a' is some initial or reference time. Then if a quantity is frame indifferent, it will transform in one of the following ways from the 'unstarred' to the 'starred' system;

$$A^* = A \qquad \text{if A is a scalar} \tag{4.2a}$$

$$\underset{\sim}{V}^* = \underset{\sim}{Q}\underset{\sim}{V} \qquad \text{if } \underset{\sim}{V} \text{ is a vector} \tag{4.2b}$$

$$\underset{\sim}{S}^* = \underset{\sim}{Q}\underset{\sim}{S}\underset{\sim}{Q}^T \qquad \text{if } \underset{\sim}{S} \text{ is a second rank tensor} \tag{4.2c}$$

Thus if $\underset{\sim}{V} = \underset{\sim}{X}-\underset{\sim}{Y}$ is objective, then $\underset{\sim}{V}^* = \underset{\sim}{X}^* - \underset{\sim}{Y}^*$ (4.3)

Upon inserting equation (4.1a) into (4.3) one obtains;

$$\underset{\sim}{V}^{*} = \underset{\sim}{Q}(X-Y) = \underset{\sim}{Q}\underset{\sim}{V} \tag{4.4}$$

If $$\underset{\sim}{V} = \underset{\sim}{S}\underset{\sim}{W} \tag{4.5}$$

where $\underset{\sim}{S}$ is an objective, second rank tensor, and $\underset{\sim}{V}$ and $\underset{\sim}{W}$ are both objective vectors, then

$$\begin{aligned}
&\underset{\sim}{V}^{*} = \underset{\sim}{Q}\underset{\sim}{V} \\
&\underset{\sim}{W}^{*} = \underset{\sim}{Q}\underset{\sim}{W} \\
&\underset{\sim}{Q}\underset{\sim}{V} = \underset{\sim}{S}^{*}(\underset{\sim}{Q}\underset{\sim}{W}) = \underset{\sim}{Q}(\underset{\sim}{S}\underset{\sim}{W}) \\
&\underset{\sim}{S}^{*}\underset{\sim}{Q} = \underset{\sim}{Q}\underset{\sim}{S} \\
&\underset{\sim}{S}^{*} = \underset{\sim}{Q}\underset{\sim}{S}\underset{\sim}{Q}^{T}
\end{aligned} \tag{4.6}$$

Let $\underset{\sim}{F} = x^{i}_{,\alpha}$ be the deformation gradient (see chapter III), then;

$$\underset{\sim}{F}^{*} = \frac{\partial x^{i*}}{\partial X^{\alpha}} = Q^{i}_{j}(t^{*})\frac{\partial x^{j}}{\partial X^{\alpha}} \tag{4.7a}$$

$$\underset{\sim}{F}^{*} = \underset{\sim}{Q}\underset{\sim}{F} \tag{4.7b}$$

Thus, $\underset{\sim}{F}$ is not an objective tensor.

The material derivative of $\underset{\sim}{F}$ is given by;

$$\dot{\underset{\sim}{F}} = \frac{\partial \dot{x}^{i}}{\partial X^{\alpha}} = V^{i}_{,K}x^{K}_{,\alpha} = \underset{\sim}{G}\underset{\sim}{F} \tag{4.8}$$

$$\dot{\underset{\sim}{F}}^{*} = \dot{\underset{\sim}{Q}}\underset{\sim}{F} + \underset{\sim}{Q}\underset{\sim}{G}\underset{\sim}{F} \tag{4.9}$$

Since $\underset{\sim}{F} = \underset{\sim}{Q}^{T}\underset{\sim}{F}^{*}$ one may write;

$$\underset{\sim}{G}^{*}\underset{\sim}{F}^{*} = \underset{\sim\sim\sim}{QGQ}^{T}\underset{\sim}{F}^{*} + \underset{\sim\sim}{\dot{Q}Q}^{T}\underset{\sim}{F}^{*} \qquad (4.10)$$

Then post-multiplying both sides of (4.10) by $(F^{*})^{-1}$ results in;

$$\underset{\sim}{G}^{*} = \underset{\sim\sim\sim}{QGQ}^{T} + \underset{\sim\sim}{\dot{Q}Q}^{T} \qquad (4.11)$$

By lowering the upper index of the term $V^{i}_{,K}$ it may be reduced to a sum of symmetric and anti-symmetric second rank tensors. Thus;

$$\underset{\sim}{G} = g_{iK}V^{K}_{,j} = 1/2(V_{i,j}+V_{j,i}) + 1/2(V_{i,j}-V_{j,i}) \qquad (4.12)$$

Then recalling that

$$D_{ij} = 1/2(V_{i,j}+V_{j,i}) \text{ is stretching} \qquad (4.13)$$

and

$$W_{ji} = 1/2(V_{i,j}-V_{j,i}) \text{ is spin} \qquad (4.14)$$

we have; $\underset{\sim}{G} = \underset{\sim}{D} + \underset{\sim}{W}$

then $\underset{\sim}{G}^{*} = \underset{\sim}{D}^{*}+\underset{\sim}{W}^{*} = \underset{\sim}{Q}(\underset{\sim}{D}+\underset{\sim}{W})\underset{\sim}{Q}^{T} + \underset{\sim}{\dot{Q}Q}^{T}$

But $\underset{\sim}{\dot{Q}Q}^{T}$ is anti-symmetric since $D/Dt(\underset{\sim}{QQ}^{T}) = \underset{\sim}{\dot{Q}Q}^{T} + \underset{\sim}{Q\dot{Q}}^{T} = 0$

Hence; $$\underset{\sim}{G}^{*} = \underset{\sim}{D}^{*}+\underset{\sim}{W}^{*} = \underset{\sim\sim\sim}{QDQ}^{T} + (\underset{\sim\sim\sim}{QWQ}^{T} + \underset{\sim\sim}{\dot{Q}Q}^{T}) \qquad (4.15)$$

4.2 Frame Indifference in Constitutive Equations

The requirement that constitutive laws be frame indifferent is equivalent to the following; let the stress-strain relationship for a simple* material be represented by[2];

$$\underset{\sim}{\tau}(t) = \overset{\infty}{\underset{s=0}{\mathcal{G}}}(\underset{\sim}{F}(t-s)) \qquad (4.17)$$

where $\underset{\sim}{\tau}(t)$ is the stress tensor; $\underset{\sim}{F}(t)$ is the deformation gradient (see Chapter III); $\mathcal{G}$ is a functional relating $\underset{\sim}{\tau}$ to $\underset{\sim}{F}$; and 't' and 's; are the current and past times respectively; then the requirements of material frame indifference are that;[2]

$$\underset{\sim}{\tau}^{*} = \overset{\infty}{\underset{s=0}{\mathcal{G}}}(F^{*}(t-s))$$

or

$$\underset{\sim}{Q}(t)\,\underset{\sim}{\tau}(t)\,\underset{\sim}{Q}^{T}(t) = \overset{\infty}{\underset{s=0}{\mathcal{G}}}(\underset{\sim}{Q}(t-s)\;\underset{\sim}{F}\;(t-s)) \qquad (4.\ldots$$

By letting

$$\underset{\sim}{R}^{T}(t) = \underset{\sim}{Q}\;(t)$$

where $\underset{\sim}{R}\;(t)$ is defined in (3.8), we may obtain

$$\underset{\sim}{\tau}(t) = \underset{\sim}{R}(t)\;\left[\;\overset{\infty}{\underset{s=0}{\mathcal{G}}}(\underset{\sim}{U}(t-s))\;\right]\;\underset{\sim}{R}^{T}(t) \qquad (4.18)$$

where $\underset{\sim}{U}(t)$ is the symmetric, pure deformation tensor and $\mathcal{G}$ is the functional relating $\underset{\sim}{\tau}$ to $\underset{\sim}{U}$.

---

*Simple materials are defined by Truesdell as those whose properties may be deduced by subjecting them to homogeneous motions.

If the constitutive equations are of the form

$$\dot{\tau}_{ij} = F_{ij}\,(D_{11}\ldots D_{33};\ \tau_{11};\ldots\ \tau_{33};\ \epsilon_{11},\ldots$$

where the dot over a quantity indicates the material [illegible] and τ_{ij}, ϵ_{ij} and D_{ij} are the stress, strain and [illegible] tensors respectively, then a difficulty arises when one attempts to apply (4.19) to a body in rigid motion [illegible], the terms on the right of (4.19) transform [illegible] the point transformation given by (4.1a) while the [illegible] on the left do not. This latter point may be [illegible] by noting that if τ_{ij} is frame indifferent [illegible]

$$\underset{\sim}{\tau}^{*} = \underset{\sim}{Q}\,\underset{\sim}{\tau}\,\underset{\sim}{Q}^{T}$$

and

$$\dot{\underset{\sim}{\tau}}^{*} = \dot{\underset{\sim}{Q}}\underset{\sim}{\tau}\underset{\sim}{Q}^{T} + \underset{\sim}{Q}\dot{\underset{\sim}{\tau}}\underset{\sim}{Q}^{T} + \underset{\sim}{Q}\underset{\sim}{\tau}\dot{\underset{\sim}{Q}}^{T}$$

Furthermore, it would appear natural [illegible] constitutive equations (4.19) from the standpoint of observer moving in time and body motion with [illegible] deforming medium. According to such an observer the [illegible] of translation and rotation should have no effect [illegible] distortion of the medium locally or [illegible]

With the above considerations in mind, [illegible] to obtain a definition of a stress rate or 'time' [illegible] frame indifference, that transforms [illegible] under the point transformation (4.1a) and that results in

consistent constitutive equations. One such definition, is the Jaumann stress rate and is obtained as follows [5]

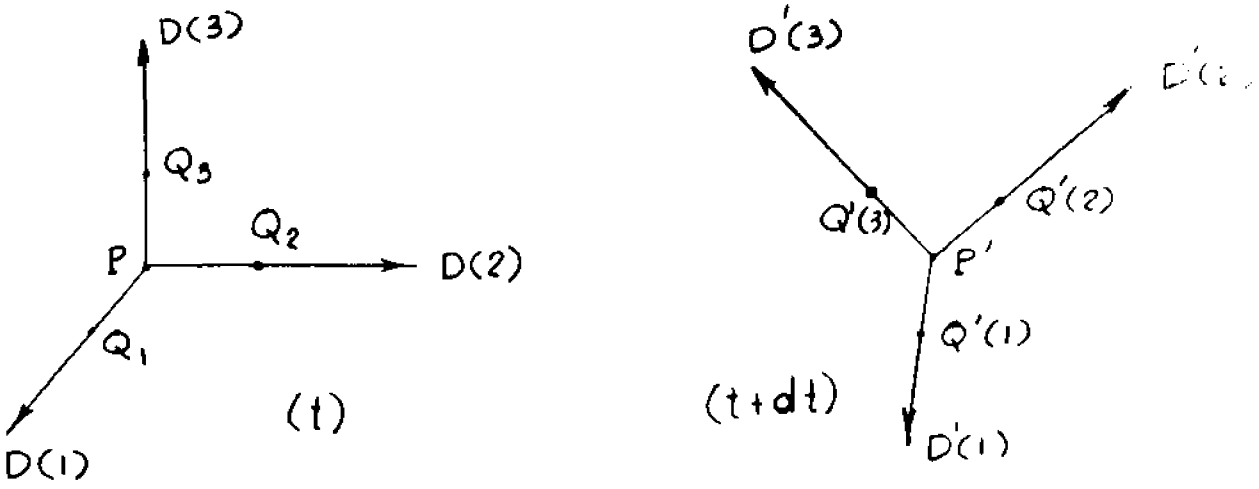

Figure 4.1

Let P, Q_i (i = 1,3) in Figure 4.1 be a cartesian system of points in a continuum at a time t such that $\overline{PQ}_i$ each lies along a principal direction of D_{ij} (the stretching tensor). At time (t + dt) the system is represented by P', Q'_i, and since shear deformation rates vanish along principal directions of D_{ij}, the system 'Q' within a small neighborhood of P is also orthogonal and consists of a system of principal directions of D'_{ij}.

Then define stress rate such that it vanishes identically when the stress tensor at P' has the same stress components with reference to $\overline{P'Q'}_i$ as it had with reference to $\overline{PQ}_i$. Thus;

$$D/Dt\ (\tau_{ij}\lambda_i\lambda_j) = 0 \qquad (4.20)$$

where λ_i, λ_j are unit vectors along the principal axes of $\overline{PQ}_i$. Expanding equation (4.20), we have;

$$D/Dt \quad (\tau_{ij}\lambda_i\lambda_j) = \dot{\tau}_{ij}\lambda_i\lambda_j + \tau_{ij}\dot{\lambda}_i\lambda_j + \tau_{ij}\lambda_i\dot{\lambda}_j \qquad (4.21)$$

But $\dot{\lambda}_i = \left\{ V_{i,j} - D_{(n)}\,\delta_{ij} \right\} \lambda_j$ (see equation (3.16))

where $D_{(n)}$ is a principal value of D_{ij} and $V_{i,j} = D_{ij} + W_{ij}$

Hence $$\dot{\lambda}_i = W_{ij}\lambda_j \qquad (4.22)$$

Then inserting (4.22) into (4.21) we obtain the following expression for stress rate or flux;

$$T_{ij}^{(J)} = \dot{\tau}_{ij} - \tau_{Kj}W_{iK} - \tau_{iK}W_{jK} \qquad (4.23)$$

Equation (4.23) for stress rate is only one of many such possible expressions, each of which satisfy the criterion of frame indifference. For example, the following expressions for stress rate are equally valid frame indifferent quantities;

$$\underset{\sim}{T}^{(n)} = (\dot{\underset{\sim}{\tau}} + \underset{\sim}{\tau}\underset{\sim}{W} - \underset{\sim}{W}\underset{\sim}{\tau}) \quad \pm \quad \tau D + D\tau + \alpha\tau \qquad (4.24)$$

where α is a scalar. The singular property of the definition given by equation (4.23) is that if $T_{ij}^{(J)}$ vanishes, the stress invariants in the continuum become stationary[55]. This is seen by the fact that stress rate is measured with respect to a set of orthogonal, principal axes that rotate with the material. It is this property that qualifies its applicability to the

constitutive equations of elasto-plasticity. For if the stress rate vanishes, the yield function is stationary for an elastic perfectly plastic material. Similarly, for a work hardening material, a vanishing stress rate implies a stationary state of hardening.

CHAPTER V

Elastic-Plastic Materials

The formable, ductile materials available to industries of today may be described, for the most part as elastic-plastic and work hardening. In most cases, the Von Mises yield criterion[3] may be used to predict the onset of plastic yielding. Large deformations, occurring well beyond the state of initial yielding may be predicted in accordance with various constitutive laws that are currently available. Thus in considering representative problems in the large deformation of dynamically loaded metals (for which analytic and experimental results exist), a Von Mises material with isotropic, linear strain hardening properties was elected.

In choosing a constitutive law to represent a strain hardening, elastic-plastic material, consideration was given to the fact that such a law must be generally applicable to all classes of dynamic loading for both the finite and infinitesmal straining. While one obvious requirement is that the constitutive law agrees with physical observations, it is also necessary that the following principles,

or axioms be adhered to; i.e., the principle of local action, determinism and frame indifference[2].

In the principle of local action, the motion of particles at some distance from the point x_i may be disregarded in calculating the stress at x_i. The principle of determinism states that the stress at a particle located at x_i in a body at a time 't', is determined by the history of the motion of the body up to the time 't'; while the principle of frame indifference requires that the material properties of the same material, as viewed by observers in different reference frames, be identical.

Constitutive theories for elastic-plastic, strain hardening materials fall into two main categories, i.e. 'deformation' and 'incremental' theories. In the latter, incremental plastic strains are a function of the current stress state, and current stress increment, while in the former, total plastic strains are a function of the current stress state. Both theories have been applied to metals during small straining.

5.1 DEFORMATION THEORY

As an example of a total deformation theory, Hencky's[3] model is illustrated. In this theory,

the total strain deviator e_{ij} and the dilitational component of the total strain ϵ_{kk}, are given at any time by the following relationships:

$$e_{ij} = (\phi + 1/2G)\,\tau'_{ij} \tag{5.1}$$

$$\epsilon_{kk} = \frac{(1-2\nu)}{E}\,\tau_{kk} \tag{5.2}$$

where ϕ is a scalar such that

$\phi > 0$ during increasing loading after plastic yielding

$\phi = 0$ during unloading or in the elastic range

The scalars G, ν, and E are the shear modulus, Poisson's ratio and Young's modulus of elasticity respectively, and τ'_{ij} is the deviator of the total stress.

The plastic components of strain are given by;

$$e^{p}_{ij} = \phi\,\tau'_{ij} \tag{5.4}$$

Thus components of total plastic strain are proportional to components of the current total stress deviators.

Hill[3] raised an objection to Hencky's theory that is based on the fact that discontinuous changes in permanent deformation are predicted during load cycling; a fact that clearly contradicts physical observation. Despite this, use has been made of total deformation theories, such as Hencky's in

simplifying analytic solutions to problems in plasticity.

It can be shown[3] that for the special case of small deformations and proportional loading, (where stress components retain a constant ratio to each other while their magnitudes increase monotonically) incremental and deformational theories produce coincident results. More recently, it has been shown that the Hencky theory may be made to produce equivalent results to the incremental theories over certain loading paths other than those of proportional loading[17]. In addition to Hencky's, other deformational theories of interest include those of Swainger[3] and Prager[3]. However, these theories fail to describe physical phenomena in sufficient generality for the purpose of this thesis.

5.2 INCREMENTAL THEORY; MISES MATERIAL

The material to be described below has the characteristics of being elastic-plastic, isotropic and linear strain hardening. It is assumed to strain harden isotropically and to yield in accordance with the Mises yield criterion.

Let $f(\tau_{ij}) = 0$ define a yield surface in stress space. Then if a vector from the origin lies within the yield surface, the material behaves elastically. If the vector lies on the yield surface and the increment in stress state is such as to cause the vector to move inwardly from the yield surface, the material once again behaves elastically. On the other hand, if the vector lies on the yield surface and the change in stress state is such as to cause the vector to move along the yield surface (for the elastic-perfectly plastic case) or outwardly from the current yield surface (for the strain hardening case), the material behaves plastically.

The flow law relating the increment in plastic deformation to the current stress state for this materials is given by[3,8]

$$de_{ij}^{p} = \lambda \frac{\partial f(\tau_{ij})}{\partial \tau_{ij}} \qquad (3.5)$$

where de_{ij}^{p} are the components of the deviators of plastic deformation increments. Since yielding is assumed to occur without change in volume, the deviators of plastic deformation increments are the same as the plastic deformation increments themselves.

The deviators of the total deformation increments may be written as the sum of their elastic and plastic components as follows[3];

$$de_{ij} = \frac{d\tau'_{ij}}{2G} + \lambda \frac{\partial f(\tau_{ij})}{\partial \tau_{ij}} \qquad (5.6)$$

where the deviators of incremental deformations and stresses are written respectively as;

$$de_{ij} = d\epsilon_{ij} - \tfrac{1}{3}\delta_{ij}\, d\epsilon_{kk} \qquad (5.7)$$

$$d\tau'_{ij} = d\tau_{ij} - \tfrac{1}{3}\delta_{ij}\, d\tau_{kk} \qquad (5.8)$$

If the expression for the yield surface is written as;

$$f(\tau_{ij}) = J_2 - (\sigma_e^2/3) = 0 \qquad (5.9)$$

where σ_e is the effective stress defined in Figure E.1, Appendix E, and

$$J_2 = \tfrac{1}{2}\, \tau'_{ij}\, \tau'_{ij} \qquad (5.9)$$

Then the expression for λ may be shown to be;

$$\lambda = \frac{3\, de^p}{2\, \sigma_e} \qquad (5.10)$$

where de^P is a scalar defined by

$$de^P = \sqrt{2/3\ (de^P_{ij} de^P_{ij})} \qquad (5.11)$$

and e^P is called the 'effective plastic strain'.

By incorporating a rate theory of elasticity proposed by Truesdell [4] into the concepts of frame indifferent constitutive laws discussed in Chapter IV we propose to rewrite equations (5.6) in the following form:

$$D'_{ij} = \frac{T'^{(J)}_{ij}}{2G} + \lambda \tau'_{ij} \qquad (5.12)$$

where D'_{ij}, $T'^{(J)}_{ij}$ and τ'_{ij} are the deviators of stretching, the Jaumann stress rate and stress respectively.

In the absence of rigid body rotations equations (5.12) lead to results that are identical to those of (5.6). When rigid body rotations occur, the difference in results are due to the presence of additional terms in $T'^{(J)}_{ij}$ consisting of the sums of products of spin and stress components (see equation (4.23)).

Equations (5.12) then represent the constitutive equations for an elastic-plastic, Von Mises material undergoing large deformations. Since thermal effects have been neglected in these equations, care must be taken to apply them to cases in which material temperatures remain

essentially constant. The work of Rice, Mcqueen, et al.[10] indicates that material temperatures vary during large elastic volume changes resulting from hydrostatic pressures in excess of 100 kilobars. Hence equations (5.12) apply to cases involving large deformations with pressures well below the 100 kilobar level. For pressures above this level, the reader is referred to the works of P. W. Bridgman[11,12,13].

Equations (5.12) now satisfy requirements of frame indifference. Satisfaction of local action is implied by the fact that (5.12) represents events occurring at a particle; while determinism is implied by the dependency of the plastic deformation increment on the previous stress path of a material particle. Finally, Hill's objection to Henky's deformation theory doesn't apply to equations (5.12); i.e. for a material particle whose stress path starts on the yield surface, unloads and then returns to a different point on the same yield surface, continuous changes occur in the plastic component of total deformation. Hence the constitutive equations, (5.12) satisfy the criteria initially set forth in this chapter.

CHAPTER VI

The Equations of Motion

Before discussing the finite element method in the next chapter, an incremental form of the equations of motion will be developed herein. These equations are derived by considering the virtual work of surface tractions and body forces acting on a body already in a deformed state.

Define;

$\overset{\nu}{T}_i$ = the traction on a surface whose outer normal is ν

F_i = body force per unit mass

S_u = that part of the boundary on which displacements are specified

S_σ = that part of the boundary on which tractions are specified

$S = S_u + S_\sigma$

V = the current volume of the body under consideration

The surface and volume of the body in Figure 6.1 are considered to be in a deformed state. Further it is assumed that there exists a class of admissible displacements, such that all boundary conditions and the equations of motion are satisfied. The field representing these displacements may be differentiated

as often as may be required. Thus, if one considers the admissible displacements $(u_i + \delta u_i)$ satisfying all boundary conditions, δu_i vanishes on S_u, and is arbitrary on S_σ. Then the virtual work of the surface tractions and body forces is;

$$\delta W = \int_V \rho F_i \delta U_i \, dV + \int_{S_u + S_\sigma} \overset{\nu}{T}_i \, \delta U_i \, dS \qquad (6.1)$$

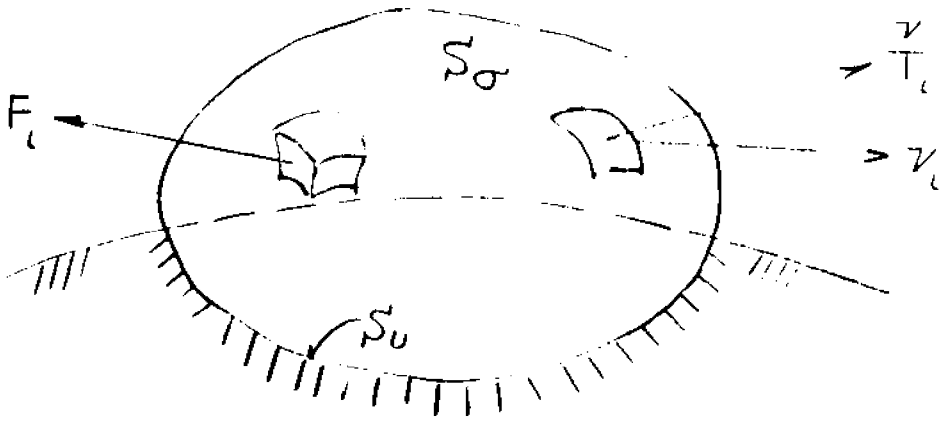

Figure 6.1

From the divergence theorem and the relationship;

$$\overset{\nu}{T}_i = \tau_{ij} \nu_j \qquad (6.2)$$

one may write;

$$\int_S (\tau_{ij} \delta U_i) \nu_j \, dS = \int_V [(\tau_{ij,j} \delta U_i) + (\tau_{ij} \delta U_{i,j})] dV \qquad (6.3)$$

From the known equilibrium relationship

$$\tau_{ij,j} + \rho F_i = 0 \tag{6.4}$$

it may be deduced that;

$$\delta W = \int_V \tau_{ij} \delta e_{ij} \, dV = \int_V \rho F_i \, \delta U_i \, dV + \int_S \bar{T}_i \, \delta U_i \, dS \tag{6.5}$$

where

$$\delta e_{ij} = \tfrac{1}{2}(\delta U_{i,j} + \delta U_{j,i}) \tag{6.6}$$

Equation (6.5) may be written in terms of stress increments occurring at a time t_n. Let ;

$$\Delta ( )_n = ( )_n - ( )_{n-1} \tag{6.7}$$

be the increment of a quantity during the time interval $(t_n - t_{n-1})$. Then equation (6.5) may be written

$$\int_V (\tau_{ij(n-1)} + \Delta \tau_{ij(n)}) \delta e_{ij(n)} dV = \int_V \rho F_{i(n)} \delta U_{i(n)} dV + \int_S \bar{T}_{i(n)} \delta U_{i(n)} dS \tag{6.8}$$

Equation (6.8) is basic to the incremental form of the finite element method to be developed herein.

CHAPTER VII

The Finite Element Method

Analytic solutions to dynamic problems in solids involving both geometric and constitutive non-linearities are infrequent. Those that do exist depend heavily on simplifying assumptions regarding symmetry, material behavior, loading paths and boundary conditions. After all of these assumptions are introduced and the governing differential equations formulated, the solution process often reduces to a numerical procedure to integrate these equations. A more direct approach to such problems would be to discretize them to begin with, in anticipation of the numerical solutions that must follow. The finite element method is one in which such an approach is made possible.

The finite element method is an outgrowth of matrix displacement methods which have been used extensively to analyze structures whose parameters may be conveniently lumped into discrete systems. The extension of these methods to the analysis of continuums was first introduced by Turner et al.[31]

In this method, the real continuum is subdivided into discrete substructures or 'elements' that are constrained to deform in such fashion that contiguous points on the boundaries of adjacent elements remain contiguous throughout their deformation history. Since stress discontinuities will occur from element to element across element boundaries, consideration of element equilibrium is accounted for by the effect of discrete forces acting at the element nodes from both external and internal sources.

Compatability of displacments at element boundaries is accomplished by choosing one of a class of displacement functions satisfying constraints along boundaries of each element. It may be shown that such a choice, in fact, is the basis of a Ritz[27] approach to formulating the equations of motion, in discrete form, for each finite element. The Ritz Method, and theorems associated with it, may be used to examine convergence of the finite element methods towards exact solutions.[54]

Two basic types of elements are used in this thesis; i.e. the triangle and the quadrilateral. The quadrilateral more accurately represents strains

since an extra degree of freedom has been introduced into its displacement function. Furthermore, the quadrilateral may be used to replace two triangles joining four nodes. However, both elements are required to assure adequate representation of irregular boundary conditions.

In the material that follows, a presentation of the discretized equations of motion, will be made. Matrices and other details associated with implementation of the finite element method, are shown in the Appendices.

7.1 Incremental Expressions for Displacement, Strain, Stress and Rotation.

The Triangular Element

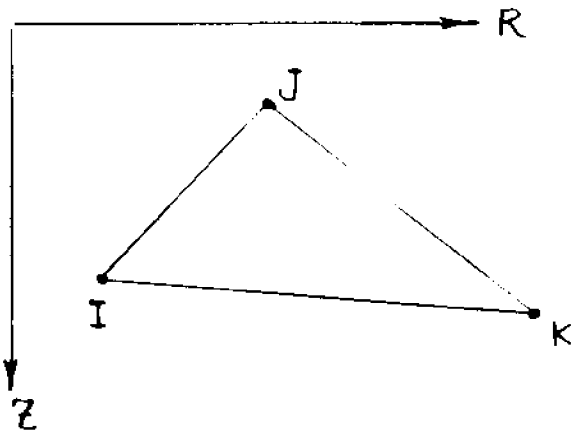

Figure 7.1

The conformable displacement function satisfying constraints along the element boundary in Figure 7.1 is given as;

$$\begin{Bmatrix} U \\ V \end{Bmatrix} = \begin{bmatrix} 1 & R & Z & 0 & 0 & 0 \\ 0 & 0 & 0 & 1 & R & Z \end{bmatrix} \begin{Bmatrix} \alpha_1 \\ \cdot \\ \cdot \\ \cdot \\ \cdot \\ \alpha_6 \end{Bmatrix} \qquad (7.1a)$$

or

$$\{U\} = [\Phi]\{\alpha\} \qquad (7.1b)$$

where U and V are the displacements in the R and Z directions respectively and α_1, through α_6 are arbitrary, time dependent coefficients corresponding to the degrees of freedom of each triangular element.

Upon inserting values for the coordinates of each of the nodes, I, J, K into equation (7.1a) and solving the resulting set of six simultaneous equations for α_L, one obtains

$$\begin{Bmatrix} \alpha_1 \\ \alpha_2 \\ \alpha_3 \\ \alpha_4 \\ \alpha_5 \\ \alpha_5 \end{Bmatrix} = \begin{bmatrix} a_I & 0 & a_J & 0 & a_K & 0 \\ b_I & 0 & b_J & 0 & b_K & 0 \\ c_I & 0 & c_J & 0 & c_K & 0 \\ 0 & a_I & 0 & a_J & 0 & a_K \\ 0 & b_I & 0 & b_J & 0 & b_K \\ 0 & c_I & 0 & c_J & 0 & c_K \end{bmatrix} \begin{Bmatrix} U_I \\ V_I \\ U_J \\ V_J \\ U_K \\ V_K \end{Bmatrix} \qquad (7.2a)$$

or

$$\{\alpha\} = [A]\{\delta\} \tag{7.2b}$$

where;

$$a_I = (\tfrac{1}{2}A)(Z_K R_J - Z_J R_K) \tag{7.3}$$

$$b_I = (\tfrac{1}{2}A)(Z_J - Z_K) \tag{7.4}$$

$$c_I = (\tfrac{1}{2}A)(R_K - R_J) \tag{7.5}$$

$$2A = \begin{vmatrix} 1 & 1 & 1 \\ R_I & R_J & R_K \\ Z_I & Z_J & Z_K \end{vmatrix} = \text{twice the element area} \tag{7.6}$$

R_I, Z_I, are the R and Z coordinate of node I, etc. and the remaining terms a_J, a_k, c_k, b_J, b_k may be obtained from (7.3), (7.4), and (7.5) by cyclically permutating indices.

It is convenient to define the following vector terms;

$$\underset{\sim}{b}^T = \begin{bmatrix} b_I & 0 & b_J & 0 & b_K & 0 \end{bmatrix} \tag{7.7a}$$

$$\underset{\sim}{\bar{b}}^T = \begin{bmatrix} 0 & b_I & 0 & b_J & 0 & b_K \end{bmatrix} \tag{7.7b}$$

$$\underset{\sim}{c}^T = \begin{bmatrix} c & 0 & c_J & 0 & c_K & 0 \end{bmatrix} \tag{7.7c}$$

$$\underset{\sim}{\bar{c}}^T = \begin{bmatrix} 0 & c_I & 0 & c_J & 0 & c_K \end{bmatrix} \tag{7.7d}$$

$$\underset{\sim}{a}^T = \begin{bmatrix} a_I & 0 & a_J & 0 & a_K & 0 \end{bmatrix} \tag{7.7e}$$

where the superscript 'T' denotes the matrix transpose and $(\underset{\sim}{\ })$ denotes a vector or a matrix.

Expressions (7.1) and (7.2) are equally valid for velocities or displacement increments provided a_I, b_I, and c_I of equations (7,3,4,5) are based on current nodal coordinates.

Now the expressions for stretching and spin are respectively; (see equations (3.12a, b)

$$D_{ij} = \tfrac{1}{2}\,(\dot{U}_{i,j} + \dot{U}_{j,i}) \qquad (7.8a)$$

$$W_{ij} = \tfrac{1}{2}\,(\dot{U}_{j,i} - \dot{U}_{i,j}) \qquad (7.8b)$$

where $(\ )_{,i}$ is defined more generally as the covariant derivative of the term in parenthesis. Hence, the vector for stretching may be written;

$$\begin{Bmatrix} D_{rr} \\ D_{\theta\theta} \\ D_{zz} \\ D_{rz} \end{Bmatrix} = \begin{bmatrix} \underset{\sim}{b}^T \\ \underset{\sim}{k}^T \\ \underset{\sim}{\bar{c}}^T \\ \tfrac{1}{2}(\underset{\sim}{c}+\underset{\sim}{\bar{b}})^T \end{bmatrix} \begin{Bmatrix} \dot{U}_I \\ \dot{V}_I \\ \dot{U}_J \\ \dot{V}_J \\ \dot{U}_K \\ \dot{V}_K \end{Bmatrix} \qquad (7.9a)$$

or $\underset{\sim}{D} = \underset{\sim}{B}\ \dot{\underset{\sim}{\delta}}$ (7.9b)

where;

$\underset{\sim}{K}^T = \underset{\sim}{0}$ for the plane strain configuration

and $\underset{\sim}{K}^T = (\underset{\sim}{a}^T + R\underset{\sim}{b}^T + Z\underset{\sim}{c}^T)/R$ for the axi-symmetric configuration

Note, that in the axi-symmetric case, the expression in (7.9a) are the physical components of stretching.

Since the only non-zero spin term lies in the (R, Z) plane, its expression is given by;

$$\omega = \tfrac{1}{2}(\dot{\lambda}_3 - \dot{\lambda}_5) = \tfrac{1}{2}(\underset{\sim}{c}-\underset{\sim}{b})^T \dot{\underset{\sim}{\delta}} \qquad (7.10)$$

The frame indifferent rate form of the stress-strain relationship for an elastic material is given by;

$$\underset{\sim}{T}^{(J)} = \underset{\sim}{E}\,\underset{\sim}{D} \qquad (7.11)$$

where;

$$\underset{\sim}{T}^{(J)} = \begin{Bmatrix} T^{(J)}_{rr} \\ T^{(J)}_{\theta\theta} \\ T^{(J)}_{zz} \\ T^{(J)}_{rz} \end{Bmatrix}$$

is the Jaumann stress rate defined in (4.23) (7.12)

$$\underset{\sim}{E} = \frac{E}{1-\nu^2}\begin{bmatrix} 1 & 0 & \nu & 0 \\ 0 & 0 & 0 & 0 \\ \nu & 0 & 1 & 0 \\ 0 & 0 & 0 & (1-\nu) \end{bmatrix} \quad \text{if plane stress} \qquad (7.13a)$$

$$\underset{\sim}{E} = \frac{E(1-\nu)}{(1+\nu)(1-2\nu)} \begin{bmatrix} 1 & \frac{\nu}{1-\nu} & \frac{\nu}{1-\nu} & 0 \\ \frac{\nu}{1-\nu} & 1 & \frac{\nu}{1-\nu} & 0 \\ \frac{\nu}{1-\nu} & \frac{\nu}{1-\nu} & 1 & 0 \\ 0 & 0 & 0 & \frac{1-2\nu}{1-\nu} \end{bmatrix} \quad \text{if plane strain , or Axi-symmetric} \qquad (7.13)$$

7.2 The Discretized form of the Equations of Motion

The total deformation rate at any time t_n is assumed to consist of an elastic and plastic component. Hence, (7.11) may be written as;

$$\underset{\sim}{T}^{(J)} = \underset{\sim}{E} \left(\underset{\sim}{D}^{(T)} - \underset{\sim}{D}^{(P)} \right) \qquad (7.14)$$

where the superscripts T and P, in parentheses denote the total and plastic components of stretching respectively.

The substitutions of (7.2b) into (7.11) results in the expression;

$$\delta \underset{\sim}{U} = \int_{\sim} \underset{\sim}{A} \, \delta \underset{\sim}{\delta} \qquad (7.15)$$

and the expression for deformation perturbation may be written as;

$$\delta \underset{\sim}{e} = \underset{\sim}{B} \, \delta \underset{\sim}{\delta} \qquad (7.16)$$

Incremental expressions for $\underset{\sim}{D}$ and ω are found by substituting displacement increments (occurring during a time interval 'h') for the velocities in equations (7.9) and (7.10) respectively. These displacement increments are obtained through the recursive integration formulae (7.47) and (7.48). In order to avoid introducing additional notation, $\underset{\sim}{D}$ and ω will hencefor designate increments in deformation and rotation rather than rates, while $\underset{\sim}{T}^{(J)}$ will be used to designate a Jaumann stress increment consistent with the above incremental expressions. With this in mind, the actual stress increment $\Delta\underset{\sim}{\tau}_n$ may be obtained from (4.23), Chapter V and written as

$$\Delta\underset{\sim}{\tau}_n = \underset{\sim}{T}_n^{(J)} + \omega_n \underset{\sim}{Y}\, \underset{\sim}{\tau}_{n-1} \qquad (7.17)$$

where

$$\underset{\sim}{Y} = \begin{bmatrix} 0 & 0 & 0 & 2 \\ 0 & 0 & 0 & 0 \\ 0 & 0 & 0 & -2 \\ -1 & 0 & 1 & 0 \end{bmatrix} \qquad (7.18)$$

Hence;

$$\Delta\underset{\sim}{\tau}_n = \underset{\sim}{E}\left(\underset{\sim}{B}_n \Delta\underset{\sim}{\delta}_n - \underset{\sim}{D}_n^{(P)}\right) + \omega_n \underset{\sim}{Y}\, \underset{\sim}{\tau}_{n-1} \qquad (7.19)$$

Then in view of equations (7.9b), (7.16), (7.19), and the above remarks on incremental notation, equation (7.8) may be written as;

$$\delta\underset{\sim}{\delta}_n^T \int_V \underset{\sim}{B}_n^T \left\{(\underset{\sim}{I} + \omega_n \underset{\sim}{Y})\,\underset{\sim}{\tau}_{n-1} + \underset{\sim}{E}\left(\underset{\sim}{B}_n \Delta\underset{\sim}{\delta}_n - \underset{\sim}{D}_n^{(P)}\right)\right\} dV =$$
$$\delta\underset{\sim}{\delta}_n^T \int_V \left(\rho_n \underset{\sim}{A}_n^T \underset{\sim}{\phi}^T \underset{\sim}{F}_n\right) dV + \delta\underset{\sim}{\delta}_n^T \int_S \left(\underset{\sim}{A}_n^T \underset{\sim}{\phi}^T \underset{\sim}{T}_n\right) dS \qquad (7.20)$$

where $\underset{\sim}{I}$ is the identity matrix

$$\underset{\sim}{F}_n = \begin{Bmatrix} F_u \\ F_v \end{Bmatrix}_n$$ is a vector of body forces per unit mass at a particle in an element

$$\underset{\sim}{T}_n = \begin{Bmatrix} T_u \\ T_v \end{Bmatrix}_n$$ is the vector of specified tractions on the external surface of an element

$$\underset{\sim}{L} = \begin{bmatrix} 1 & 0 & 0 & 0 \\ 0 & 1 & 0 & 0 \\ 0 & 0 & 1 & 0 \\ 0 & 0 & 0 & 2 \end{bmatrix}$$

and the subscript n denotes values at a time t_n.

The integral $\int_S A^T{}_n \Phi_n T_n \, dS$ in equation (7.20) above is shown evaluated in Appendix B. The integral is zero except for those elements having specified surface tractions.

The first integral on the right of (7.20) may be altered somewhat by extending the definition of a body force to include inertial forces. Then if $\underset{\sim}{F} = -\underset{\sim}{\ddot{U}}$, we have

$$\underset{\sim}{F} = -\underset{\sim}{\Phi} \underset{\sim}{A} \underset{\sim}{\ddot{\delta}} \qquad (7.22)$$

and;

$$\int_V (\rho_n A_n^T \underset{\sim}{\Phi}^T \underset{\sim}{F}_n) dV = -\left\{ \int_V \rho_n A_n^T \Phi^T \Phi \, A \, dV \right\} \ddot{\delta}_n \qquad (7.23)$$

The term in brackets on the right of (7.23) is referred to in the literature as a 'consistent' mass matrix. This matrix is consistent with the admissible motion of an element when the element mass is regarded as distributed through the element volume rather than concentrated at the element nodes. Since it is nodal equilibrium that we are ultimately interested in, contributions to the equivalent mass of each node could be obtained from the distributed mass matrices of each element containing that node. These contributions taken together for all the nodes in continuum add up to the "assembled mass matrix". Unfortunately, any solution of the equations of motion would require the inversion of this matrix. If we are to solve problems of any reasonable size, the computer time and core storage requirements would be of sufficient proportion as to render this procedure unsuitable. Hence, the bracketed term in (7.23) will be replaced by a less accurate, but operationally more suitable, diagonalized mass matrix; i.e. one in which the element mass is treated as if it were concentrated at the element nodes.

The conditions imposed upon the relationship of concentrated to distributed mass in each element are discussed in Appendix A. In view of the above discussion, the equations of motion (7.20) may be written;

$$\int_V \underset{\sim}{B}_n^T \underset{\sim}{L} \left\{ (\underset{\sim}{I} + \omega_n \underset{\sim}{Y}) \underset{\sim}{T}_{n-1} + \underset{\sim}{E}(\underset{\sim}{B}_n \Delta\underset{\sim}{\delta}_n - \underset{\sim}{D}_n^{(P)}) \right\} dV = -\underset{\sim}{M}\ddot{\underset{\sim}{\delta}}_n + \underset{\sim}{T}_{n} \tag{7.24}$$

The integral on the left of (7.24) may be evaluated in terms of the initial configuration of each element by making the substitution; $JdV_o = dV$ in the integrand and V_o in the limits of integration; where J is the Jacobian of transformation (See Chapter III). The Jacobian is evaluated as;

$$J_n = 1 + \left\{ (\underset{\sim}{b} + \underset{\sim}{\bar{c}})^T + \underset{\sim}{\delta}_n^T (\underset{\sim}{b}\,\underset{\sim}{\bar{c}}^T - \underset{\sim}{c}\,\underset{\sim}{\bar{b}}^T) \right\} \underset{\sim}{\delta}_n \tag{7.25}$$

for the plane stress and plane strain cases and as

$$J_n = \left[1 + \frac{1}{R}(\underset{\sim}{a}^T + R\,\underset{\sim}{b}^T + Z\,\underset{\sim}{c}^T)\underset{\sim}{\delta}_n \right] \left\{ 1 + ([\underset{\sim}{b} + \underset{\sim}{\bar{c}}]^T + \underset{\sim}{\delta}_n^T [\underset{\sim}{b}\,\underset{\sim}{\bar{c}}^T - \underset{\sim}{c}\,\underset{\sim}{\bar{b}}^T])\underset{\sim}{\delta}_n \right\} \tag{7.26}$$

for axial symmetry. Note, that $\underset{\sim}{b}$, $\underset{\sim}{c}$, $\underset{\sim}{\bar{b}}$, and $\underset{\sim}{\bar{c}}$ are based on initial nodal coordinates.

Equation (7.24) may now be written in the shorter, and more useful form;

$$\ddot{\underset{\sim}{\delta}}_n = \underset{\sim}{M}^{-1} \left\{ \underset{\sim}{T}_n - \underset{\sim}{K}_n - \underset{\sim}{P}_n + \underset{\sim}{H}_n \right\} \qquad (7.27)$$

where: $\underset{\sim}{T}_n$ = the specified surface traction at time t_n,

$$\underset{\sim}{K}_n = \int_{V_o} \left(\underset{\sim}{B}_n^T \underset{\sim}{L} \underset{\sim}{E} \underset{\sim}{B}_n \Delta \underset{\sim}{\delta}_n \right) J_n \, dV_o \qquad (7.28a)$$

$$\underset{\sim}{P}_n = \int_{V_o} \left(\underset{\sim}{B}_n^T (\underset{\sim}{I} + \omega_n \underset{\sim}{Y}) \underset{\sim}{\tau}_{n-1} \right) J_n \, dV_o \qquad (7.28b)$$

$$\underset{\sim}{H}_n = \int_{V_o} \left(\underset{\sim}{B}_n^T \underset{\sim}{L} \underset{\sim}{E} \underset{\sim}{D}_n^{(P)} \right) J_n \, dV_o \qquad (7.28c)$$

In the plane strain and plane stress cases the integrals in equations (7.28) are simply the bracketed terms in the integrands multiplied by the element areas, since the integrands are constant over the element volumes at any time t. In the axi-symmetric case, however, the integrals are evaluated at each time step by the application of Gaussian quadrature over the volume of each element. (See Appendix C).

7.3 The Quadrilateral Element [22].

Except for certain details, the presentation of the quadrilateral element is identical to that of the triangular element. The advantages of using

this element are improved accuracy achieved by including an extra degree of freedom in the displacement relationships and the smaller number of elements required to represent a given continuum. Computational advantages are further achieved in the numerical integration over the element volume (See Appendix C) and in storage of element properties.

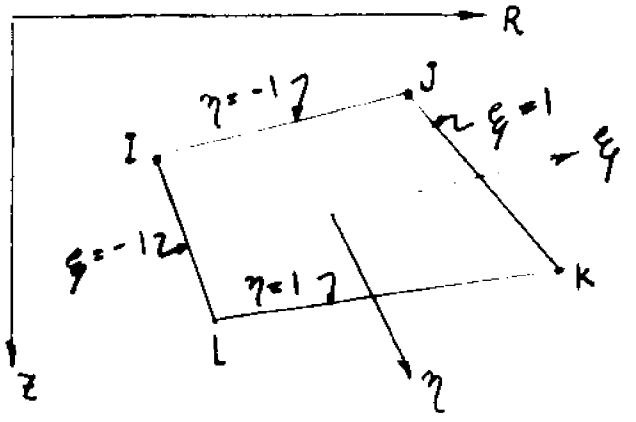

Figure 7.2

(Quadrilateral Element Referred to a Spatial (current) Coordinate System)

The conforming displacement function for the element of Figure 7.2, above is expressed in terms of the (ξ,η) coordinate system as [22];

$$\begin{Bmatrix} U \\ V \end{Bmatrix} = \begin{bmatrix} 1 & \xi & \xi\eta & \eta & 0 & 0 & 0 & 0 \\ 0 & 0 & 0 & 0 & 1 & \xi & \xi\eta & \eta \end{bmatrix} \begin{Bmatrix} \alpha_1 \\ \alpha_2 \\ \vdots \\ \alpha_7 \\ \alpha_8 \end{Bmatrix} \quad (7.29)$$

By substituting the values of (ξ_I, η_I) into equations (7.29) one may arrive at ;

$$\begin{Bmatrix} \alpha_1 \\ \alpha_2 \\ \alpha_3 \\ \alpha_4 \\ \alpha_5 \\ \alpha_6 \\ \alpha_7 \\ \alpha_8 \end{Bmatrix} = \frac{1}{4} \begin{bmatrix} 1 & 0 & 1 & 0 & 1 & 0 & 1 & 0 \\ -1 & 0 & 1 & 0 & 1 & 0 & -1 & 0 \\ 1 & 0 & -1 & 0 & 1 & 0 & -1 & 0 \\ -1 & 0 & -1 & 0 & 1 & 0 & 1 & 0 \\ 0 & 1 & 0 & 1 & 0 & 1 & 0 & 1 \\ 0 & -1 & 0 & 1 & 0 & 1 & 0 & -1 \\ 0 & 1 & 0 & -1 & 0 & 1 & 0 & -1 \\ 0 & -1 & 0 & -1 & 0 & 1 & 0 & 1 \end{bmatrix} \begin{Bmatrix} U_I \\ V_I \\ U_J \\ V_J \\ U_K \\ V_K \\ U_L \\ V_L \end{Bmatrix} \quad (7.30)$$

The values of α_i may be substituted into (7.29) to obtain;

$$\begin{Bmatrix} U \\ V \end{Bmatrix} = \begin{bmatrix} N_I & 0 & N_J & 0 & N_K & 0 & N_L & 0 \\ 0 & N_I & 0 & N_J & 0 & N_K & 0 & N_L \end{bmatrix} \underset{\sim}{\delta} \quad (7.31)$$

where;

$$\begin{aligned} N_I &= \tfrac{1}{4} (1 - \xi)(1 - \eta) \\ N_J &= \tfrac{1}{4} (1 + \xi)(1 - \eta) \\ N_K &= \tfrac{1}{4} (1 + \xi)(1 + \eta) \\ N_L &= \tfrac{1}{4} (1 - \xi)(1 + \eta) \end{aligned} \quad (7.32)$$

and

$$\underset{\sim}{\delta}^T = [U_I \; V_I \; U_J \; V_J \; U_K \; V_K \; U_L \; V_L] \quad (7.33)$$

Since a linear relationship of the form of (7.31) exists between the two coordinate system shown in Figure 7.2, one may also write;

$$\begin{Bmatrix} R \\ Z \end{Bmatrix} = \begin{bmatrix} N_I & 0 & N_J & 0 & N_K & 0 & N_L & 0 \\ 0 & N_I & 0 & N_J & 0 & N_K & 0 & N_L \end{bmatrix} X \quad (7.34)$$

where:

$$\underset{\sim}{X}^T = [R_I \; Z_I \; R_J \; Z_J \; R_K \; Z_K \; R_L \; R_L] \quad (7.35)$$

Now, in order to write expressions for the components of the stretching tensor referred to the (R,Z) coordinate system, the following relationships are used;

$$\begin{Bmatrix} (\;)_{,R} \\ (\;)_{,Z} \end{Bmatrix} = \frac{1}{|\mathcal{J}|} \begin{bmatrix} Z_{,\zeta} & -Z_{,\xi} \\ -R_{,\zeta} & R_{,\xi} \end{bmatrix} \begin{Bmatrix} (\;)_{,\xi} \\ (\;)_{,\zeta} \end{Bmatrix} \quad (7.36)$$

$$U_{,\xi} = \underset{\sim}{A}\,\underset{\sim}{\delta} = \underset{\sim}{\delta}^T \underset{\sim}{A}^T \quad (7.37a)$$

$$U_{,\zeta} = \underset{\sim}{B}\,\underset{\sim}{\delta} = \underset{\sim}{\delta}^T \underset{\sim}{B}^T \quad (7.37b)$$

$$V_{,\zeta} = \underset{\sim}{\bar{B}}\,\underset{\sim}{\delta} = \underset{\sim}{\delta}^T \underset{\sim}{\bar{B}}^T \quad (7.37c)$$

$$V_{,\xi} = \underset{\sim}{\bar{A}}\,\underset{\sim}{\delta} = \delta^T \bar{A}^T \quad (7.37d)$$

where:

$$\underset{\sim}{J} = \begin{bmatrix} R_{,\xi} & Z_{,\xi} \\ R_{,\eta} & Z_{,\eta} \end{bmatrix} = \frac{1}{4}\begin{bmatrix} -(1-\eta) & (1-\eta) & (1+\eta) & -(1+\eta) \\ -(1-\xi) & -(1+\xi) & (1+\xi) & (1-\xi) \end{bmatrix}\begin{bmatrix} R_I & Z_I \\ R_J & Z_J \\ R_K & Z_K \\ R_L & Z_L \end{bmatrix} \quad (7.38)$$

$|J|$ = Determinant of J

$$\underset{\sim}{A} = \tfrac{1}{4}[-(1-\eta)\ 0\ (1-\eta)\ 0\ (1+\eta)\ 0\ -(1+\eta)\ 0] \quad (7.39a)$$

$$\underset{\sim}{\bar{A}} = \tfrac{1}{4}[0\ -(1-\eta)\ 0\ (1-\eta)\ 0\ (1+\eta)\ 0\ -(1+\eta)] \quad (7.39b)$$

$$\underset{\sim}{B} = \tfrac{1}{4}[-(1-\xi)\ 0\ -(1+\xi)\ 0\ (1+\xi)\ 0\ (1-\xi)\ 0] \quad (7.39c)$$

$$\underset{\sim}{\bar{B}} = \tfrac{1}{4}[0\ -(1-\xi)\ 0\ -(1+\xi)\ 0\ (1+\xi)\ 0\ (1-\xi)] \quad (7.39d)$$

and we further define:

$$\underset{\sim}{N} = [N_I\ \ 0\ \ N_J\ \ 0\ \ N_K\ \ 0\ \ N_L] \quad (7.39e)$$

Then the matrix expression for stretching becomes;

$$\begin{Bmatrix} D_{RR} \\ D_{\theta\theta} \\ D_{ZZ} \\ D_{RZ} \end{Bmatrix} = \begin{bmatrix} (1/|J|)\ \underset{\sim}{X}^T(\underset{\sim}{\bar{B}}^T\underset{\sim}{A} - \underset{\sim}{\bar{A}}^T\underset{\sim}{B}) \\ \underset{\sim}{K} \\ (1/|J|)\ \underset{\sim}{X}^T(\underset{\sim}{A}^T\underset{\sim}{\bar{B}} - \underset{\sim}{B}^T\underset{\sim}{\bar{A}}) \\ (1/2|J|)\ \underset{\sim}{X}^T(\underset{\sim}{\bar{B}}^T\underset{\sim}{\bar{A}} - \underset{\sim}{B}^T\underset{\sim}{A} + \underset{\sim}{A}^T\underset{\sim}{B} - \underset{\sim}{\bar{A}}^T\underset{\sim}{\bar{B}}) \end{bmatrix} \underset{\sim}{\dot{\delta}} \quad (7.40)$$

where:

$$\underset{\sim}{K} = \begin{cases} 0 & \text{if plane strain} \\ \underset{\sim}{N}/R;\ (R = \underset{\sim}{N}\ \underset{\sim}{X}) & \text{if axi-symmetric} \end{cases}$$

Equations (7.40) may be written more conveniently as;

$$\underset{\sim}{D} = \underset{\sim}{B}\ \dot{\underset{\sim}{\delta}} \tag{7.41}$$

and used directly in the equilibrium equations (7.27). The integrals are evaluated numerically over the current volume of each element, so that;

$$\underset{\sim}{K}_n = \int_V \left(\underset{\sim}{B}_n^T\ \underset{\sim}{L}\ \underset{\sim}{E}\ \underset{\sim}{B}_n\ \Delta\ \underset{\sim}{\delta}_n\right) dV \tag{7.42a}$$

$$\underset{\sim}{P}_n = \int_V \left(\underset{\sim}{B}_n^T\ \underset{\sim}{L}\ (\underset{\sim}{I}+\omega_n \underset{\sim}{Y})\ \underset{\sim}{\tau}_{n-1}\right) dV \tag{7.42b}$$

$$\underset{\sim}{H}_n = \int_V \left(\underset{\sim}{B}_n^T\ \underset{\sim}{L}\ \underset{\sim}{E}\ \underset{\sim}{\square}_n^{(P)}\right) dV \tag{7.42c}$$

and $\underset{\sim}{X}$ represents the vector of current coordinates of the element node.

7.4 Solution of the Equations of Motion

In equation (7.27), the equations of motion for a single finite element are written as;

$$\ddot{\underset{\sim}{\delta}}_n = \underset{\sim}{M}^{-1}\ [\underset{\sim}{T}_n - \underset{\sim}{K}_n - \underset{\sim}{P}_n - \underset{\sim}{H}_n] \tag{7.27}$$

The terms in brackets on the right side of equation (7.27) above, may be considered to be a combination of externally applied and internal resisting forces of the element acting on the element nodes. Therefore, it is possible to deal with the sum total of such loadings acting

on a node that is common to several elements. For example in Figure 7.3 below, node 6 is common to elements 1 through 5.

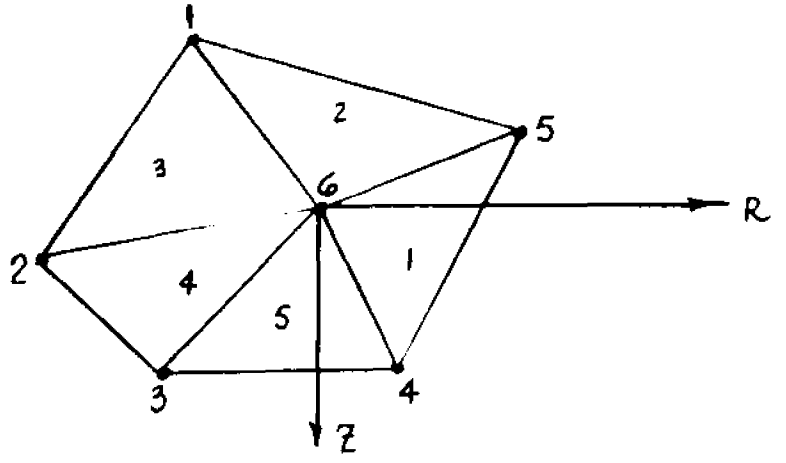

Figure 7.3

The expanded form of equations (7.27) above may be written for element 3 as;

$$\begin{Bmatrix} U_1 \\ V_1 \\ U_6 \\ V_6 \\ U_2 \\ V_2 \end{Bmatrix} = \begin{bmatrix} 1/M_1 & & & & & \\ & 1/M_1 & & & & \\ & & 1/M_6 & & & \\ & & & 1/M_6 & & \\ & & & & 1/M_2 & \\ & & & & & 1/M_2 \end{bmatrix} \begin{Bmatrix} Tu_1 - Ku_1 - Pu_1 + Hu_1 \\ Tv_1 - Kv_1 - Pv_1 + Hv_1 \\ Tu_6 - Ku_6 - Pu_6 + Hu_6 \\ Tv_6 - Kv_6 - Pv_6 + Hv_6 \\ Tu_2 - Ku_2 - Pu_2 + Hu_2 \\ Tv_2 - Kv_2 - Pv_2 + Hv_2 \end{Bmatrix}$$

(7.43)

Then the combination of loadings from elements 1 through 5 produce an acceleration in node 6 as follows;

$$\begin{Bmatrix} \ddot{U}_6 \\ \ddot{V}_6 \end{Bmatrix} = \begin{bmatrix} 1/M_6 & 0 \\ 0 & 1/M_6 \end{bmatrix} \left[\begin{Bmatrix} Tu_6 \\ Tv_6 \end{Bmatrix} - \begin{Bmatrix} Ku_6 \\ Kv_6 \end{Bmatrix} - \begin{Bmatrix} Pu_6 \\ Pv_6 \end{Bmatrix} + \begin{Bmatrix} Hu_6 \\ Hv_6 \end{Bmatrix} \right]_{1+2\cdots+5} \tag{7.44}$$

Hence, equations (7.27) also represent the equations of motion for every node in the finite element system.

Solving the set of equations (7.27) is equivalent to solving the set of ordinary differential equations;

$$\ddot{\underset{\sim}{X}}(X,t) = \underset{\sim}{F}(X,t) \tag{7.45}$$

with initial conditions;

$$\begin{aligned} \underset{\sim}{X}(X,t_o) &= \underset{\sim}{X}_o \\ \dot{\underset{\sim}{X}}(X,t_o) &= \dot{\underset{\sim}{X}}_o \end{aligned} \tag{7.46}$$

7.5 Integration Schemes for Solution

In choosing an integration scheme to solve equations (7.27), it was deemed desirable that this scheme have the following properties;

(a) A 'reasonable' solution accuracy be attainable in the interval of integration.

(b) In any 'step-by-step' procedure the conditions at a time t_n are entirely predicted using earlier conditions.

(c) Storage of data at each integration step be kept to a minimum.

(d) The method requires no major alteration of solution algorithm to be started.

(e) The solutions obtained are stable throughout the integration interval.

(f) The use of computer time is minimal in completing any integration step.

The Runge-Kutta methods[23] and the predictor-corrector methods of Milne[28] and Adams[23] each require the calculation of at least four values of the dependent variable and/or its first derivative for each integration step. Although applicable to systems of differential equations of all orders, systems must first be reduced to a system of first order equations.

A number of methods are available that are directly applicable to systems of second order equations without reducing their order. The Stormer-Corwell[29] method, for example requires the calculation of only two values of the dependent variable per integration step and is not self starting. The Newmark 'β' method with 'β'=o is also directly applicable to systems of second order equations. It requires a calculation of the dependent variable and its first derivative for each integration step. The simplicity of starting as well as the accuracy in results obtained by earlier investigators[46,47,55,30]

make it a particularly attractive method for application to the problems solved in this thesis.

The recursive equations are;

$$\dot{\delta}_{n+1} = \dot{\delta}_n + \tfrac{1}{2} (\ddot{\delta}_{n+1} + \ddot{\delta}_n) h \qquad (7.47)$$

and

$$\delta_{n+1} = \delta_n + \dot{\delta}_n h + \tfrac{1}{2} \ddot{\delta}_n h^2 \qquad (7.48)$$

where h = the increment in time, Δt.

The stability of this method may be examined by considering a simple mass, spring system with one degree of freedom and no external force acting unit. For a given initial displacement and velocity the motion of the system is purely oscillatory with a circular frequency of;

$$\omega = \sqrt{K/m} \qquad (7.49)$$

where K is the spring constant and m is the mass.
If the system is linear, then the acceleration is given by;

$$\ddot{\delta} = -\omega^2 \delta \qquad (7.50)$$

Then if we define the term;

$$\Theta = \omega h = \frac{2\pi h}{T} \qquad (7.51)$$

we may derive the difference equation;

$$\delta_{n+1} - (2 - \theta^2)\delta_n + \delta_{n-1} = 0 \qquad (7.52)$$

which corresponds to the differential equation;

$$\ddot{\delta} + \left(\frac{\theta}{h}\right)^2 \delta = 0 \qquad (7.53)$$

The solution to the difference equation may be written;

$$\delta_n = \delta_o \cos(2\pi t/T_s) + B \sin(2\pi t/T_s) \qquad (7.54)$$

where δ_o is the initial mass displacement, B is a constant and, Ts is a pseudo period corresponding to the solution of the difference equation. The comparable solution to the exact equation (7.53) is;

$$\delta = \delta_o \cos(2\pi t/T_s) + \frac{V_o}{\omega} \sin(2\pi t/T) \qquad (7.55)$$

where T is the exact system period and V_o is an initial velocity.

Using this approach, Newmark[30] developed the following approximate expressions for the ratios Ts/T and $B/(V_o/\omega)$;

$$T_s/T = 1 - \theta^2/24 - 17\theta^4/5760 - \cdots \qquad (7.56)$$

$$B/(V_o/\omega) = 1 + \theta^2/8 + \cdots \qquad (7.57)$$

From these the following (partially reproduced) table of relative errors in period and maximum response to an initial velocity were obtained[30].

Table 7.1

$\beta = 0$

h/T	Relative error in Period $\left(\frac{T_s}{T} - 1\right)$	Relative error in maximum Response to an initial Velocity $\left(\frac{B}{V_o/\omega} - 1\right)$
0.05	-0.004	0.012
0.10	-0.017	0.052
0.20	-0.076	0.209
0.25	-0.130	0.614
0.318	-0.363	infinite

The stability limit of the system occurs when θ^2 is greater than 4. At this value, the solution

to equation (7.52) oscillates without bound. Hence at $\Theta^2=4$, we have at the stability limit;

$$\frac{hs}{Ts} = \frac{1}{\pi} = 0.318 \qquad (7.58)$$

It is seen in Table (7.1) that h/T must be considerably less than the value given by (7.58) if large errors are not to occur during each integration step.

The criterion used to determine 'h' is that 'h' be less than the minimum period of the discretized system. An approximate means of estimating this period is demonstrated in Appendix F.The actual ratio h/T used, is governed by consideration of stability and the amount of error that may be tolerated in generating the solution to the initial value problem. Using Table 7.1 as a guide, the value of h/T chosen for the problems solved in this thesis was 0.05. The algorithm used in solving the initial value problem may then be outlined as follows:

It is first assumed that the entire solution of the physical problem is known at some time t_n. The known solution will include such terms as displacements, velocities stresses, etc. so that all terms appearing in brackets on the right side of

equation (7.27), including any time dependent applied surface tractions, are known. Then;

a) solve for $\ddot{\delta}_n$ in equation (7.27).

b) solve for δ_{n+1} in equation (7.48).

c) solve; $\dot{\delta}'_{n+1} = \dot{\delta}_n + 1/2\ \ddot{\delta}_n h$

d) find the current nodal coordinates and update the strain displacement matrix B_{n+1}.

e) find the Jacobian J_{n+1}; the stress increment $\Delta\tau_{n+1}$; the plastic deformation increment $D^{(P)}_{n+1}$; the total deformation increment $D^{(T)}_{n+1}$; the increment in effective plastic strain Δe^P_{n+1}; and the increment in particle rotation ω_{n+1}

f) add the (components of) stress increment to τ_{n+1}. Find the total effective plastic strain; $e^P_{n+1} = e^P_n + e^P_{n+1}$

g) evaluate K_{n+1}, P_{n+1}, H_{n+1} in equation (7.27).

h) solve for $\ddot{\delta}_{n+1}$ in equation (7.27).

i) solve; $\dot{\delta}_{n+1} = (\dot{\delta}_{n+1})' + 1/2\ \ddot{\delta}_{n+1} h$

Repeat steps b) through i) for each successive cycle of integration.

Note that although $\dot{\delta}_{n+1}$ is not used directly in (7.27), it must be evaluated at each time step in order to find δ_{n+1}.

7.6 Numerical Evaluation of the Plastic Deformation Increment

From equation (5.10) and 5.11), the plastic components of deformation increment are given in incremental from as;

$$D_i^P = \left(\frac{3\Delta e_i^P}{2\sigma_{e(i-1)}}\right)\tau'_{i-1} \qquad (7.59)$$

where $\underset{\sim}{D}_i$ is understood to be the increment of deformation over a given time interval from $t_{(i-1)}$ to t_i corresponding to the subscripts used in (7.59). In the numerical integration scheme described above, the value of Δe_i^P in (7.59) must be evaluated for each time interval based on information that is known in the preceding interval. These intervals must be sufficiently small so that one may be able to consider Δe_i^P as effectively uniform over the entire interval. The values of Δe_i^P must then be positive, real values.

In general;

$$\underset{\sim}{\tau}_i = \underset{\sim}{\tau}_{i-1} + \Delta\underset{\sim}{\tau}_i \qquad (7.60)$$

and

$$\underset{\sim}{T}_i^{(J)} = \underset{\sim}{E}\,(\underset{\sim}{D}_i - \underset{\sim}{D}_i^P) \qquad (7.61)$$

where, again, $\underset{\sim}{T}_i^{(J)}$ is understood to be a stress increment over the time from $t_{(i-1)}$ to t_i.

Then from (7.17), (7.61) and (7.59)

$$\underset{\sim}{\tau}_i = (\underset{\sim}{I} + W_i \underset{\sim}{Y})\, \underset{\sim}{\tau}_{i-1} + \underset{\sim}{E}\,(\underset{\sim}{D}_i - \frac{3\,\Delta e^P_i}{2\,\sigma_{e(i-1)}}\, \underset{\sim}{\tau}'_{i-1}) \tag{7.62}$$

By defining

$$\underset{\sim}{\bar{\tau}}_i = (\underset{\sim}{I} + \underset{\sim}{WY})\, \underset{\sim}{\tau}_{i-1} + \underset{\sim}{ED}_i \tag{7.63}$$

we may write;

$$\underset{\sim}{\tau}_i = \underset{\sim}{\bar{\tau}}_i - \left(\frac{3\,\Delta e^P_i}{2\,\sigma_{e(i-1)}}\right) \underset{\sim}{E}\, \underset{\sim}{\tau}'_{i-1} \tag{7.64}$$

The expression for the deviatoric stress is given by;

$$\underset{\sim}{\tau}' = \underset{\sim}{G}\, \underset{\sim}{\tau} \tag{7.65}$$

where

$$\underset{\sim}{G} = \frac{1}{3} \begin{bmatrix} 2 & -1 & -1 & 0 \\ -1 & 2 & -1 & 0 \\ -1 & -1 & 2 & 0 \\ 0 & 0 & 0 & 3 \end{bmatrix} \tag{7.66}$$

The expression for effective stress is given by;

$$\sigma_e = \sqrt{3\, J_2}$$

so that;

$$2\,\sigma^2_{e(i)} = \underset{\sim}{\tau}_i^T\, \underset{\sim}{\bar{G}}\, \underset{\sim}{\tau}_i \tag{7.67}$$

where the superscript, T, designates the matrix transpose; and;

$$\underset{\sim}{\bar{G}} = \begin{bmatrix} 2 & -1 & -1 & 0 \\ -1 & 2 & -1 & 0 \\ -1 & -1 & 2 & 0 \\ 0 & 0 & 0 & 6 \end{bmatrix} \tag{7.68}$$

Substituing (7.64) into (7.67) and expanding, results in;

$$2\sigma_{e(i)}^2 = \underset{\sim}{\bar{\tau}}^T \underset{\sim}{\bar{G}}\, \underset{\sim}{\bar{\tau}} + \left(\frac{3\Delta e_i^p}{2\sigma_{e(i-1)}}\right)^2 \underset{\sim}{\tau'^T_{i-1}}\, \underset{\sim}{E}\, \underset{\sim}{\bar{G}}\, \underset{\sim}{E}\, \underset{\sim}{\tau'_{i-1}} - 2\left(\frac{3\Delta e_i^p}{2\sigma_{e(i-1)}}\right) \underset{\sim}{\bar{\tau}}^T \underset{\sim}{\bar{G}}\, \underset{\sim}{E}\, \underset{\sim}{\tau'_{i-1}} \tag{7.69}$$

In addition to the above, we have the expression;

$$\sigma_{e(i)} = \sigma_{e(i-1)} + H\Delta e_i^p \tag{7.70}$$

from the effective stress-effective plastic strain curve (Appendix E, Figure E.1). This furnishes the additional equation;

$$2\sigma_{e(i)}^2 = 2\sigma_{e(i-1)}^2 + 4H\Delta e_i^p \sigma_{e(i-1)} + 2\left(H\Delta e_i^p\right)^2 \tag{7.71}$$

Equating the right hand sides of (7.71) and (7.69) results in the quadratic;

$$A\,(\Delta e_i^P)^2 + B\,(\Delta e_i^P) + C = 0 \qquad (7.72)$$

where;

$$A = \left(\frac{3}{2\sigma_{e(i-1)}}\right)^2 \left(\underset{\sim}{\tau}'^{T}_{i-1}\,\underset{\sim}{E}\,\underset{\sim}{G}\,\underset{\sim}{E}\,\underset{\sim}{\tau}'_{i-1}\right) - 2H^2 \qquad (7.73a)$$

$$B = -\left[2\left(\frac{3}{2\sigma_{e(i-1)}}\right)\underset{\sim}{\bar{\tau}}^{T}\underset{\sim}{\bar{G}}\,\underset{\sim}{E}\,\underset{\sim}{\tau}'_{i-1} + 4H\sigma_{e(i-1)}\right] \qquad (7.73b)$$

$$C = \underset{\sim}{\bar{\tau}}^{T}\underset{\sim}{\bar{G}}\,\underset{\sim}{\bar{\tau}} - 2\sigma^2_{e(i-1)} \qquad (7.73c)$$

Hence

$$\underset{\sim}{D}_i^P = \frac{3}{2\sigma_{e(i-1)}}\left(\frac{-B \pm \sqrt{B^2-4AC}}{2A}\right)\underset{\sim}{\tau}_{i-1} \qquad (7.74)$$

The choice of root in equation (7.74) may be discussed in terms of Figure 7.4 below. Point i' represents the effective stress at time t_i if the material behavior were elastic during the time interval from t_{i-1} to t_i. This corresponds to the stress defined by $\bar{\tau}$ in (7.63). The quadratic curve for Δe_i^P passes through i' and intersects the line of effective stress versus effective plastic strain at two points. Since Δe_i^P must be positive and real, the choice of root is simple when one root is positive and the other negative. When both roots are positive, consideration is given to the fact that Δe_i^P is small for small intervals. Hence for this case the smaller of the two positive roots applies.

When both roots are negative or complex, the implication is that the interval over which Δe_i^P is expected to be constant, is too long. Hence, at such times, the interval is further subdivided until positive real values of Δe_i^P are obtained.

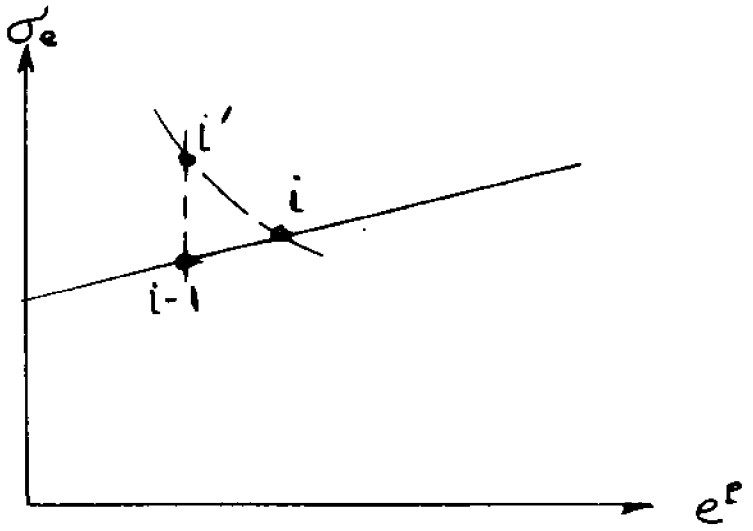

Figure 7.4

CHAPTER VIII

Results of the Finite Element Code

8.1 Effects of Rigid Body Rotation on the Stress Field in an Element

It is recalled in an earlier discussion that consideration of frame indifference in constitutive equations resulted in the definition of a stress rate in which an observer, moving in rigid motion with a particle, would see distortion of the local medium if he observed a change in stress referreed to his moving reference frame. Logically, if such an observer sees no change in stress, then a fixed observer would see only a rotation of a constant stress field when a particle undergoes rigid body rotation.

Since elements in the ensueing problems undergo large rotations as well as deformations, it is of interest to check this point of logic and the accuracy of its confirmation. Hence, a single finite element, shown in Fig. 8.0 below was subjected to two cases of rigid body rotation; one in which a null stress acted, and one in which a constant, normal stress acted in the R direction.

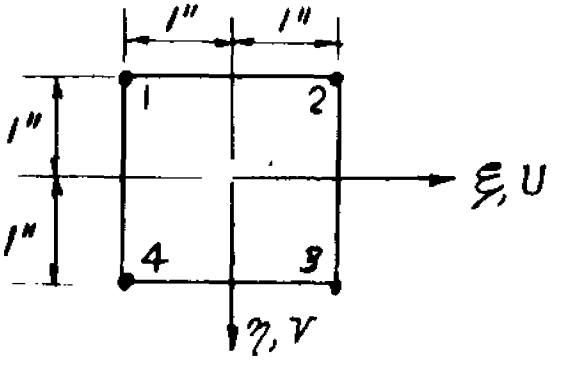

FIGURE 8.0

The element underwent a total rotation of $\pi/6$ in increments of $\pi/6000$. For the initially null stress field acting on the element, the final stress field was also null; thus indicating that no stresses or strains were numerically induced by the finite element program during rigid body rotation. For the initial stress of $\tau_{rr}=10^5$ psi acting on the element, with all other stress components zero, the following table was prepared;

Final Stress in Square Element Undergoing a Total Rigid Body Rotation of $\pi/6$

Stress Component	Predicted Stress (psi)	Computed Stress (psi)
τ_{rr}	$3/4 \times 10^5$	74998.40
$\tau_{\theta\theta}$	0	0
τ_{zz}	$1/4 \times 10^5$	24983.31
τ_{rz}	$\sqrt{3}/4 \times 10^5$	43318.32

The node displacements for the above rotation are given below;

Node	R-Displacement (inches)	Z-Displacement (inches)
1	0.6339426	-0.3660069
2	0.3660069	0.6339426
3	-0.6339426	0.3660069
4	-0.3660069	-0.6339426

The logic has thus been checked with acceptable accuracy.

8.2 Solid Cylindrical Bar

In order to test the validity of the finite element code for an elastic-plastic, linear strain hardening material, results were obtained for the cylindrical bar shown in Figure 8.4a. The bar is shown laterally restrained to assure one dimensional wave propagation along its axis.

Figure 8.4b is a plot of the distribution of longitudinal displacements, velocities and stresses along the axis of the bar at time $t = 3.67 \times 10^{-5}$ seconds after the application of the uniform stepped pressure pulse at the left end of the bar. The theoretical values for these distributions (as obtained in Appendix H) are shown for comparison. While the theoretical analysis reveals clear, sharp fronts for the elastic and plastic waves, the computer code indicates a 'smearing' or averaging effect at the theoretical wave fronts for both stress and velocity. Furthermore, stress and velocity as obtained by the computer code, oscillate about the true, theoretical

values of these quantities, with the amplitudes decreasing as points fall further behind the wave front. (Shown moving towards the right in Figure 8.4b). Similar phenomena have been known to occur in finite difference methods.

8.3 Spherical Shell

As a further test of the finite element codes' validity for large deformations, as well as for elastic-plastic material, numerical results were obtained for the spherical shell shown in Figure 8.5a, subjected to an internal triangular pressure pulse. This problem was first investigated by Baker[25] using deformation theory on elastic-plastic materials with linear strain hardening. Baker also included the effects of shell thinning and the variation of shell radius by assuming material incompressibility.

Figure 8.5b shows the radial displacement of the shell as a function of time for materials with two different strain hardenings. These correspond to slopes of the uniaxial stress-strain curves of S = 0 and S = 22.5 x 10^6 psi, in the plastic yield region. The super-position of Baker's results on the finite

element code results, indicate excellent agreement through the entire range of deformation histories considered.

Some idea regarding how large the resulting strains are is seen by comparing the second order terms in;

$$\epsilon_{\theta\theta} = \frac{U_R}{R_o} + \tfrac{1}{2}\left(\frac{U_R}{R_o}\right)^2$$

with the total resulting strain. At a maximum radial displacement of 38.7×10^{-3} inches, the lagrangian circumferential strain is

$$\epsilon_{\theta\theta} = 2583 \times 10^{-6}$$

and the second order term is;

$$\tfrac{1}{2}\left(U_R/R_o\right)^2 = 0.00128\,\epsilon_{\theta\theta}$$

Thus, comparison with Baker's solution, though excellent, falls somewhat short of validating the computer code for 'large' deformations.

3.4 Circular Plate with Simple Supports

The problem, as defined in Figure 8.6a, consists of a circular plate of 4" radius and 0.241" thickness subjected to a uniformly distributed impulse. The

material properties, etc., are as indicated and correspond to experimental results obtained earlier by Florence[26].

Wang[27] considered a circular plate consisting of a rigid plastic material obeying the Tresca yield criterion and its associated flow laws. In this treatment, based on the theories of Hopkins and Prager[7], the plate is regarded as rigid if both the radial moment, M, and the circumferential moment, N, are below the critical moment, Mo, where;

$$Mo = \sigma_o^2 \, h^2$$

σ_o is the yield stress in simple tension and h is twice the plate thickness.

Further, if M = N = Mo, then the rate of radial curvature

$$\kappa = - \frac{\partial^3 w}{\partial t \, \partial r^2}$$

and the rate of circumferential curvature

$$\lambda = \frac{1}{r} \quad \frac{\partial^2 w}{\partial t \, \partial r}$$

are non-negative. On the other hand, if N = Mo and $0<M<Mo$, κ vanishes while λ is non-negative.

The presumed mechanism for deformation is then considered to be as follows:

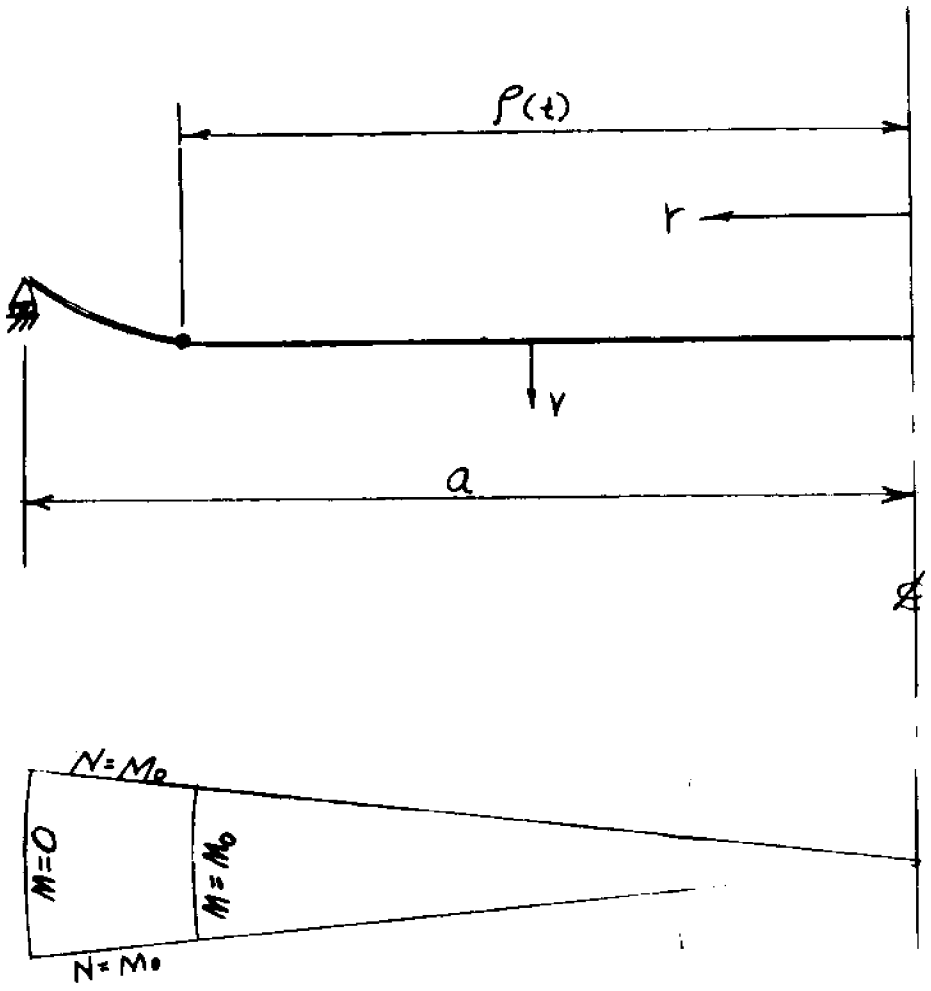

Figure 8.1

Immediately following the application of the impulse to the plate, a hinge circle forms at the supports and starts to move radially inward towards the plate center. At the hinge circle, shown in Figure 8.1 as located at ρ(t), N = Mo and M = Mo. The region inside the hinge

circle moves with constant velocity;

$$V = \frac{I}{m}$$

where 'I' and 'm' are the impulse and mass per unit of plate area respectively. Outside the hinge circle, the plate elements undergo rigid body rotations given by;

$$\omega = \frac{V}{a(1-\beta)}$$

Furthermore, the circumferential moment N is equal to Mo at the simple support while the radial moment M increases from zero at the support to Mo at the hinge circle.

After the hinge circle reaches the center of the plate, the entire elemental sector is assumed to rotate about the support as a rigid body. The terminal deflection is found by Wang to be;

$$W = \frac{I^2 a^2}{24 m M_o} (1 - r/a) (3 + 2 r/a + (r/a)^2)$$

and the central deflection is given by (at r = 0)

$$\delta = \frac{I^2 a^2}{8 m M_o}$$

Florence's[26] experiments on aluminum and steel plate subjected to blast loads indicated that Wang's analysis predicted excessive permanent plate deflections when the ratios of central plate deflection to thickness

were large. He reasoned that this was due to the effects of membrane stresses which were ignored in Wang's analysis.

Jones[55] considered the same problem as Wang, but used Reissner's[61] equilibrium expressions for the finite deflection of a circular plate with membrane stresses. The mechanism for deformation is assumed to consist of two stages; an initial stage identical to the mechanism described above, in which bending moments are dominant, and a second stage in which membrane stresses predominate.

The results of the computer code for data corresponding to Florence's experiment #7 for steel are shown in Figure 7.6b along with Florence's experimental and Wang's analytic results. Figure 8.6c indicate displacement profiles for the plate at various stages of its deformation history.

The finite element grid, consisting of fourteen quadrilateral elements is relatively coarse for this problem in that it does not enable one to obtain a variation of stress and strain through the plate thickness. Nevertheless, it represents an initial attempt at finding solutions for this problem by the

finite element code prior to undertaking the more detailed and longer solution on a faster and larger computer. The difference of approximately 19% based on experimental results indicated in Figure 8.6b, between the finite element and experimental results, may in large part be due to the difference between ideally assumed and actual experimental conditions. For the solutions obtained by the finite element code, an impulse was considered to be uniformly distributed over the plate area and was assumed to occur over a time span that approached zero.

8.5 The Impulsive Expansion of a Cylindrical Shell with Ring Reinforcements.

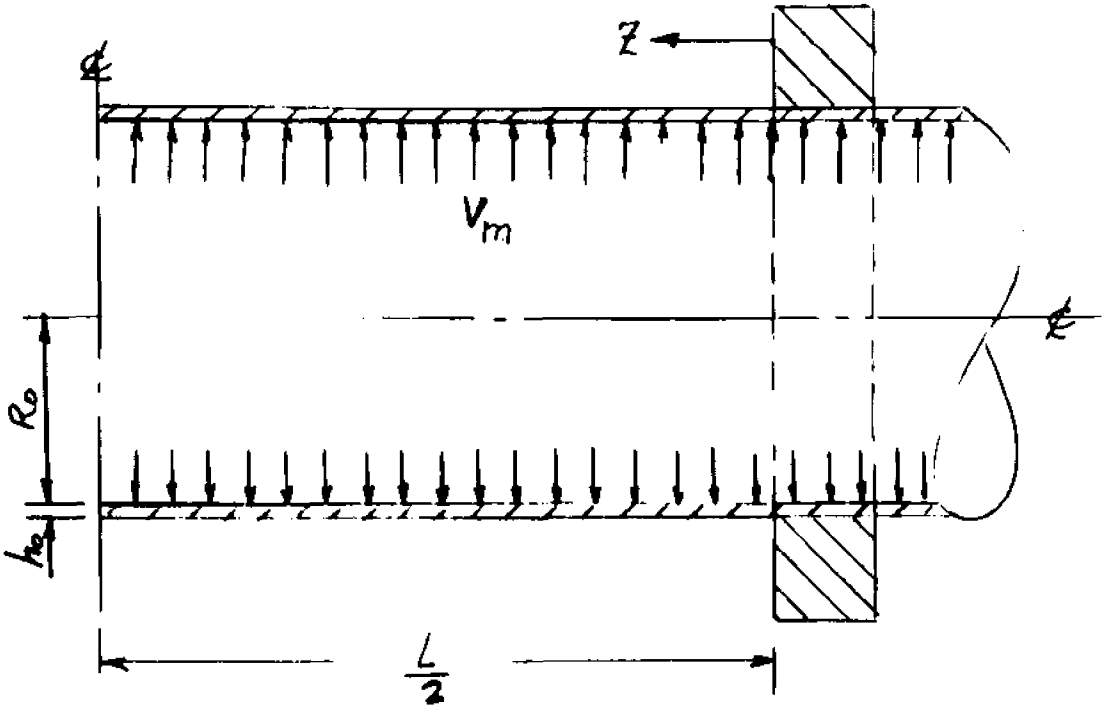

Figure 8.2

The problem illustrated in Figures 8.2 and 8.7a, was treated kinematically by Masaki[33]. In this analysis, a perfectly rigid plastic material, obeying the Mises flow rule was considered.

The cylinder of initial radius R_o and initial thickness h_o is subjected to a uniform, radial impulse I, which results in the uniform, initial velocity, V_m. The shell thickness, h_o, is taken as constant throughout the deformation history and is regarded as sufficiently thin to permit neglecting the effect of longitudinal bending on the final solution.

The deformation mechanism, as assumed by Masaki, may be described as follows: (See Figure 8.3 below).

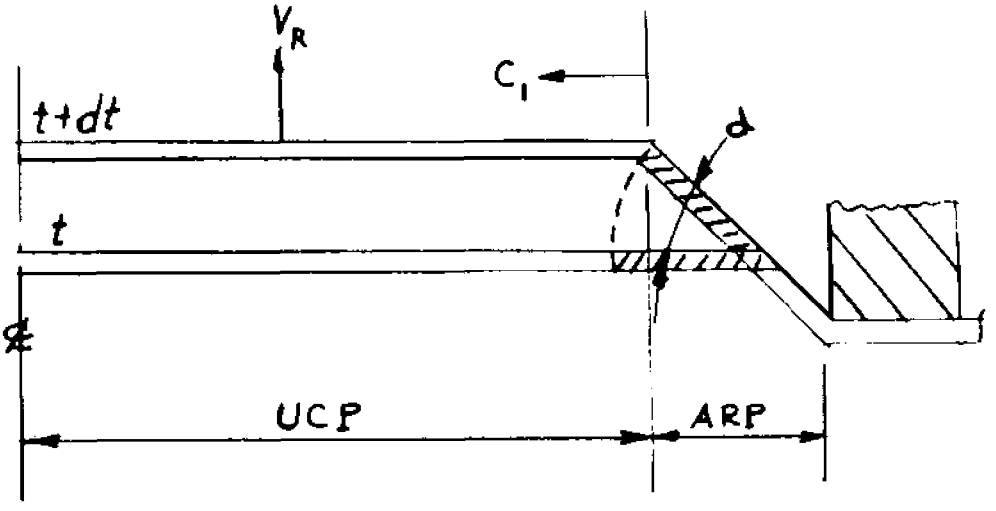

Figure 8.3

Two 'bending' waves, starting at the ring reinforcements, move axially towards the cylinder center line at a velocity C_1. As the wave advances into the undisturbed central portion, (the region marked 'UCP') an initially horizontal element, at time 't', tilts by the angle 'α' into a conical frustum, at time 't + dt'. As this occurs, the horizontal element in the undisturbed central portion undergoes a uniform elongation. The axially rotated portion of the shell already swept over by the 'bending' wave (the region marked 'ARP') comes to rest while the uniform central portion has a uniform radial velocity V_r.

The time'te' at which the shell deformation is considered to end is then distinguished by two cases; i.e.,

Case 1: The 'bending' wave reaches the centerline of the cylinder before the radial motion of the uniform central portion comes to rest.

Case 2: The uniform central portion comes to rest before the 'bending' wave reaches the cylinder centerline.

Then the terminal times of deformation are:

<u>Case 1:</u> $te_1 = \frac{L}{2C_1}$

<u>Case 2:</u> $te_2 = \frac{R_o}{2C_2} \; Ln\left(\frac{C_2+V_m}{C_2-V_m}\right)$

<u>Where</u>:

$$C_1 = \sqrt{\frac{T_{zz}}{\rho}}$$

$$C_2 = \sqrt{\frac{T_{\theta\theta}}{\rho}}$$

The finite element results presented herein are based on a copper cylinder of inside radius R_o = 15 mm and initial thickness h_o = 1 mm. The clear distance between the rigid reinforcing rings is L = 40 mm and the initial, uniformly distributed radial velocity of the shell wall outwardly is V_m = 4,740 "/sec. The material properties of the copper material are given in Figure 8.7a.

Figure 8.7b shows the displacement history of the median surface of the cylinder at the plane of symmetry bisecting the clear distance between the two reinforcing rings. Close agreement is shown with Masaki's results during the first half of the deformation history. However, during the second half, the finite element code

predicts a more rapid rise in central deflection. The maximum deflection of 0.2114" occurs 76 x 10^{-6} seconds after the application of the initial velocity. This compares with a time of 90.5 x 10^{-6} sec and a radial displacement of 0.201" as found by Masaki. The maximum circumferential strain recorded at the center of the cylinder is:

$$\epsilon_{\theta\theta} = 404,980 \times 10^{-6}$$

for which the second order term may be calculated as:

$$\frac{1}{2}\left(\frac{U_R}{R_o}\right)^2 = 0.16\,\epsilon_{\theta\theta}$$

The finite element results shown in Figure 8.7b indicate that the central deflection drops slightly after it reaches its peak value. This drop is accompanied by elastic unloading that occurs throughout the cylinder.

Figure 8.7c shows the radial displacement of the inner surface of the tube at various stages of its deformation history. During the early stages, the uniform central portion of the cylinder appears to be in a state of plane strain while the radial velocities along the cylinder axis are approximately uniform. At later stages, an 'envelope' of permanent radial

displacement develops and moves axially inward towards the cylinder center.

Figures 8.7d and 8.7e show the progression of the transverse shear wave and the effective plastic strain with time. Effective plastic strains are averaged over the volume of each element and are plotted at points along the abscissa that correspond to element centers. Shear stresses are plotted at node points and represent the average of the averaged stresses of elements having the node point in common. Since effective plastic strain in an element increases with the plastic work done on the element, it may be seen that the permanent radial displacement of the cylinder occurs just after the plastic work increment is zero. The velocity of the discontinuity representing the null increment of plastic work may therefore be interpreted as the 'bending' velocity C_1, in reference[33].

Values for τ_{zz} and $\tau_{\theta\theta}$ may be obtained approximately from reference[33], equations (12), (43), (44) and (45). The membrane stresses are presumed to occur in the undisturbed central portion of the tube during active deformation and are;

$$\tau_{zz} \approx 16,000 \text{ psi}$$
$$\tau_{\theta\theta} \approx 33,000 \text{ psi}$$

Typical values of these stresses, obtained through the finite element code, are shown plotted along the tube axis in Figures 7.7f,g for various times after the initial radial impulse.

8.6 Flat Circular Plate Impinging on a Rigid Parabolic Die

The motivation for this problem may be found in the field of high energy rate forming. When a flat circular plate recieves an impulsive load and impinges upon a curved die, it is of interest to know the extent to which the die shape will be followed. Further, if the plate acts as a component of a larger piece of equipment, design considerations make it of interest to know how much thinning and distortion occur throughout the plate.

In the problem presented, a flat circular plate 1/4" thick by 5" radius (Figure 8.8a) is given an initial vertical velocity of 4000 "/sec. and allowed to impinge on a smooth circular, parabolic die whose contour is given by $Z=0.1R^2$. As mechanical means are frequently used to 'hold down' a plate during forming, it will be assumed in this problem that the center point of the plate is constrained to be in contact with the die throughout its deformation history.

At the exact instant that a nodal mass of the finite element grid contacts the die surface, the mass velocity normal to the die surface becomes zero. At the same time, a reactive force normal to the surface at this point causes a change in the subsequent direction of motion to occur in the mass. Solutions of the equations of motion may be carried out without explicitly solving for these reactions. However, displacement boundary conditions must be known at these points of contact along the die. Since no other constraint is imposed on the mass in contact with the die, the mass may have velocity components tangential to and normally outward from the die surface subsequent to its initial contact with the die.

Figures 8.8b,c show the deformation of the bottom surface of the plate in historical sequence. It is noted that in the early stages of deformation, (prior to 209.862 μ sec. past the intial impulse) initial contact is maintained. In an intermediate stage (in the interval from 209.862 μ sec. to 507.537 μ sec.) the vertical motion is upward in the central region of the plate and downward in the outer region. Contact is maintained over a relatively small region of the die during this time. In the final stages of deformation, (from 507.537 μ sec. onward) all movement is in an upward direction until the entire plate motion is reduced to purely elastic

oscilations. The permanent plate shape at a time 857.598 μ sec. from the initial impulse is then seen to be a dimpled bowl shaped plate whose contour differs from that of the die it impinged upon.

Figure 8.8d represents a plot of the grid distortion at the time of final plate deformation. Note that plate thinning occurs in elements 1 through 11, i.e. in those elements where contact occurred between the plate and the die. Maximum thinning occurs in element 1 (as seen in Table 8.1). The maximum distortion of any element is also seen to occur in element 1 which has been transformed from a flat circular disk to a 45° $\pm$ cone. The severity of this distortion is in part due to the rigidity of the quadrilateral element itself but is mainly due to the proximity of the local constraint on node 1.

Average Thinning of Elements in Figure 8.8d

Element Number	Plate Thinning (%)
1	32.
2	8.
3	12.
4	8.
5	8.
6	12.
7	12.
8	12.
9	12.
10	8.
11	4.
12	0.
13	0.
14	0.
15	0.
16	0.

[Note: % thinning $= \Delta h/h \times 10^2$, where h is the initial plate thickness]

Table 8.1

8.7 Impact of an Ogive Nosed Projectile on a Smooth, Flat Rigid Surface

Up to this point, the problems in large deformations under impulsive loadings have been solved for plates and shells with regular geometries. By solving this last problem it is demonstrated the the present finite element program has the capability for solutions in solids of revolution having irregular geometry.

The projectile shown in Figure 8.9a with the material properties of mild steel, is given an initial velocity of 3000 inches/sec. in a direction parallel to its longitudinal axis. At this velocity, it impinges upon a flat, rigid surface normal to its direction of travel and represented by the plane Z=0. The problem then consists of finding the maximum and permanent distortion of the missile after impact. The nose section approximates an ellipse having semi axes of 2" and 1" in the axial and radial directions respectively. Since solutions to ogive nosed impact problems have not appeared in the open literature,this represents the first solution of its kind. As in the earlier impact problem, provision has been made for possible 'bouncing' of nodal masses from the rigid surface.

Since maximum deformation may be expected in the nose section, the finite element mesh has been refined in this region.

Results have been plotted for two conditions; i.e. maximum overall deformation and permanent deformation Maximum deformation occurs shortly after all points on the projectile have achieved an upward velocity. These results are shown in Figures 8.9b and 8.9c. In these and in subsequent figures, the dashed lines represent the initial, undistorted configurations, the solid lines represent the deformed configuration and the indicated time is measured from the instant of impact. At the time indicated, maximum strain occurs at mode 41 (tip) and is given as;

axial strain	$\epsilon_{zz} = -24.0\%$
radial strain	$\epsilon_{rr} = 19.3\%$
circumferential strain	$\epsilon_{\theta\theta} = 21.0\%$

The slight inconsistency between radial and circumferential strains is due to the manner in which strain is averaged for each node; i.e. the nodal strain is the average of the strains in the elements having the node in common. This averaging procedure is only used for output purposes and has no effect on computations.

The distortions shown in Figure 8.9d and e indicate the deformation of the projectile shortly after rebound (velocity of node 41 becomes negative). Since the elastic

stresses are relatively small, this configuration represents the permanent distortion of the projectile.

Table 8.2 lists the effective plastic strain averaged over each element volume. This table indicates the extent to which yielding occurred throughout the projectile. As expected, maximum yielding occurs in element 26 (tip) while elements 1 and 2 display no yielding at all.

Figure 8.9f shows the variation of effective plastic strain along the projectile axis at various times during its deformation history. The times corresponding to maximum deformation and the condition shortly after rebound of the projectile are also included. It is seen that the plastic work increment is zero at the rear of the missile long before it is zero at the nose section.

8.8 Conclusions

In conclusion, the validity of the finite element code for impulsively loaded elastic-plastic media undergoing large deformation has been verified by comparisons with several known results of a diverse nature. These include the results for the solid cylindrical bar, the thin spherical shell, the simply supported flat circular plate and the ring reinforced cylindrical tube. The results shown for the flat circular plate and the ogive nosed projectile impinging on rigid surfaces were not based on any previously known work. Hence their validity must be inferred from those of the previous comparisons. However, their inclusion represents potential applications to impulsive die forming and missile deformation not previously investigated.

One of the main advantages of using the finite element method is that bodies with odd surface geometries may be conveniently dealt with in any computational procedure. Bodies undergoing severe finite deformations will develop such odd geometries as the computation proceeds, even when the initial geometries are simple. Hence a development of a finite element method to deal with dynamic problems in large deformations is clearly necessary if solutions are

required for general geometric configurations. Improvements may always be made in numerical procedures that will reduce core storage and increase computational speed. This is certainly true for the present case. As this work is complex in concept, programming requirements are equally complex and the time to run through each integration step is large. Hence future developments should be directed towards reducing the total number of integration steps required to bring a problem to a conclusion.

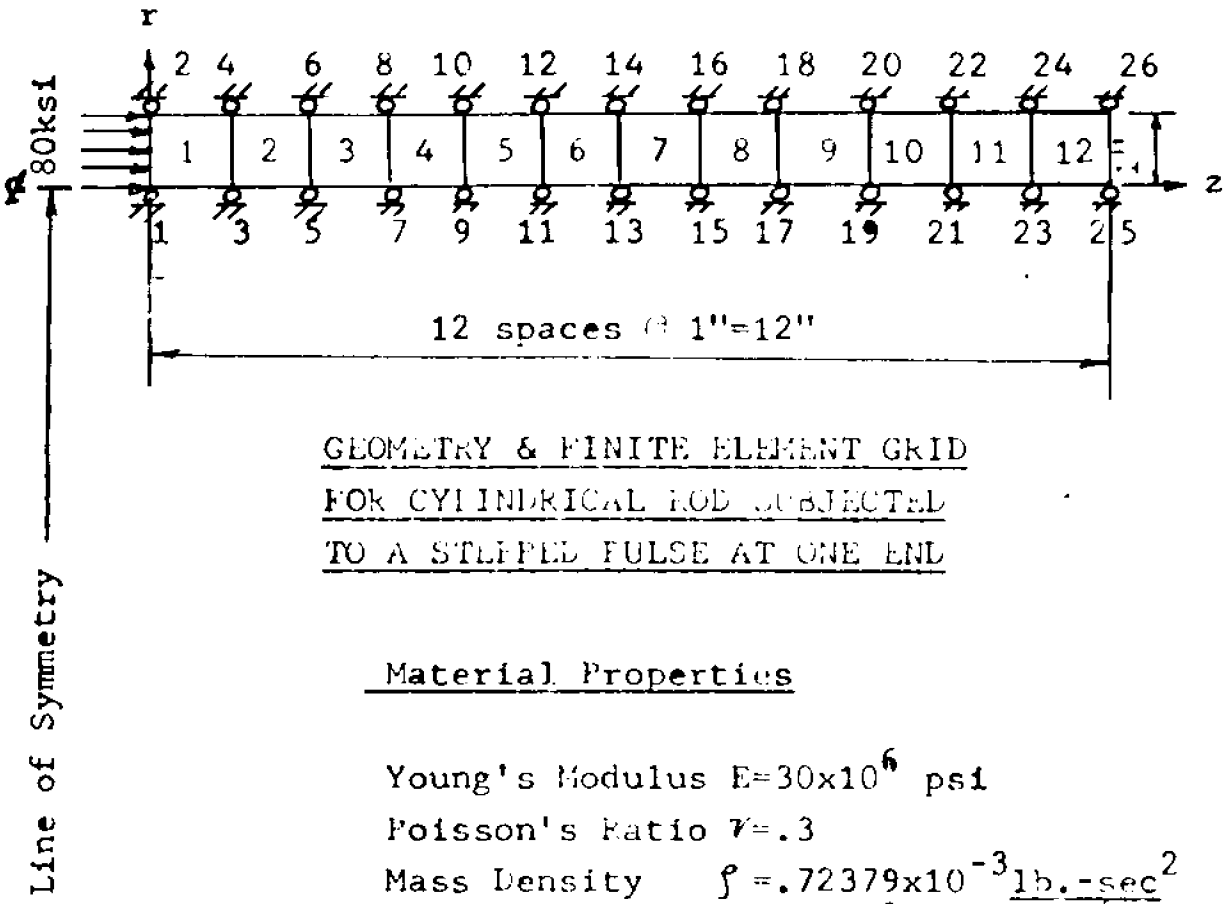

GEOMETRY & FINITE ELEMENT GRID FOR CYLINDRICAL ROD SUBJECTED TO A STEPPED PULSE AT ONE END

Material Properties

Young's Modulus $E=30\times10^{6}$ psi

Poisson's Ratio $\nu=.3$

Mass Density $\rho=.72379\times10^{-3}\frac{\text{lb.-sec}^2}{\text{in.}^4}$

Yield Stress $\sigma_Y=30\times10^{3}$psi

Slope of Eff. Stress-Eff. Plast. Strain Line: $h=15\times10^{6}$psi

FIGURE 8.4a

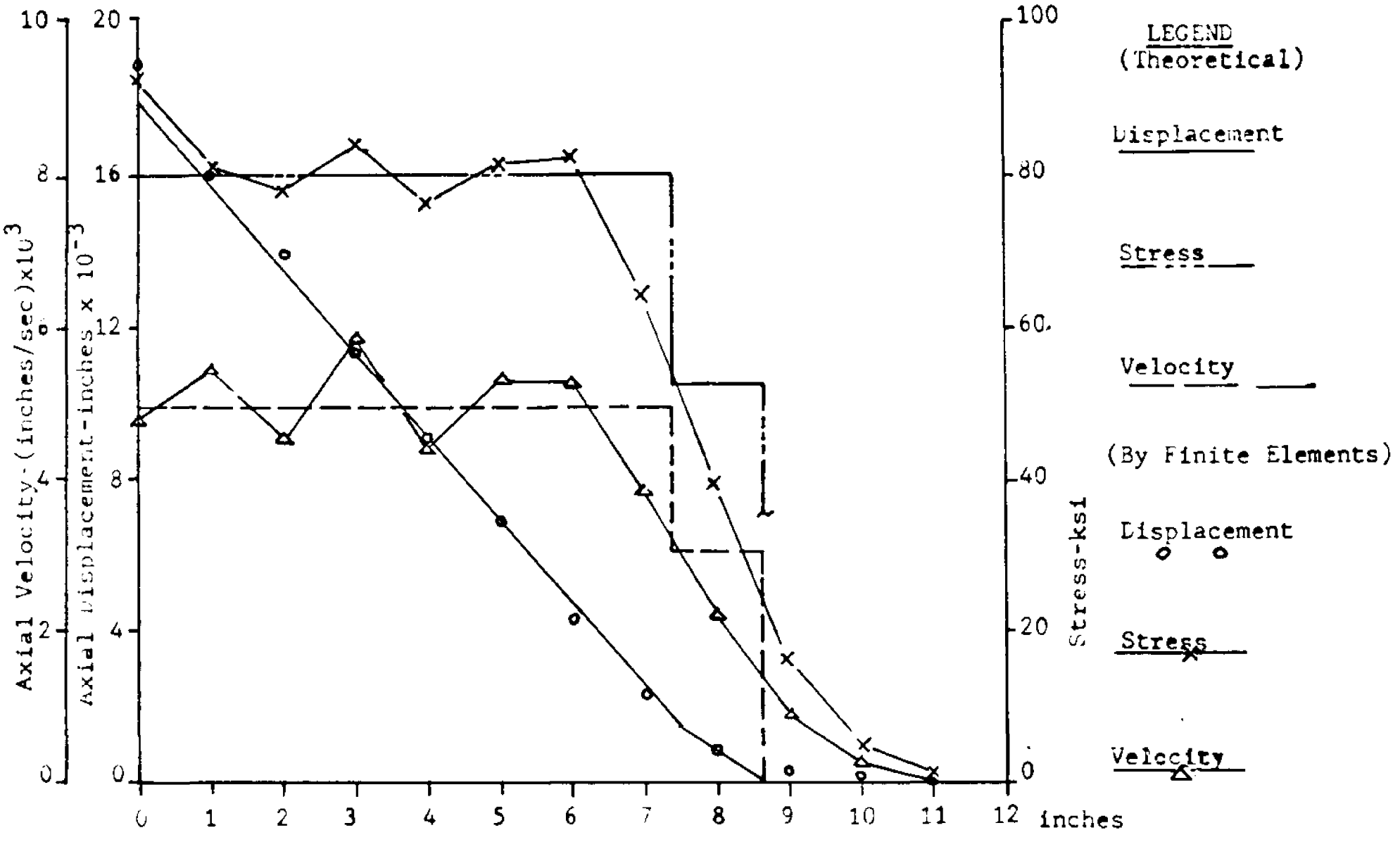

RESPONSE OF A CYLINDRICAL BAR TO AN AXIAL STEP PULSE

FIGURE 3.4b

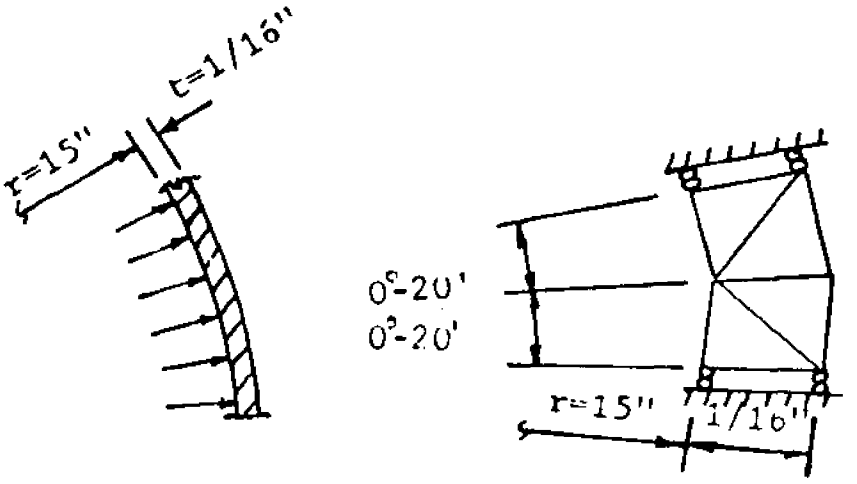

GEOMETRY & FINITE ELEMENT GRID REPRESENTATION FOR SPHERICAL SHELL SUBJECTED TO A RADIAL PRESSURE PULSE

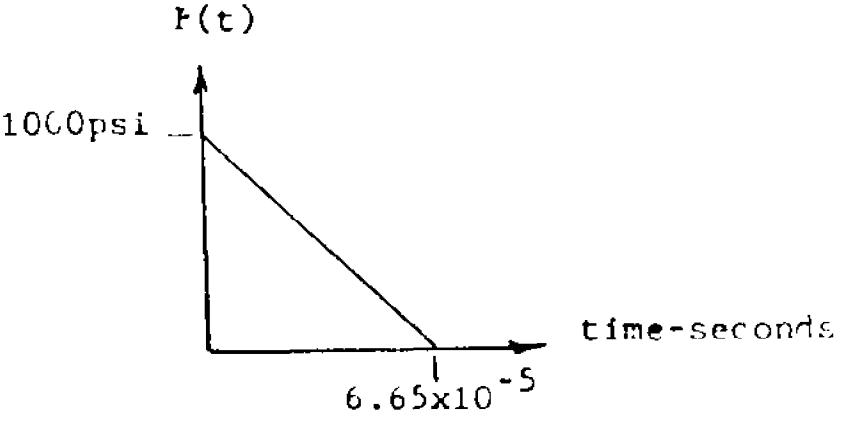

PRESSURE PULSE

Material Properties

Young's Modulus $E=30\times10^{6}$psi

Poisson's Ratio $\nu=.3$

Specific Weight $\rho g=.283$ lb/in^3

Yield stress $\sigma_y=40\times10^{3}$psi

Slope of Plastic Part of Stress Strain Curve: s=0, s=22.5x10^{6}psi

FIGURE 8.5a

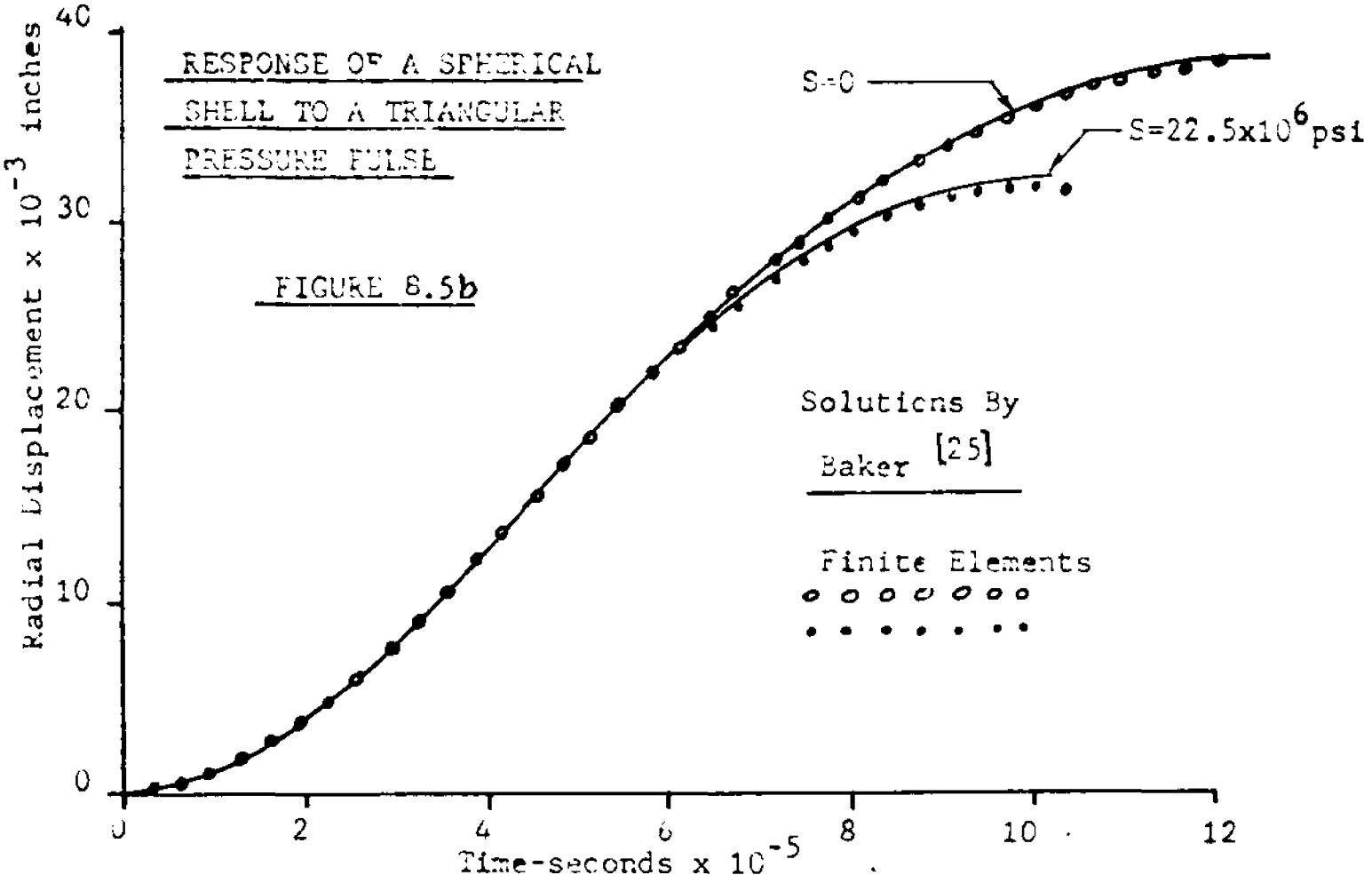
RESPONSE OF A SPHERICAL SHELL TO A TRIANGULAR PRESSURE PULSE
S=0
S=22.5x10^6 psi
Solutions By
Baker [25]
Finite Elements
Radial Displacement x 10^-3 inches
Time-seconds x 10^-5
0
10
20
30
40
2
4
6
8
10
12

FIGURE 8.5b

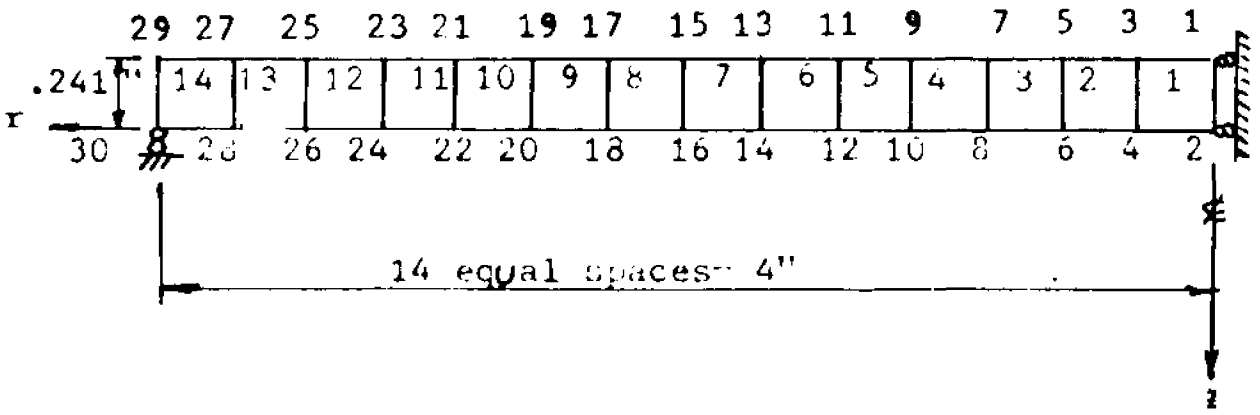

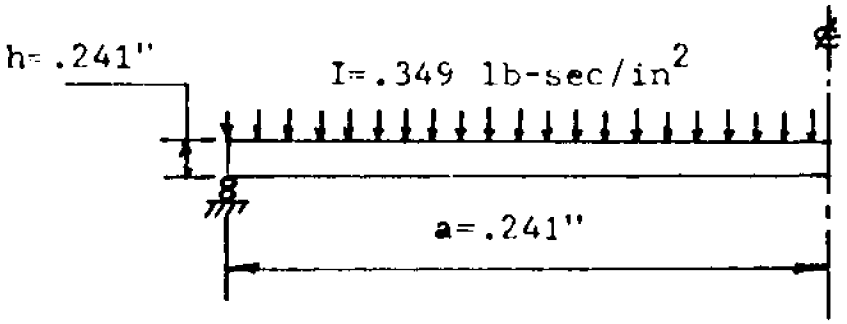

GEOMETRY & FINITE ELEMENT GRID FOR SIMPLY SUPPORTED CIRCULAR PLATE SUBJECTED TO A UNIFORM IMPULSE

Definitions for Fig.7.6b

I=impulse/unit area of plate

$M_o = \sigma_y h_o^2/4$ =fully plastic moment

W=vertical displacement of plate

m=mass density of plate/unit area

Material (steel)

Young's modulus $E = 30 \times 10^6$ psi

Poisson's Ratio $\nu = .3$

Yield Stress $\sigma_y = 79 \times 10^2$ psi

Mass Density $\rho = .732 \times 10^{-3}$ lb-sec^2/in^4

FIGURE 8.6a

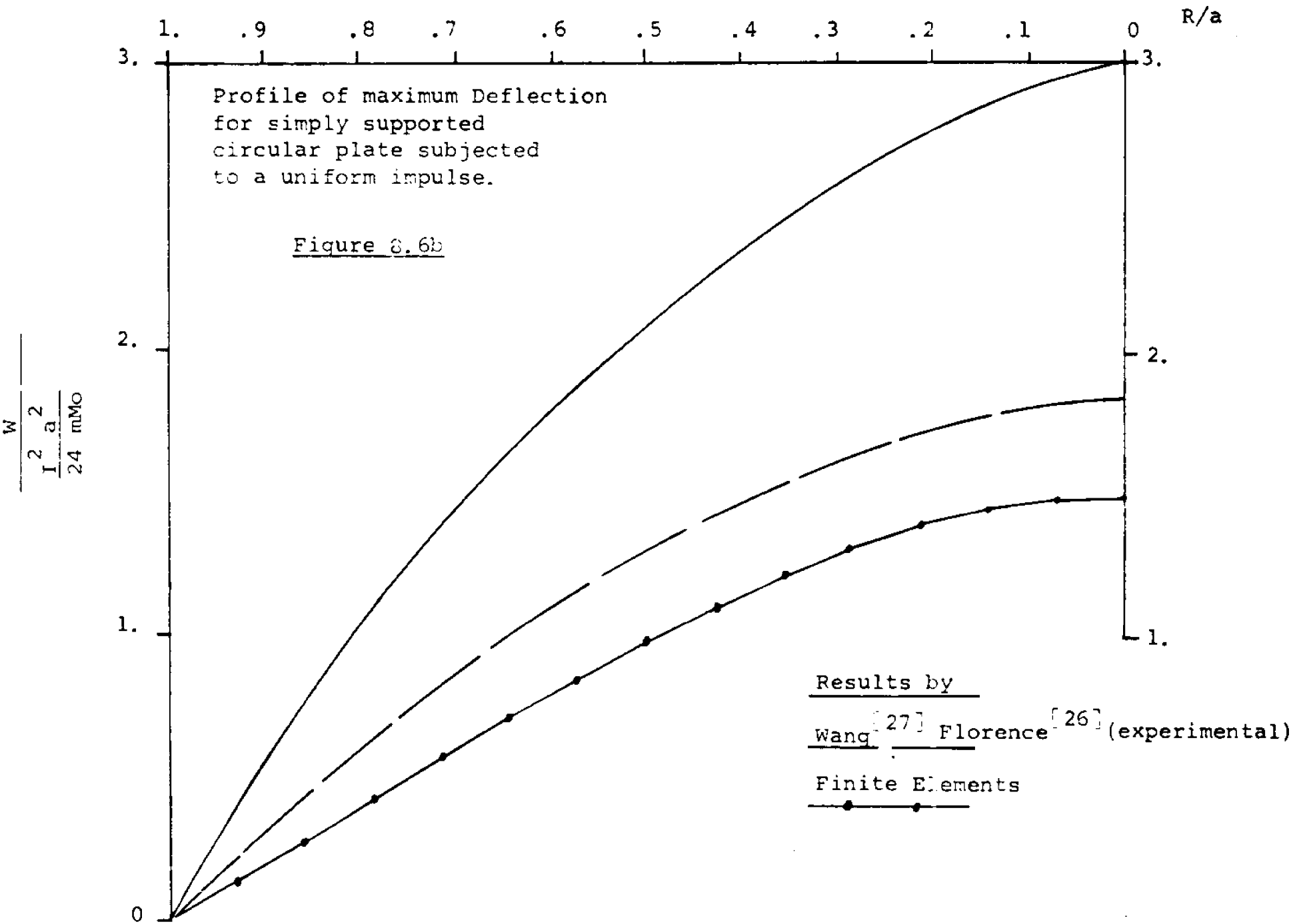
R/a
1.
.9
.8
.7
.6
.5
.4
.3
.2
.1
0
3.
2.
1.
0
$\frac{w}{\frac{I^2 a^2}{24\ mMo}}$
Profile of maximum Deflection
for simply supported
circular plate subjected
to a uniform impulse.
Figure 8.6b
Results by
Wang [27]
Florence [26] (experimental)
Finite Elements

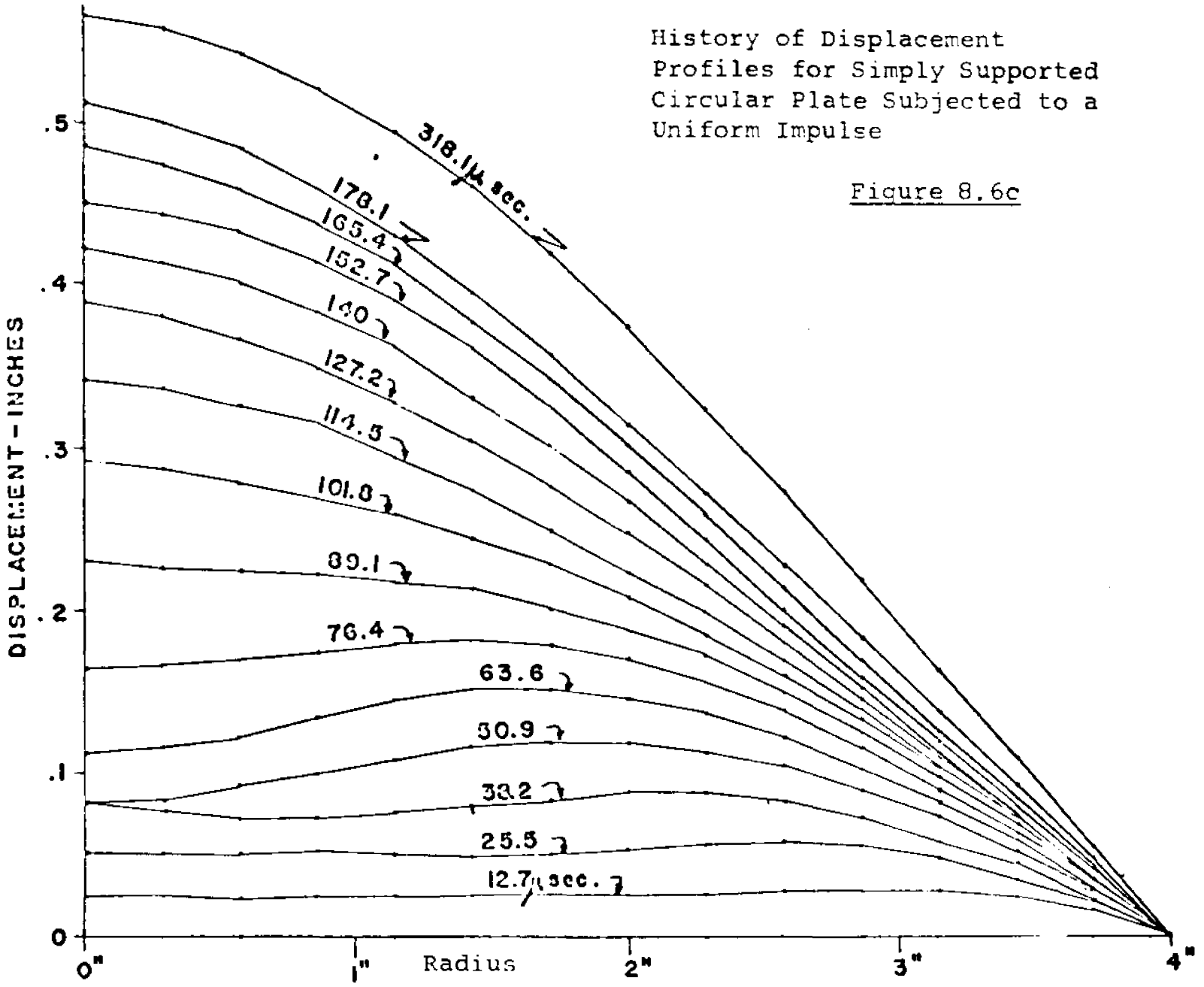

History of Displacement Profiles for Simply Supported Circular Plate Subjected to a Uniform Impulse

Figure 8.6c

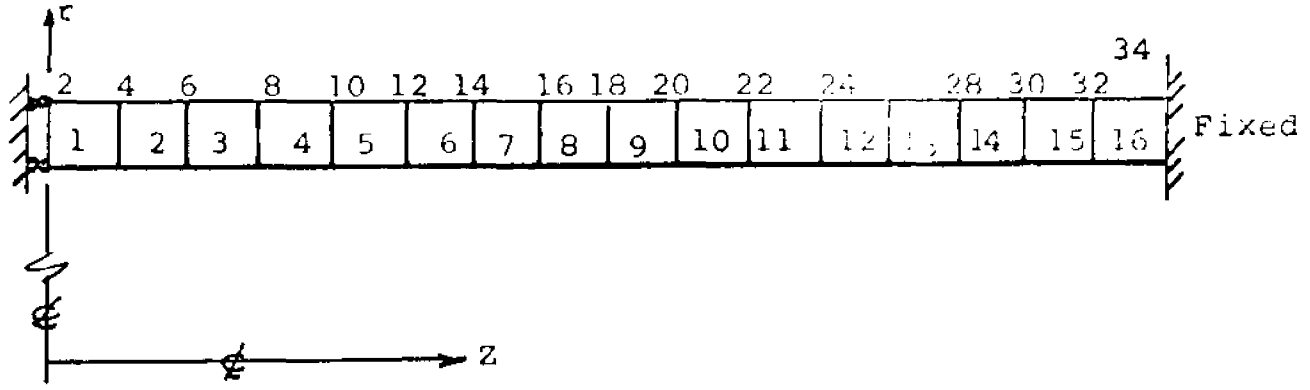

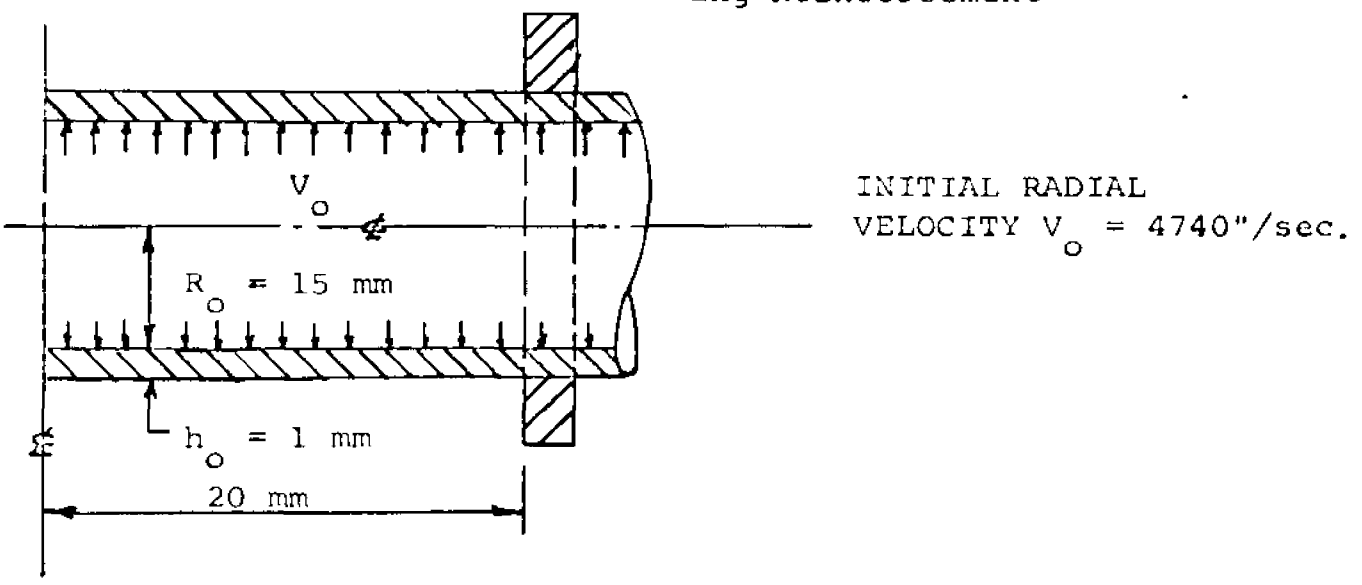

GEOMETRY AND FINITE ELEMENT GRID FOR RING REINFORCED TUBE

Material Properties

Copper

Young's Modulus $E = 16 \times 10^6$ psi

Poisson's Ratio $\nu = 0.3$

Mass Density $\rho = 0.828 \times 10^{-3} \frac{\text{lb - sec}^2}{\text{in}^4}$

Yield Stress $\sigma_y = 28{,}440$ psi

Slope of Eff. Stress Versus Eff. Plastic Strain Curve $H = 0$

Figure 8.7a

History of Radial Displacement
at Centerline for Ring Reinforced
Tube Subjected to Radial Impulse

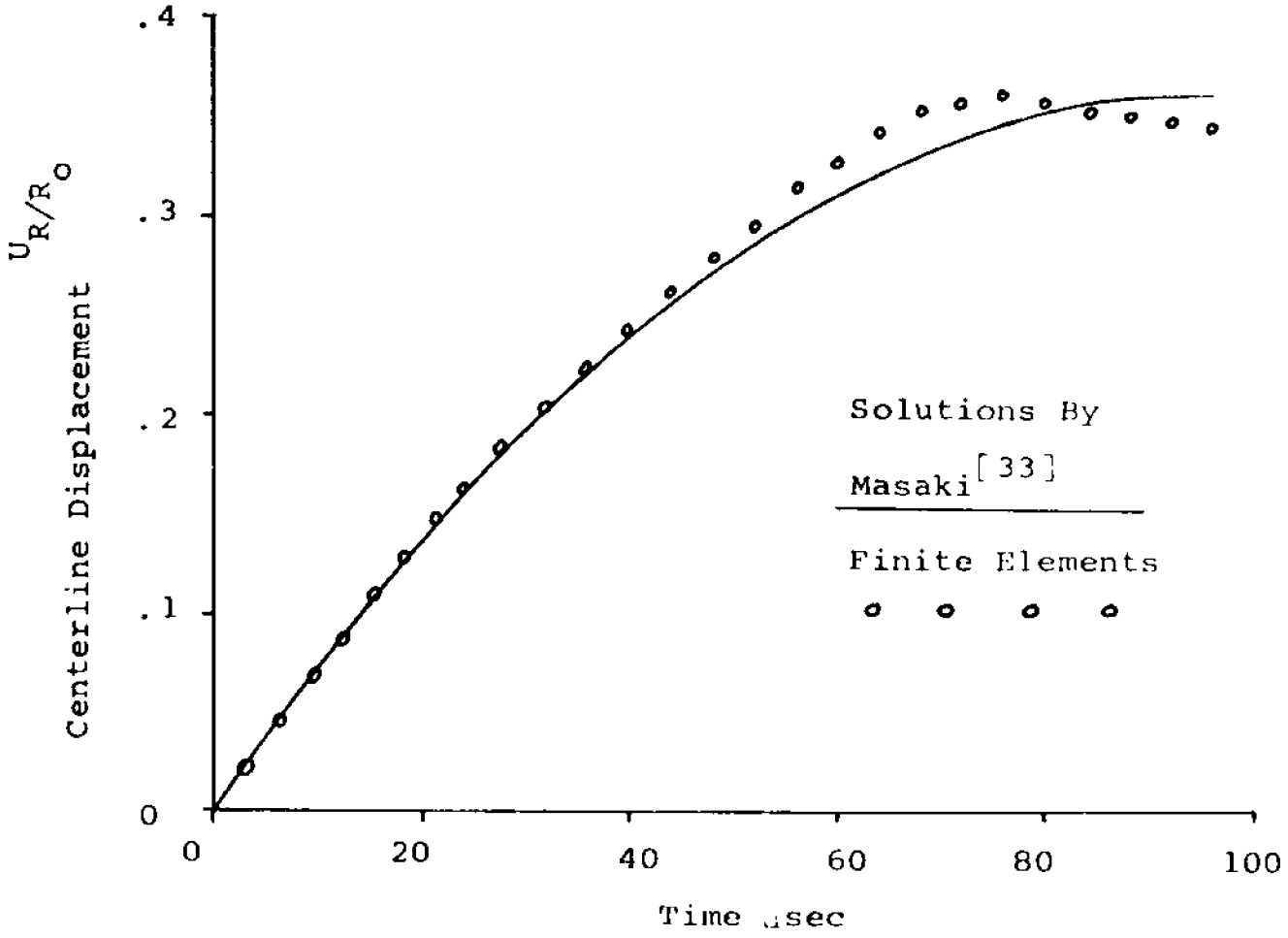

Figure 3.7b

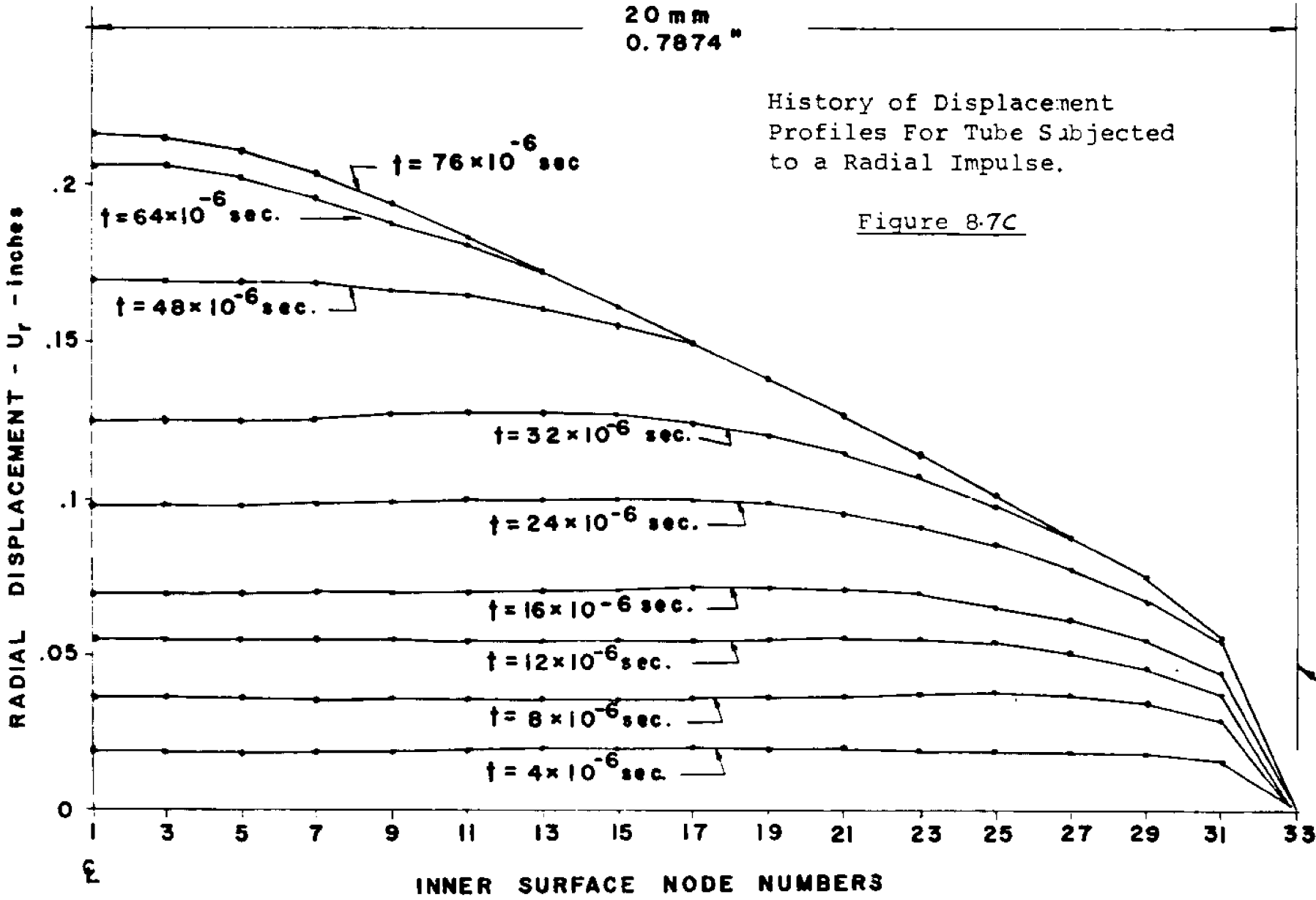

History of Displacement Profiles For Tube Subjected to a Radial Impulse.

Figure 8.7C

History of Effective Plastic Strain and τ_{RZ} for Ring Reinforced Tube Subjected to a Radial Impulse.

Figure 8.7d

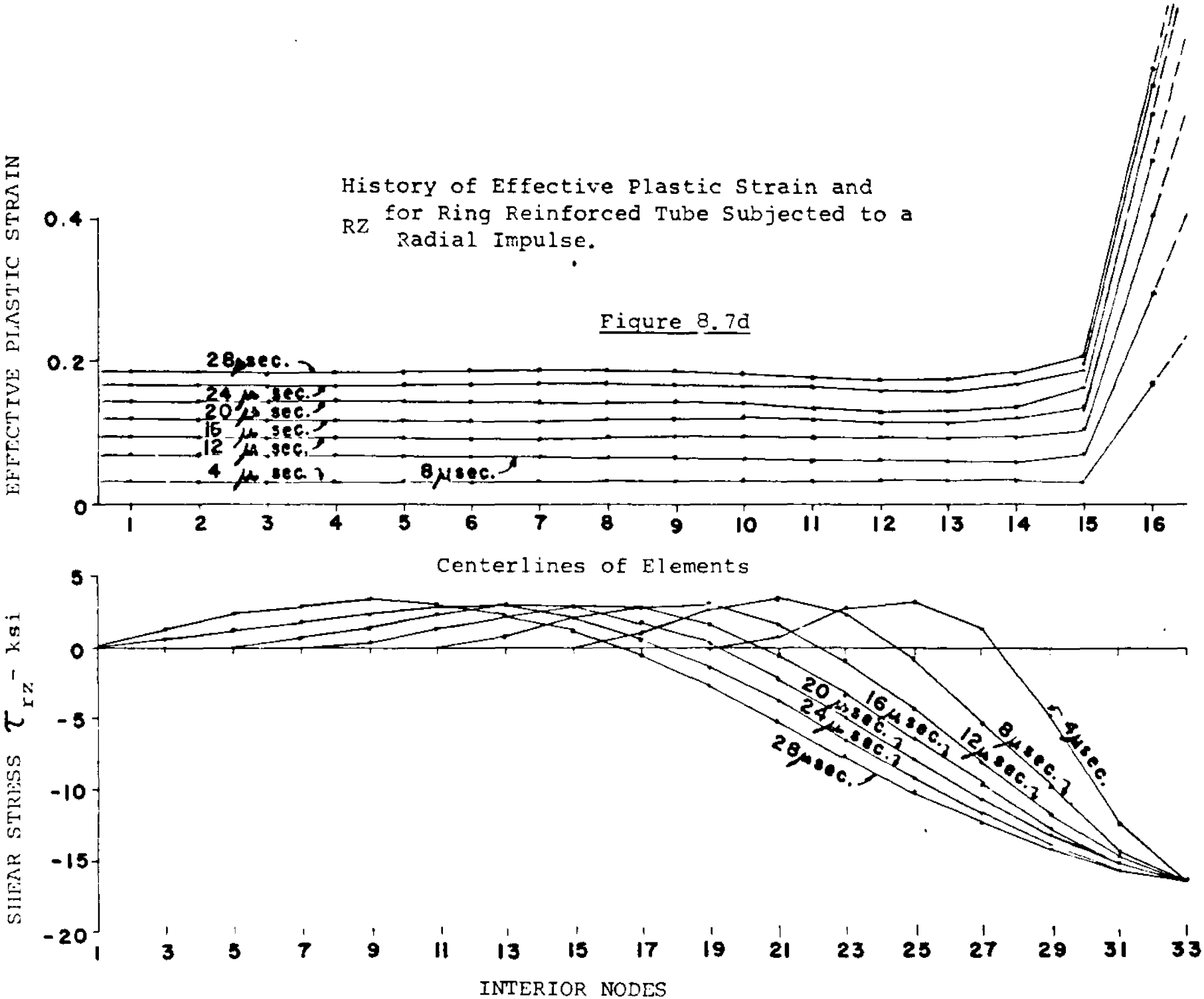

History of Effective Plastic Strain and τ_{RZ} for Ring Reinforced Tube subjected to a Radial Impulse.

Figure 8.7e

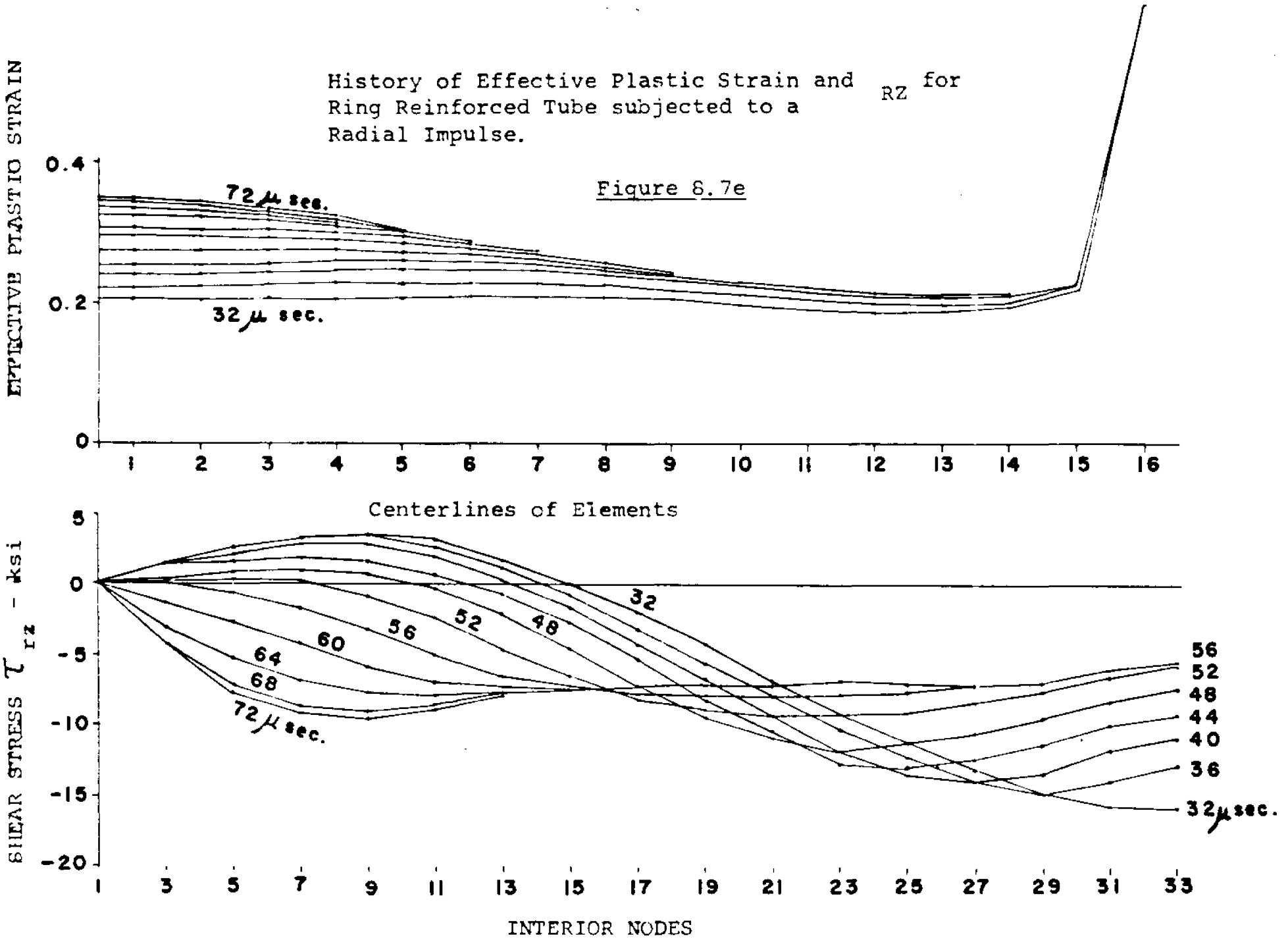

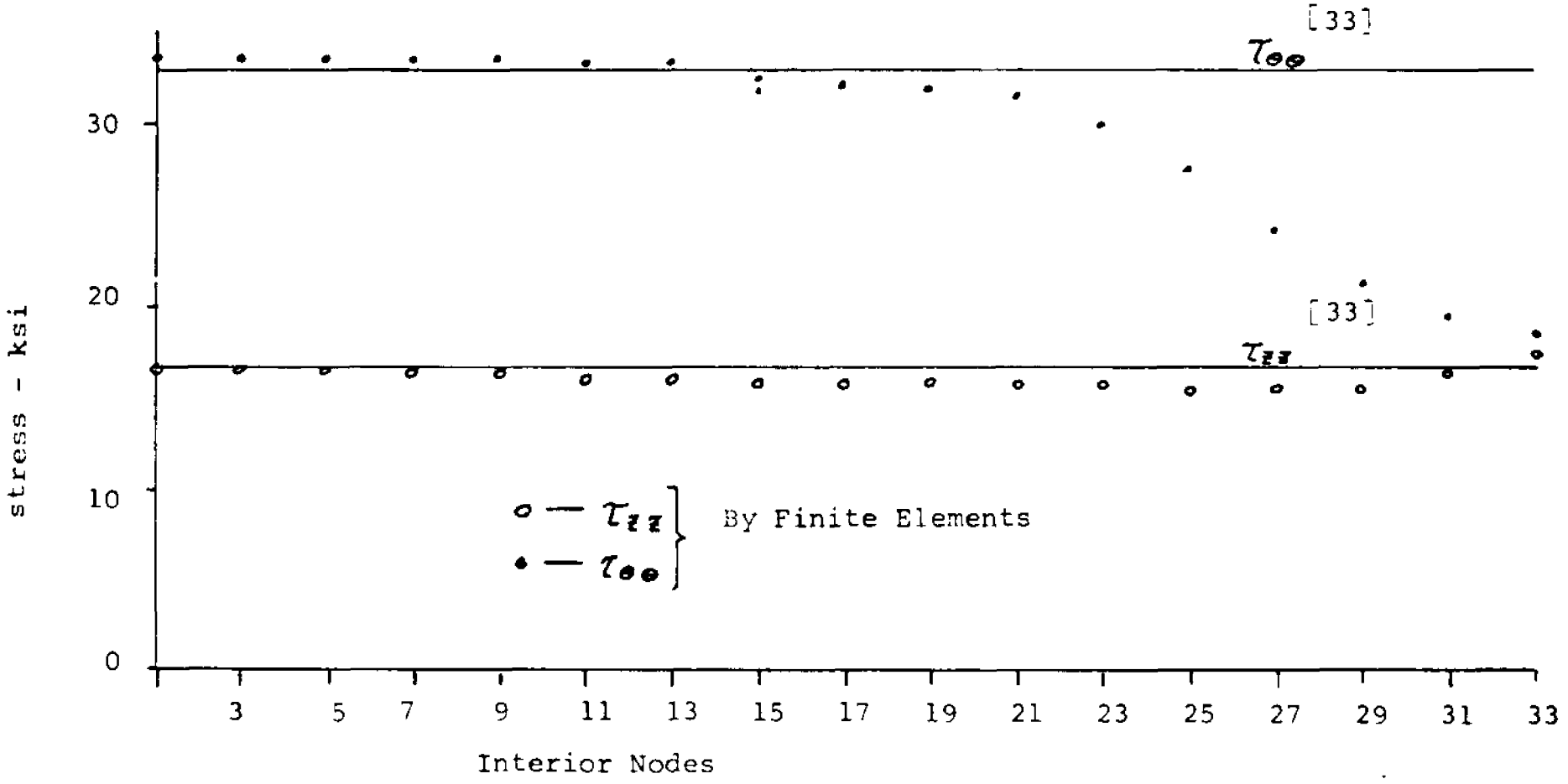

Longitudinal and Circumferential Stress
Along Tube axis at 16 μ sec. After initial Impulse.

Figure 8.7f

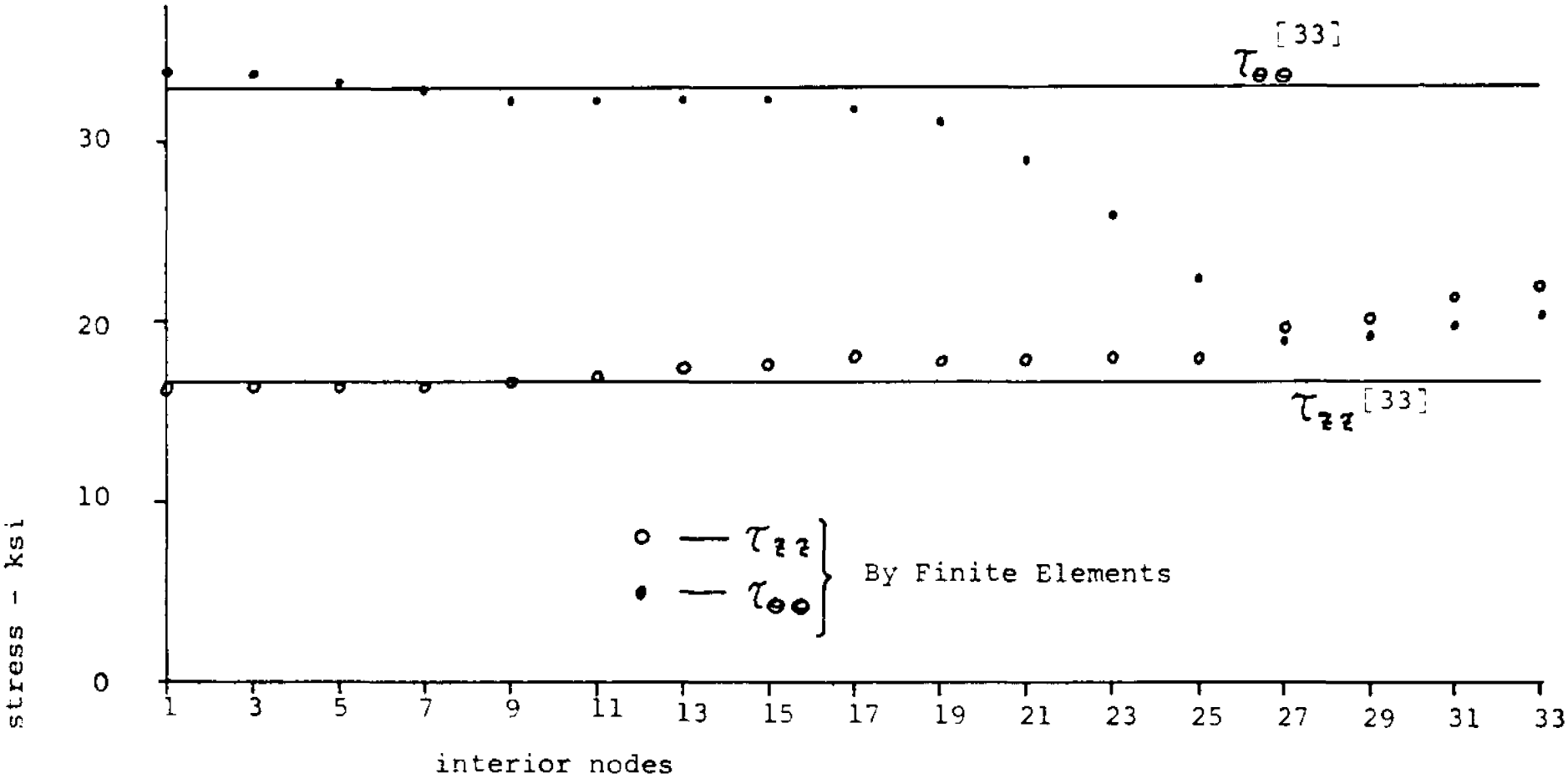

Longitudinal and Circumferential Stress Along
Tube Axis at 32 μ sec. after Initial Radial Impulse

Figure 6.7g

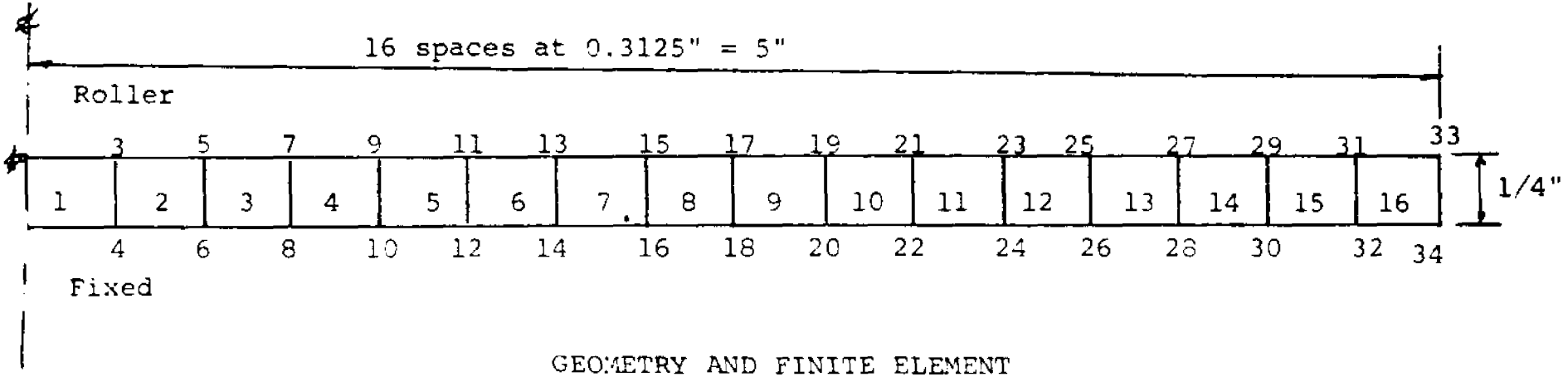

GEOMETRY AND FINITE ELEMENT GRID FOR CIRCULAR PLATE IMPINGING ON RIGID DIE MATERIAL PROPERTIES

Young's Modulus $E = 30 \times 10^6$ psi

Poisson's Ratio $\nu = .3$

Mass Density $\rho = .72379 \times 10^{-3} \frac{\text{lb.sec.}^2}{\text{in.}^4}$

Strain Hardening; $H = 0$

FIGURE 8.8a

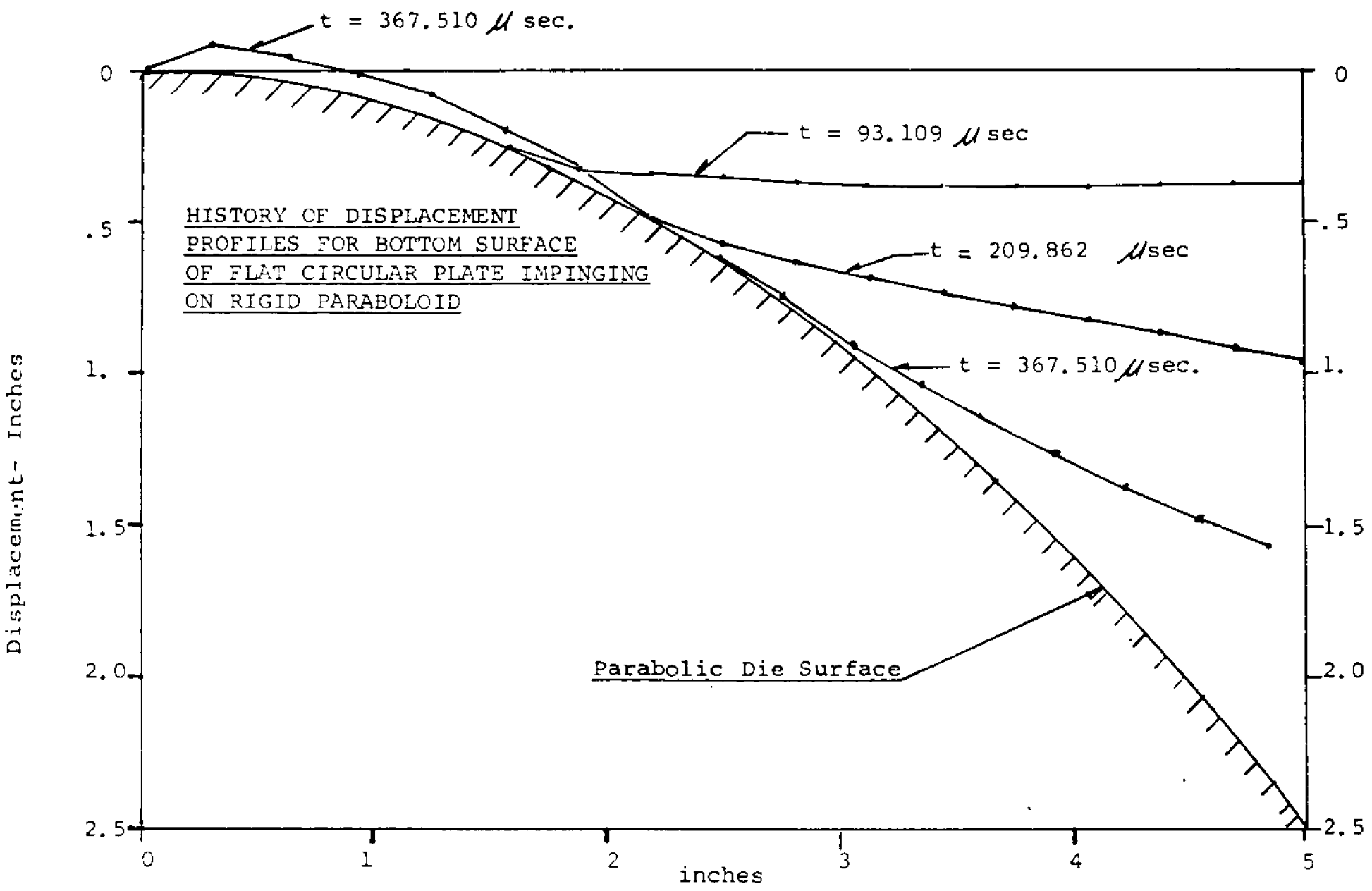
t = 367.510 μ sec.
t = 93.109 μ sec
t = 209.862 μsec
t = 367.510 μsec.
HISTORY OF DISPLACEMENT
PROFILES FOR BOTTOM SURFACE
OF FLAT CIRCULAR PLATE IMPINGING
ON RIGID PARABOLOID
Parabolic Die Surface
Displacement- Inches
0
.5
1.
1.5
2.0
2.5
0
1
2
3
4
5
inches

Figure 8.8b

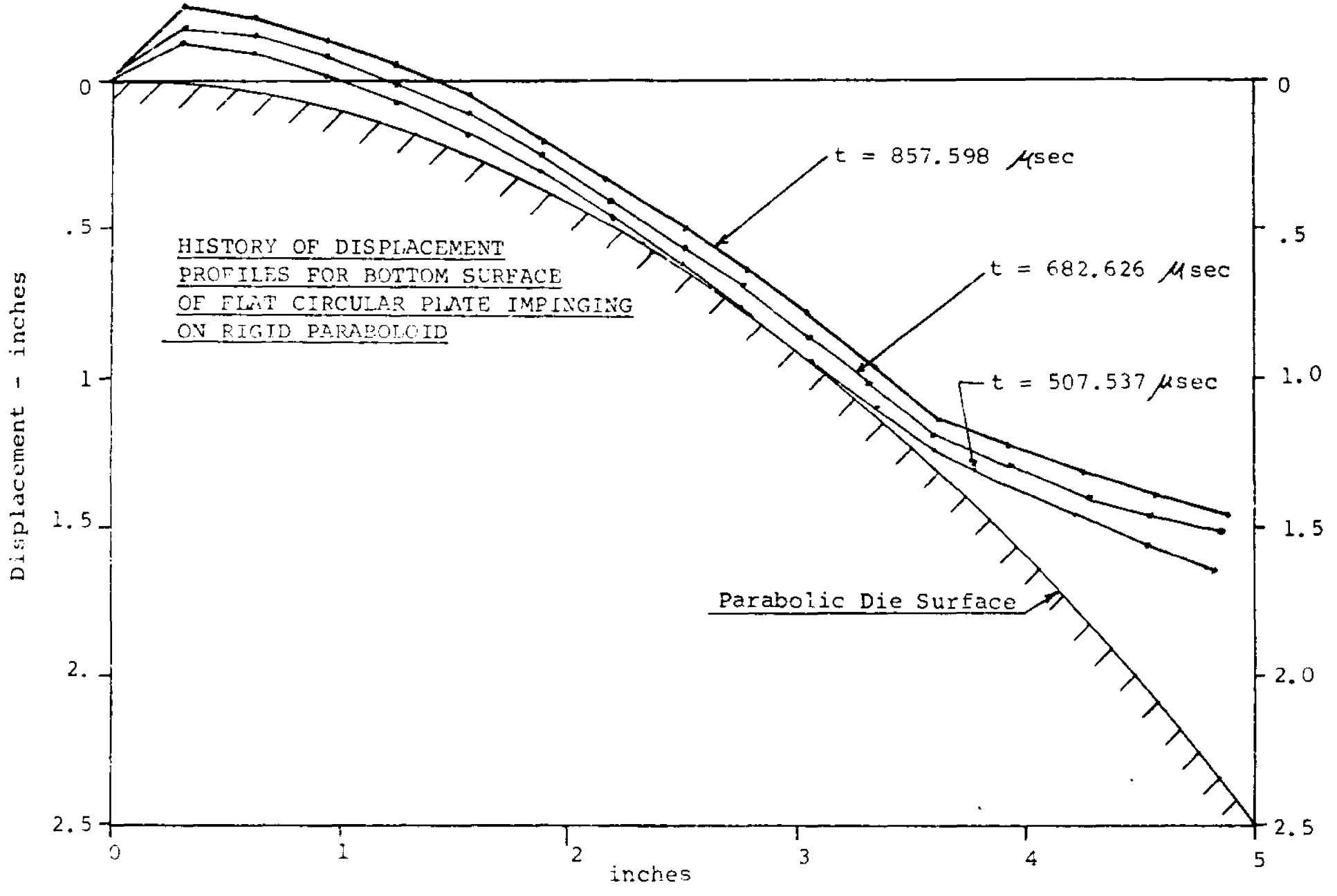
HISTORY OF DISPLACEMENT
PROFILES FOR BOTTOM SURFACE
OF FLAT CIRCULAR PLATE IMPINGING
ON RIGID PARABOLOID
t = 857.598 μsec
t = 682.626 μsec
t = 507.537 μsec
Parabolic Die Surface
Displacement - inches
inches
0
.5
1
1.5
2.
2.5
0
1
2
3
4
5
0
.5
1.0
1.5
2.0
2.5

Figure 8.8c

FINITE ELEMENT GRID DISTORTION AT

FINAL PLATE DEFORMATION

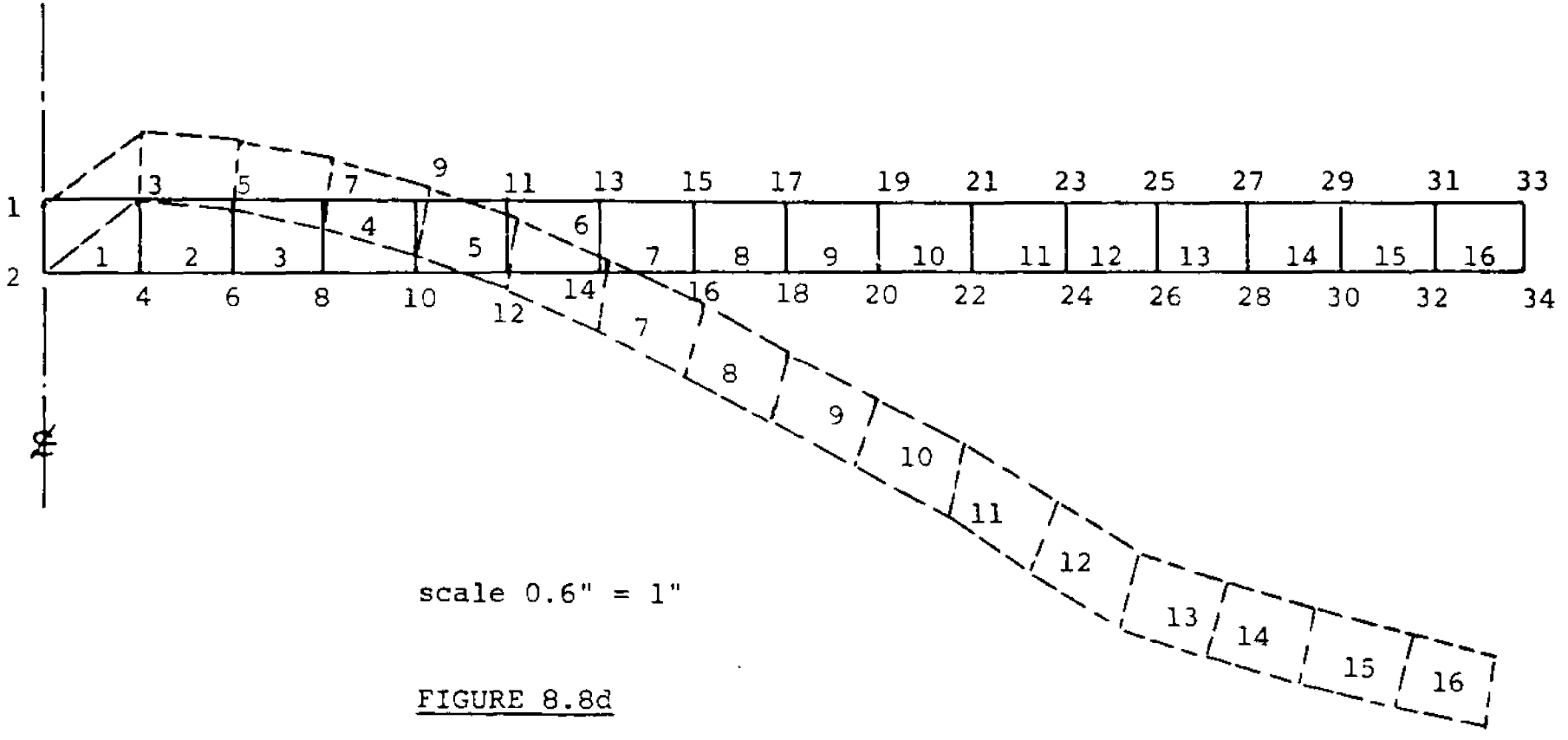

scale 0.6" = 1"

FIGURE 8.8d

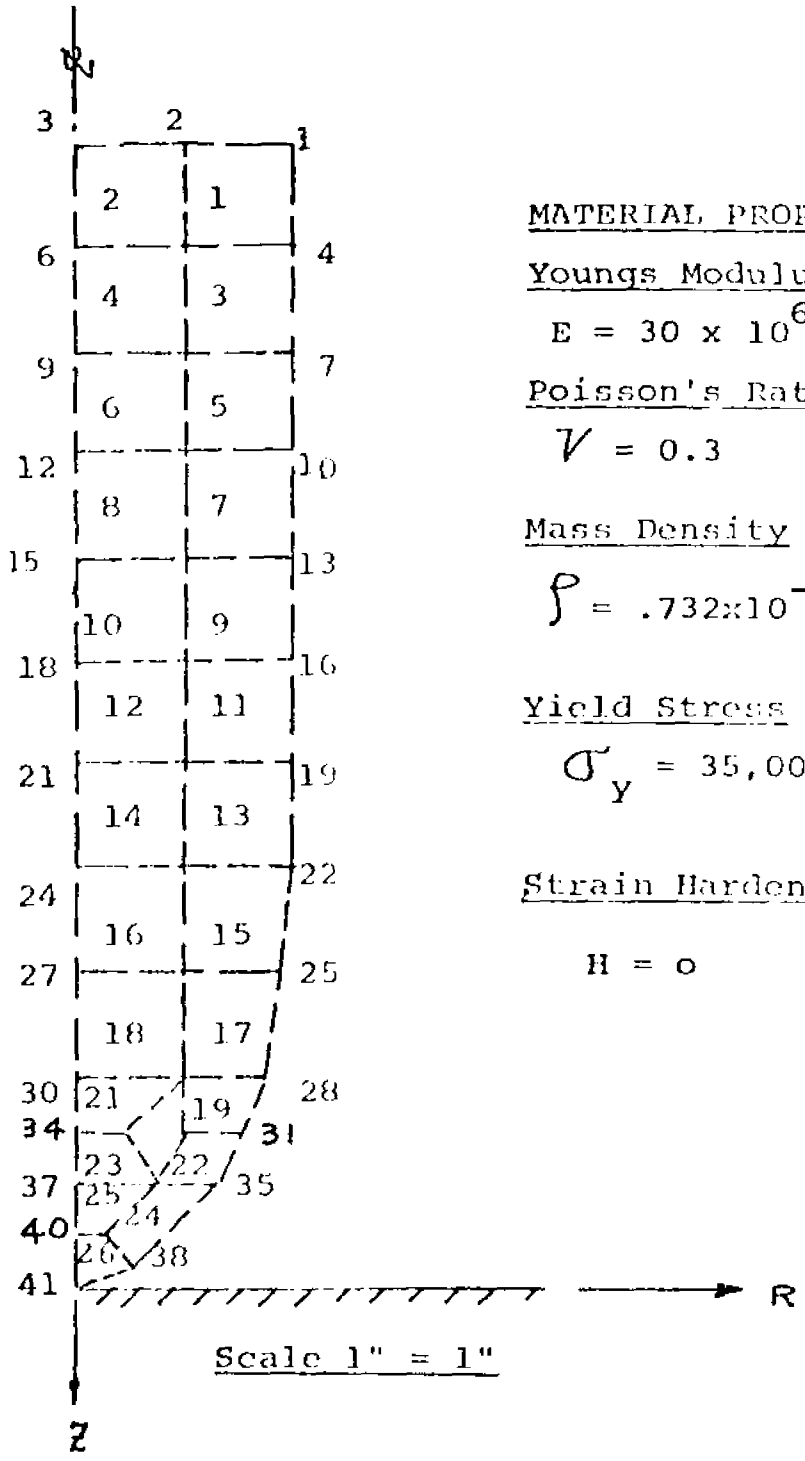

MATERIAL PROPERTIES

Youngs Modulus

$E = 30 \times 10^6$ psi

Poisson's Ratio

$\nu = 0.3$

Mass Density

$\rho = .732 \times 10^{-3}$ lb.-sec^2/in^4

Yield Stress

$\sigma_y = 35{,}000$ psi

Strain Hardening Modulus

$H = o$

FINITE ELEMENT MESH FOR OGIVE NOSED PROJECTILE

FIGURE 8.9a

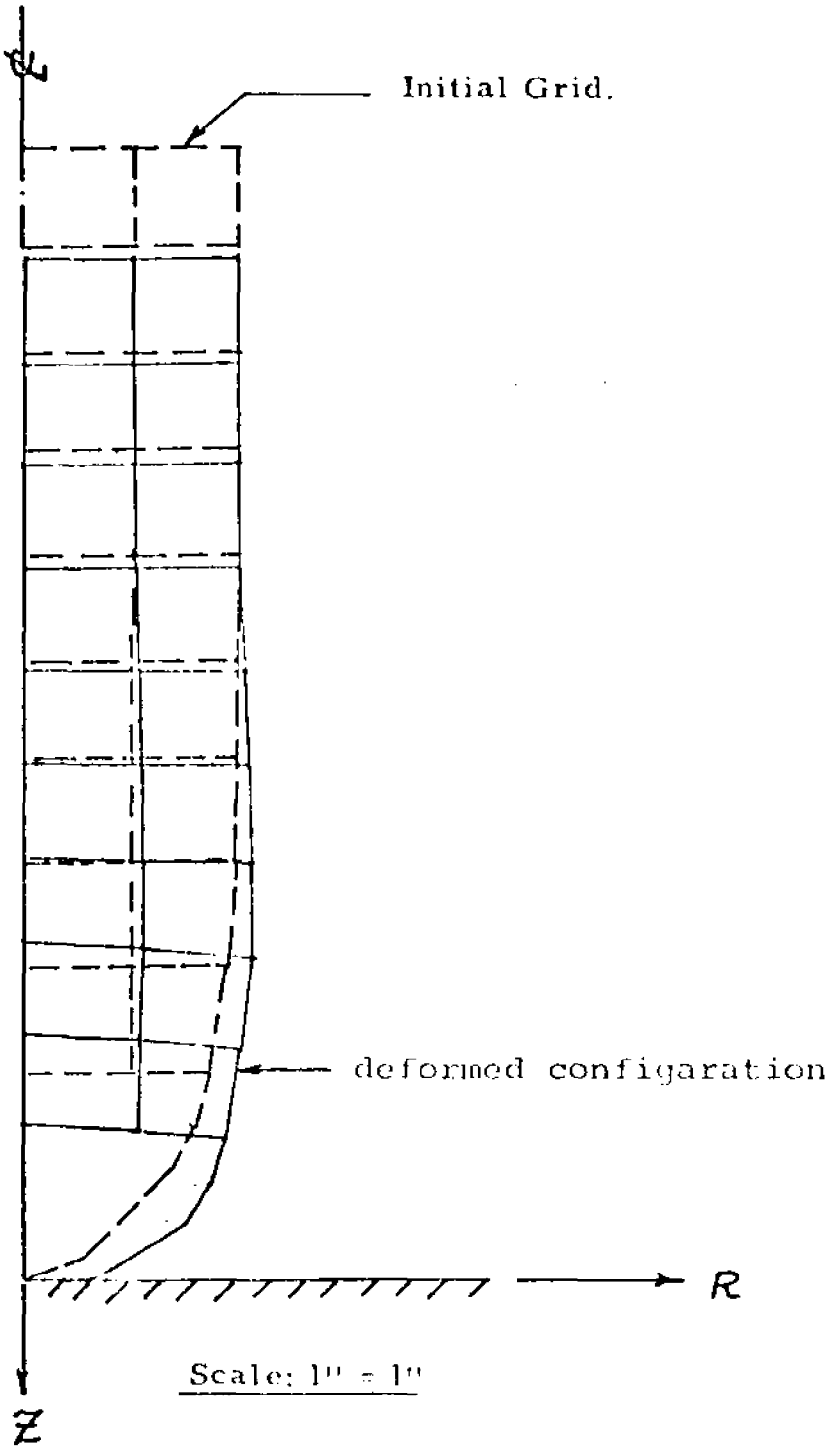

MAXIMUM DISTORTION OF PROJECTILE

Time = 280.1367 μsec.

FIGURE 8.9b

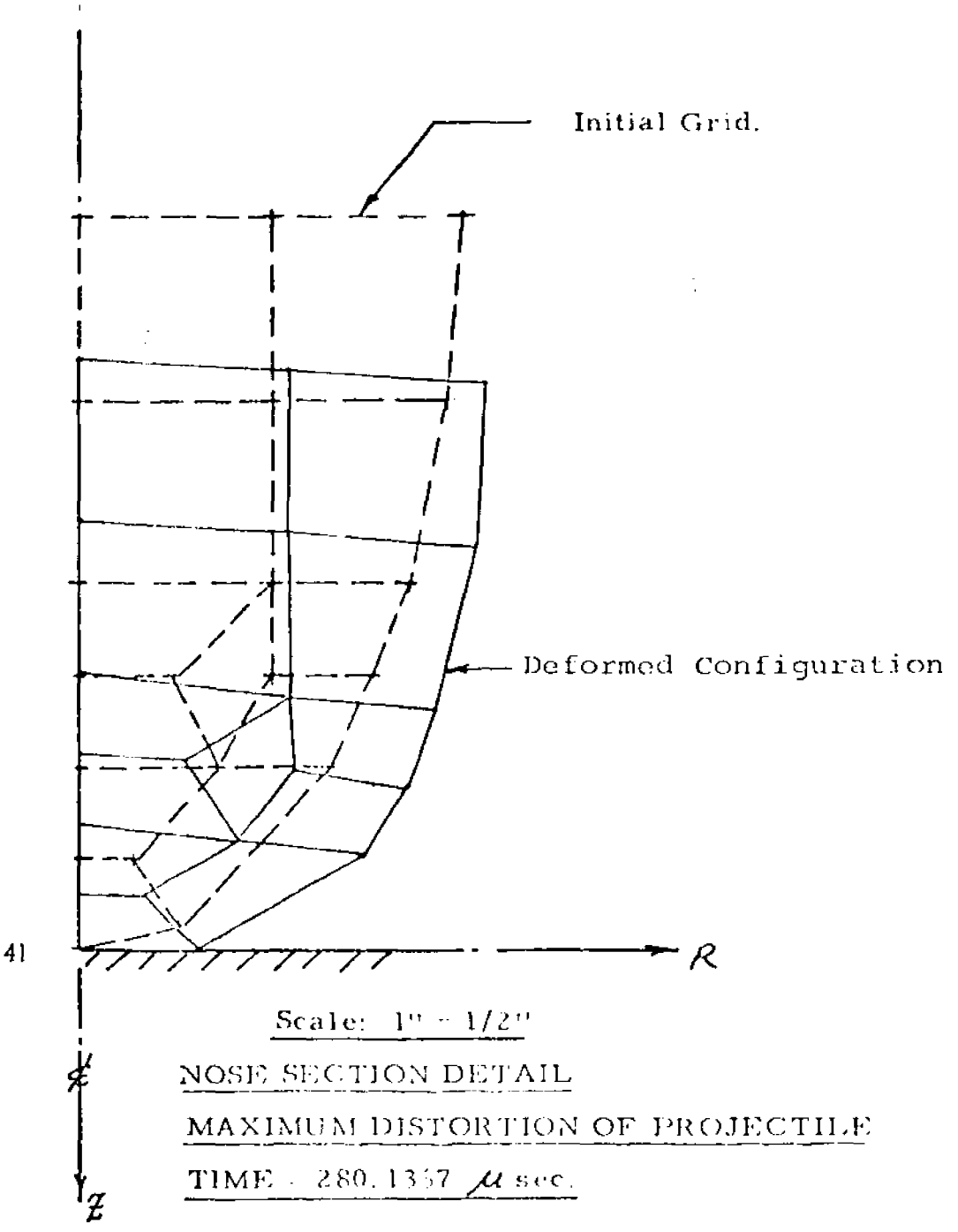
Initial Grid.
Deformed Configuration
41
R
Z
Scale: 1" = 1/2"
NOSE SECTION DETAIL
MAXIMUM DISTORTION OF PROJECTILE
TIME - 280.1367 μ sec.

FIGURE 8.9c

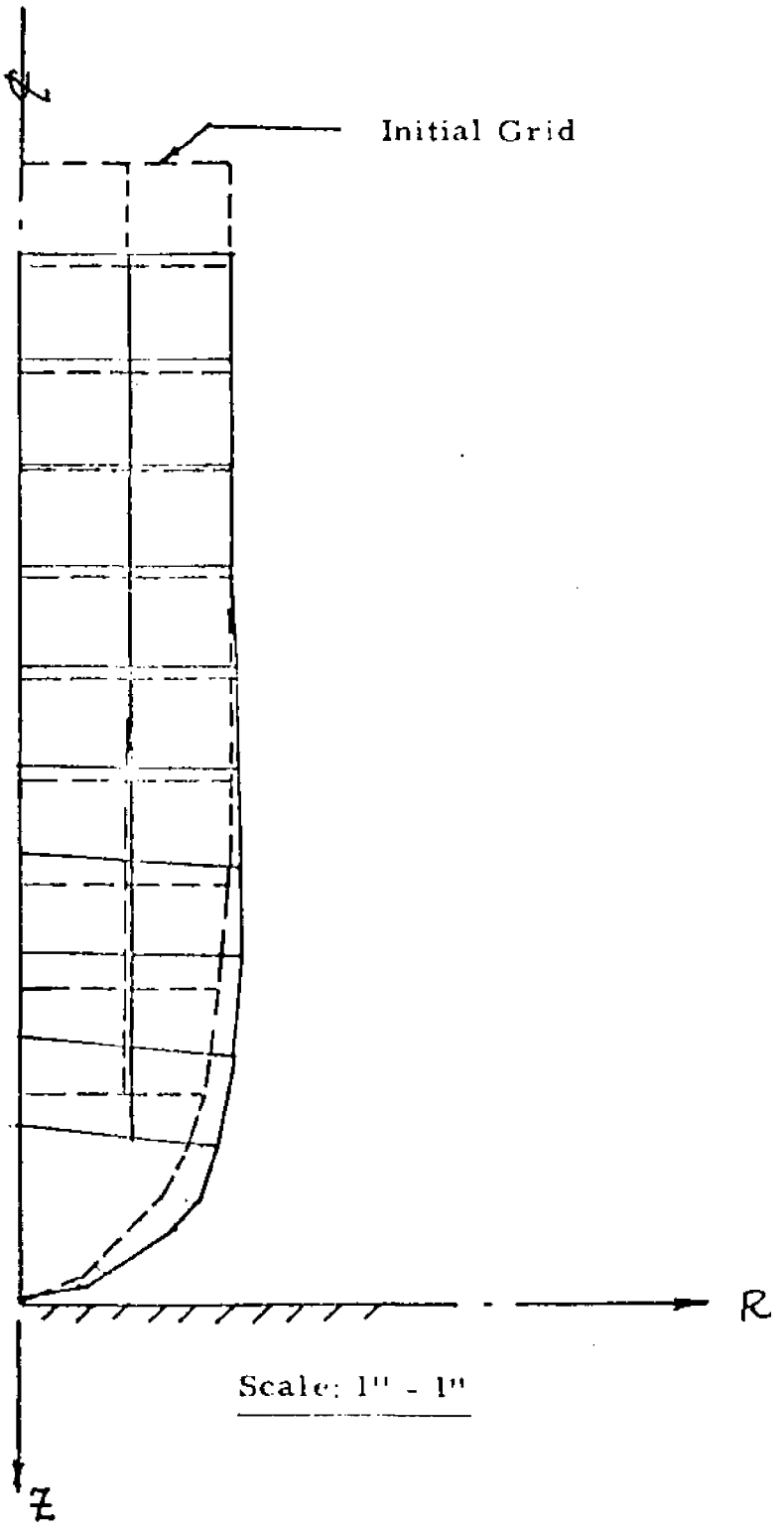

PERMANENT DISTORTION OF PROJECTILE

TIME = 502. 3058 μ sec.

FIGURE 8. 9d

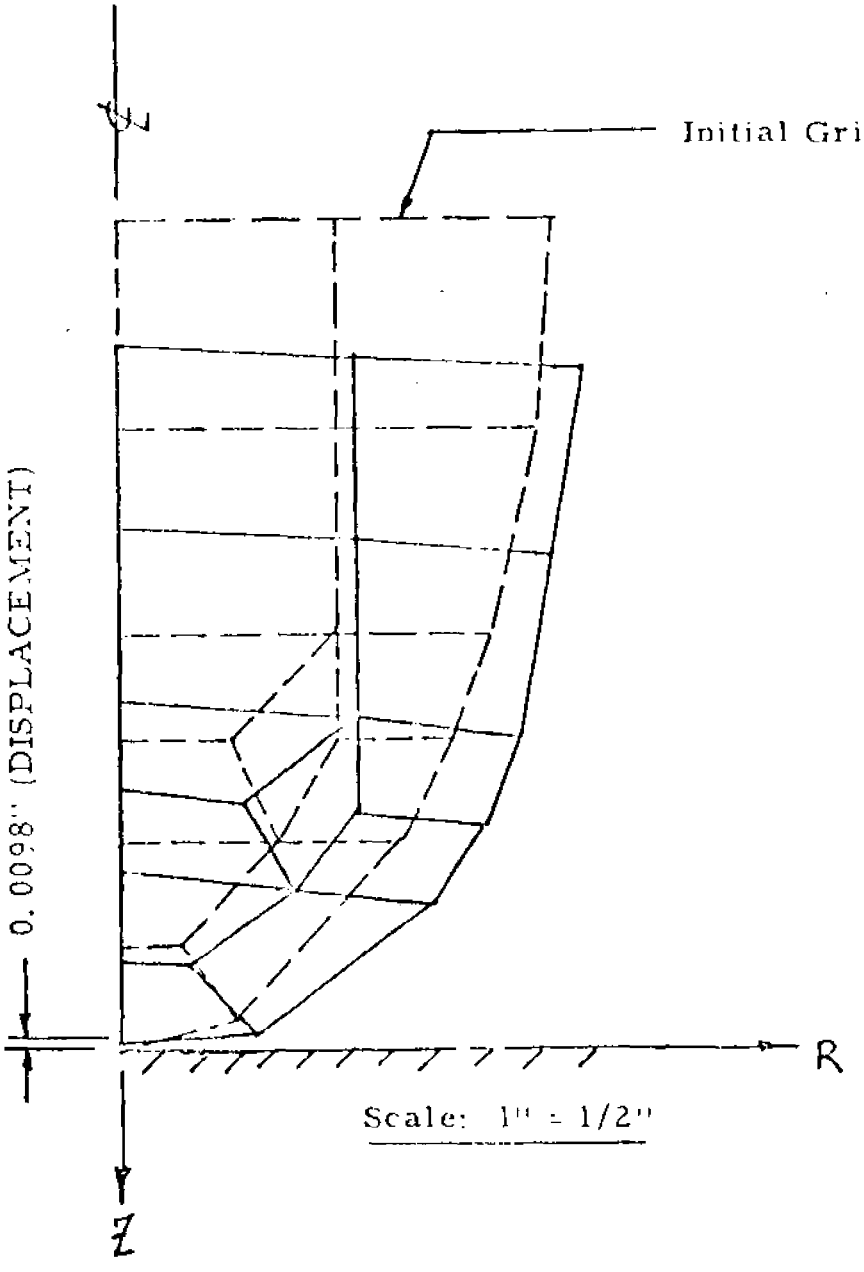

NOSE SECTION DETAIL

PERMANENT DISTORTION OF PROJECTILE

TIME = 502.3058 μ sec.

FIGURE 8.9e

Element No.	% Effective Plastic Strain
1	0
2	0
3	0.2
4	0 1
5	1.0
6	1.2
7	2.5
8	3.1
9	4 6
10	. 7
11	6.9
12	8 2
13	9 4
14	11.0
15	12 1
16	13 9
17	15.5
18	17 5
19	24.2
20	28.0
21	22 5
22	31.9
23	34 6
24	38 3
25	39.2
26	50.4

TABLE 8.2

Effective Plastic Strain In Each Element Of The Ogive Nosed Missile At Time t = 502.3058 μ sec.

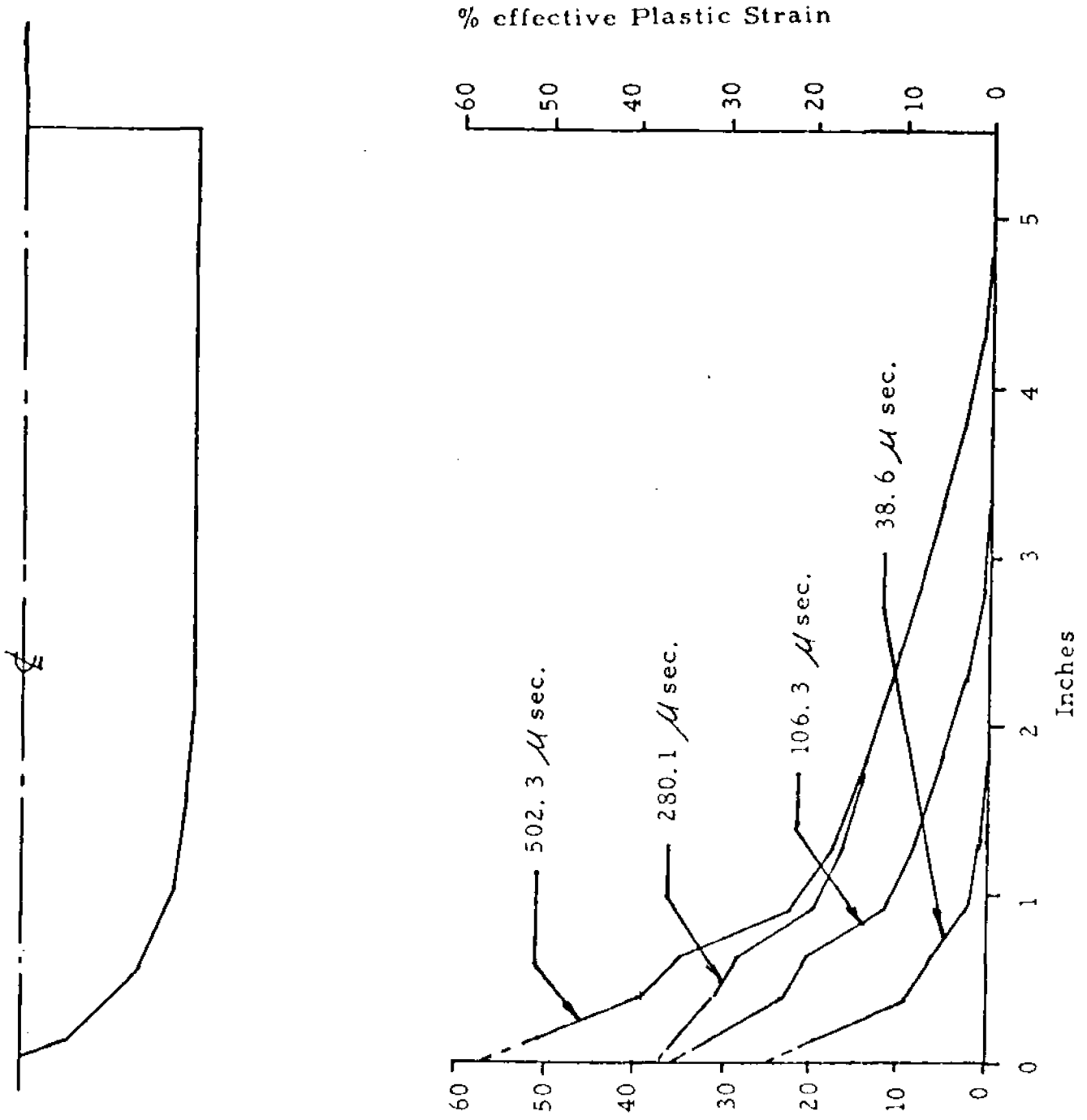

EFFECTIVE PLASTIC STRAINS

ALONG PROJECTILE AXIS AT VARIOUS TIMES

FIGURE 8.9f

APPENDIX A

The Equivalent Nodal Mass

Criteria for establishing the equivalent nodal masses within an element should at least include the following;

(1) The sum of the equivalent nodal masses must equal the total element mass.

(2) The centers of gravity of the equivalent nodal masses and the distributed element mass must coincide.

(3) If the element possesses any symmetry about a line within the element, the equivalent nodal masses must have the same symmetry.

The above criteria are sufficient to uniquely define nodal masses for plane triangles and quadrilaterals and for the axi-symmetric triangular element. However quadrilateral elements having no symmetry about a line through the element require yet another criterion. This difficulty is circumvented by considering the quadrilateral element as being made up of two triangular elements.

The necessary equations required to satisfy the above criteria are shown for the axi-symmetric, triangular element. For plane triangular and rectangular elements the application of these criteria leads to equivalent nodal masses that are the same at each of the element nodes.

A.1 Equivalent Nodal Mass of the Axi-symmetric Triangular Element

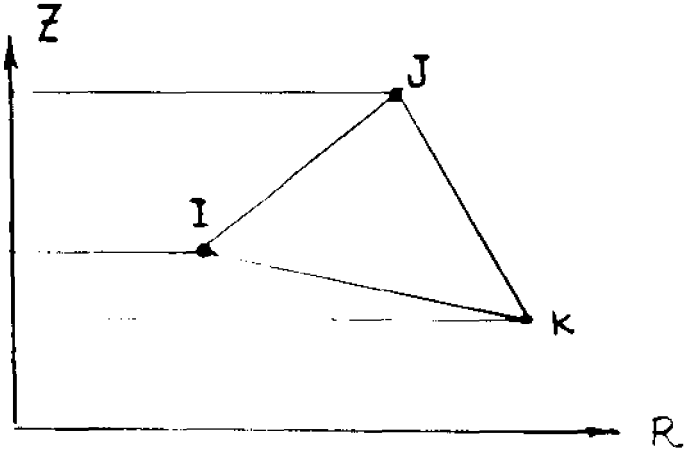

Figure A.1

The nodal masses M_I, M_J, M_K are found by solving the set of equations;

$$\begin{bmatrix} 1 & 1 & 1 \\ R_I & R_J & R_K \\ Z_I & Z_J & Z_K \end{bmatrix} \begin{Bmatrix} M_I \\ M_J \\ M_K \end{Bmatrix} = \rho \begin{Bmatrix} I_1 \\ I_2 \\ I_3 \end{Bmatrix} \qquad (A.1)$$

where ρ = the mass density of the element material

$$I_1 = \frac{1}{6}\left\{(R_J-R_K)[Z_J(2R_J+R_I) + Z_I(2R_I+R_J)]\right.$$
$$+ (R_K-R_I)[Z_K(2R_K+R_J) + Z_J(2R_J+R_K)]$$
$$\left.+ (R_I-R_J)[Z_I(2R_I+R_K) + Z_K(2R_K+R_I)]\right\}$$

$$I_2 = \frac{1}{12}\left\{(R_J-R_I)^3(3Z_J+Z_I) + (R_K-R_J)^3(3Z_K+Z_J)\right.$$
$$\left.+ (R_I-R_K)^3(3Z_I+Z_K)\right\} - \frac{1}{2}\left\{R_I^2(R_J-R_I)(Z_J+Z_I)\right.$$
$$+ R_J^2(R_K-R_J)(Z_K+Z_J) + R_K^2(R_I-R_K)(Z_I+Z_K)\left.\right\}$$
$$+ 2(R_I I_1^{(I)} + R_J I_1^{(J)} + R_K I_1^{(K)})$$

$$I_3 = \frac{1}{24}\left\{(R_J-R_I)^2[(Z_J+Z_I)^2 + 2Z_J^2] + 4R_I(R_J-R_I)[(Z_J+Z_I)-Z_IZ_J]\right.$$
$$+ (R_K-R_J)^2[(Z_K+Z_J)^2+2Z_K^2] + 4R_J(R_K-R_J)[(Z_K+Z_J)-Z_JZ_K]$$
$$\left.+ (R_I-R_K)^2[(Z_I+Z_K)^2+2Z_I^2] + 4R_K(R_I-R_K)[(Z_I+Z_K)-Z_KZ_I]\right\}$$

$$I_1^{(I)} = \frac{1}{6}(R_J-R_K)(Z_J(2R_J+R_I) + Z_I(2R_I+R_J); \text{ etc.} \qquad \text{(A.2)}$$

The resulting solution of (A.1) is;

$$\begin{Bmatrix} M_I \\ M_J \\ M_K \end{Bmatrix} = \rho \begin{bmatrix} a_I & b_I & c_I \\ a_J & b_J & c_J \\ a_K & b_K & c_K \end{bmatrix} \begin{Bmatrix} I_1 \\ I_2 \\ I_3 \end{Bmatrix} \qquad \text{(A.3)}$$

where a_I, b_I, c_I are defined in Chapter VII.

APPENDIX B

The Equivalent Nodal Forces for a Surface With Specified Tractions

In Chapter VII equation (7.20), we encounterd the term;

$$\int \underset{\sim}{\delta}_n^T \int_S (\underset{\sim}{A}^T \underset{\sim}{\Phi}^T \underset{\sim}{T}_n) dS \qquad (B.1)$$

where integration is carried out along the loaded surface boundaries. A direct approach to evaluating this integral is as follows; We first rewrite the integral in its more general form as;

$$\int_S (\underset{\sim}{U}_n^T \underset{\sim}{T}_n) dS \qquad (B.2)$$

where $\underset{\sim}{U}_n = \underset{\sim}{\Phi} \underset{\sim}{A} \underset{\sim}{\delta}_n$ is the displacement along the loaded surface (since the integral is zero, identically along all other surfaces).

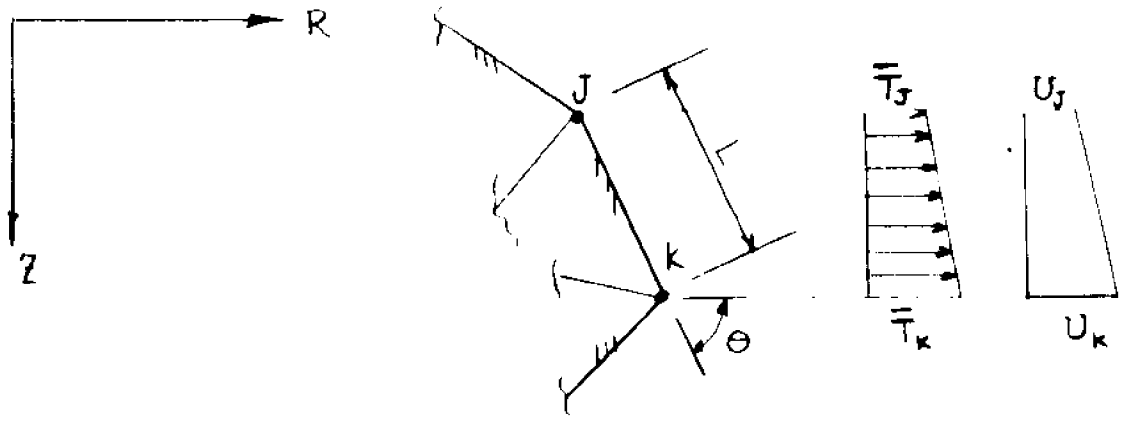

Figure B.1

In Figure B.1, above, a surface traction in the positive R direction is assumed to vary linearly along the surface JK. Since displacement functions for both the triangular and the quadrilateral elements are chosen to permit only linear variations of displacement along the element boundaries, a linear variation of the U displacement is shown to exist in Figure B.1. Then along the boundary JK, we may write:

$$\bar{T} = \bar{T}_J + \left(\frac{\bar{T}_K - \bar{T}_J}{Z_K - Z_J}\right)(Z - Z_J) \qquad (B.3a)$$

$$U = U_J + \left(\frac{U_K - U_J}{Z_K - Z_J}\right)(Z - Z_J) \qquad (B.3b)$$

Considering the plane stress and plane strain cases first, the virtual work performed by the surface tractions is;

$$\delta W = \frac{1}{\sin\Theta} \int_{Z_J}^{Z_K} \left(T_J + \left(\frac{\bar{T}_K - \bar{T}_J}{Z_K - Z_J}\right)(Z - Z_J)\right)\left(\delta U_J + \left(\frac{\delta U_K - \delta U_J}{Z_K - Z_J}\right)(Z - Z_J)\right) dZ$$

$$\text{or} \quad \delta W = \frac{1}{6}\left\{(2\bar{T}_J + \bar{T}_K)\,\delta U_J + (2\bar{T}_K + \bar{T}_J)\,\delta U_K\right\} \qquad (B.4)$$

It is then evident that the equivalent forces acting on each of the surface nodes J and K, due to the surface pressure are;

$$P_J = \frac{L}{6}\left(2\bar{T}_J+\bar{T}_K\right)$$

$$P_K = \frac{L}{6}\left(2\bar{T}_K+\bar{T}_J\right) \qquad (B.5)$$

For the axi-symmetric case, the virtual work of the surface traction will be found after first rewriting equations (B.3) as;

$$\bar{T} = \bar{T}_J + \left(\frac{\bar{T}_K-\bar{T}_J}{R_K-R_J}\right)(R-R_J) \qquad (B.6a)$$

$$U = U_J + \left(\frac{U_K-U_J}{R_K-R_J}\right)(R-R_J) \qquad (B.6b)$$

Then;

$$\delta W = \frac{1}{\cos\Theta}\int_{R_J}^{R_K}\left(\bar{T}_J+\left(\frac{\bar{T}_K-\bar{T}_J}{R_K-R_J}\right)(R-R_J)\right)\left(\delta U_J + \left(\frac{\delta U_K-\delta U_J}{R_K-R_J}\right)(R-R_J)\right)R\,dR \qquad (B.7)$$

The expanded integral becomes;

$$W = \frac{R_K-R_J}{12\cos\Theta}\left\{\left[\bar{T}_J(R_K+3R_J)+\bar{T}_K(R_K+R_J)\right]\delta U_J + \left[\bar{T}_J(R_K+R_J)+\bar{T}_K(3R_K+R_J)\right]\delta U_K\right\} \qquad (B.8)$$

and since the length of the external boundary of the element is;

$$L = \frac{R_K - R_J}{\cos \theta} \tag{B.9}$$

the equivalent forces acting on the surface nodes J and K per radian of arc are;

$$P_J = \frac{L}{12} \left\{ (R_K + 3R_J)\bar{T}_J + (R_K + R_J)\bar{T}_K \right\} \tag{B.10a}$$

$$P_K = \frac{L}{12} \left\{ (R_K + R_J)\bar{T}_J + (3R_K + R_J)\bar{T}_K \right\} \tag{B.10b}$$

APPENDIX C

Gaussian Integration Formulae for Triangles and Quadrilaterals [22,24]

Formulae for the iterated integrals that occur over two dimensional regions are derived from the Gauss-Legendre quadrature formulae;

$$\int_{-1}^{1} f(x)dx \approx \sum_{i=1}^{n} H_i f_i(a_i) \qquad (C.1)$$

where a_i are the zeros of the Legendre polynominal of degree n, and H_i are the weighting functions.

C.1 The Triangular Element

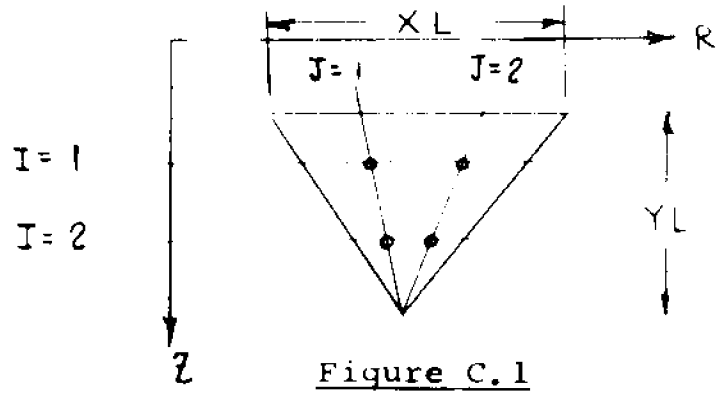

Figure C.1

For the triangular element, a one to one mapping along the R and Z directions occurs as illustrated below;

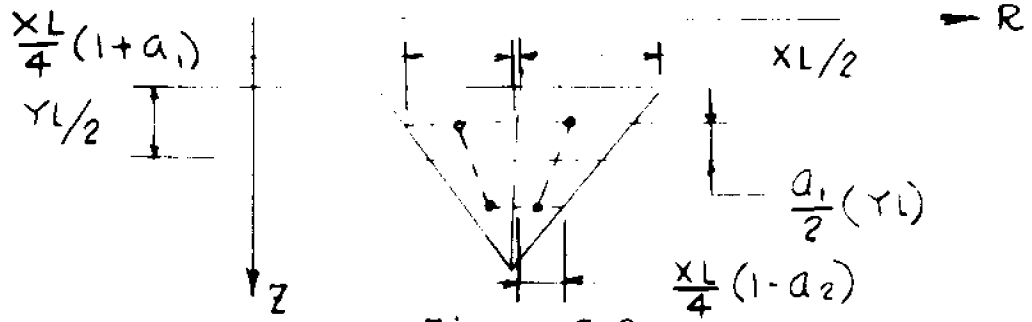

Figure C.2

Then the integrals along the R direction at each Z level are;

$$I_I = (1-a_I)XL(H_1\ f_{I1}+H_2\ f_{I2})/4 \qquad (C.2)$$

and the total, iterated integral is then;

$$I_T = YL(H_1\ I_1 + H_2\ I_2)/2 \qquad (C.3)$$

For the two point Gaussian integral used in this thesis, $H_1 = H_2 = 1$, and $a_1 = -.5773503$; $a_2 = .5773503$, while f_{IJ} is the function in the integrand on the left side of equation (C.1) but evaluated at the Gaussian points (I,J). Since these formulae apply only when the base of the triangular element is parallel to the R axis, a rotation of local reference axes must be effected.

C.2 The Quadrilateral Element

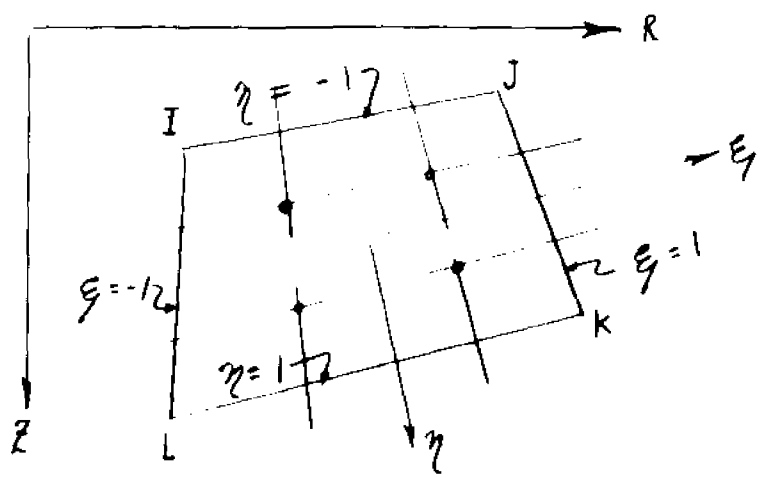

Figure C.3

It is first noted that;

$$\iint_A f(R,Z)\,dR\,dZ = \iint_{A'} f(\xi,\eta)\,|\mathcal{J}|\,d\xi\,d\eta \qquad (C.4)$$

where $|\mathcal{J}|$ is the jacobian of transformation from the (R,Z) to the (ξ,η) system.

Then;

$$\iint_A f(R,Z)\,dR\,dZ \approx \sum_{j=1}^{n} \sum_{i=1}^{n} f(a_i,b_j) H_i H_j \left|\mathcal{J}\,(a_i,b_j)\right| \qquad (C.5)$$

where a_i and b_j are the zeros of the Legendre polynominal of second degree. Note that, since this integration occurs in the (ξ,η) system, no preferential axis orientation exists.

APPENDIX D

Expanded Kinematic Expressions

For the plane strain and plane stress cases, a cartesian system of coordinates is chosen, thus enabling us to lower all superscripts where indicial notation is used.

The deformation gradient is then given by;

$$X^{i}_{,\alpha} = \begin{bmatrix} (1 + U_{r,R}) & U_{r,Z} \\ U_{z,R} & (1 + U_{z,Z}) \end{bmatrix} \qquad (D.1)$$

The jacobian of transformation is given by;

$$J = \left| X^{i}_{,\alpha} \right| = (1 + U_{r,R})(1 + U_{z,Z}) - U_{r,Z}\, U_{z,R} \qquad (D.2.)$$

The components of Lagrangian strain are;

$$\begin{Bmatrix} \epsilon_{RR} \\ \epsilon_{ZZ} \\ \epsilon_{RZ} \end{Bmatrix} = \begin{Bmatrix} U_{r,R} + \frac{1}{2}(U^2_{r,R} + U^2_{z,R}) \\ U_{z,Z} + \frac{1}{2}(U^2_{z,Z} + U^2_{r,Z}) \\ \frac{1}{2}(U_{r,Z} + U_{z,R}) + \frac{1}{2}(U_{r,Z}U_{r,R} + U_{z,R}U_{z,Z}) \end{Bmatrix}$$

D.1 Cylindrical Coordinates;

For cylindrical coordinates, the definition of the symbol $(\ )_{,j}$ will be extended to mean the covariant derivative as defined below:

$$(\ )^{i}_{,j} = \frac{\partial(\ )^{i}}{\partial x^{j}} + \left\{ \begin{matrix} i \\ j \ K \end{matrix} \right\} (\ )^{K} \qquad (D.4)$$

$$(\ )_{i,j} = \frac{\partial(\ )_{i}}{\partial x^{j}} - \left\{ \begin{matrix} K \\ j \ i \end{matrix} \right\} (\ )_{K} \qquad (D.5)$$

where $\left\{ \begin{matrix} i \\ j \ K \end{matrix} \right\}, \left\{ \begin{matrix} K \\ j \ i \end{matrix} \right\}$ are the christoffel symbols of the second kind. The only none zero christoffel symbols are;

$$\left\{ \begin{matrix} R \\ \Theta \ \Theta \end{matrix} \right\} = -R \quad ; \quad \left\{ \begin{matrix} \Theta \\ R \ \Theta \end{matrix} \right\} = \left\{ \begin{matrix} \Theta \\ \Theta \ R \end{matrix} \right\} = \frac{1}{R} \qquad (D.6)$$

From equation (3.4) we have;

$$x^{i}_{,\alpha} = g^{i}_{\alpha} + U^{i}_{,\alpha}$$

where g^{i}_{α} is the 'shifter' that transforms vectors from an initital to a current coordinate reference frame. When these reference frames coincide, g^{i}_{α} is simply the kronecker delta, δ^{i}_{α}, and we may write;

$$x^{i}_{,\alpha} = \delta^{i}_{\alpha} \ (\delta^{\alpha}_{\beta} + U^{\alpha}_{,\beta}) \qquad (D.7)$$

Then the axi-symmetric form of the deformation gradient without torsion becomes;

$$x^{i}_{,\beta} = \begin{bmatrix} (1 + U^{r}_{,R}) & 0 & U^{z}_{,R} \\ 0 & (1 + \frac{U^{r}}{R}) & 0 \\ U^{z}_{,z} & 0 & (1 + U^{z}_{,z}) \end{bmatrix} \qquad (D.8)$$

The physical components of a tensor are defined as those components that are tangent to base unit vectors having the same physical dimensions for that tensor. Then the physical components of $x^{i}_{,\beta}$ in (D.8) are given by:

$$\bar{X}_{i,\alpha} = X^{i}_{,\alpha} \sqrt{g^{\alpha\alpha} \; g_{ii}} \qquad (D.9)$$

where $$g^{\alpha\alpha} = \begin{bmatrix} 1 & & \\ & 1/R^{2} & \\ & & 1 \end{bmatrix}$$

$$g_{ii} = \begin{bmatrix} 1 & & \\ & r^{2} & \\ & & 1 \end{bmatrix}$$

while r and R are radii respectively in a current and initial coordinate system that coincide. For the case given by (D.8), the physical components are identical to the tensor components.

The jacobian of transformation in axial symmetry is given by:

$$J = (1 + U_{r}/R) \left\{ (1 + U_{r,R}) (1 + U_{z,z}) - U_{z,R} U_{r,z} \right\} \qquad (D.10)$$

The physical components of the Lagrangian strain are given by;

$$\begin{Bmatrix} \epsilon_{RR} \\ \epsilon_{\theta\theta} \\ \epsilon_{ZZ} \\ \epsilon_{RZ} \end{Bmatrix} = \begin{Bmatrix} U_{r,R} + \frac{1}{2}\,(U_{r,R}^2 + U_{z,R}^2) \\ U_r/R + \frac{1}{2}\,(U_r/R)^2 \\ U_{z,Z} + \frac{1}{2}\,(U_{r,Z}^2 + U_{z,Z}^2) \\ \frac{1}{2}\,(U_{r,Z}+U_{z,R}) + \frac{1}{2}\,(U_{r,R}U_{r,Z}+U_{z,Z}U_{z,R}) \end{Bmatrix} \qquad (D.11)$$

APPENDIX E

Effective Stress versus Effective Plastic Strain

The results of a uniaxial tension or compression test may be presented as follows;

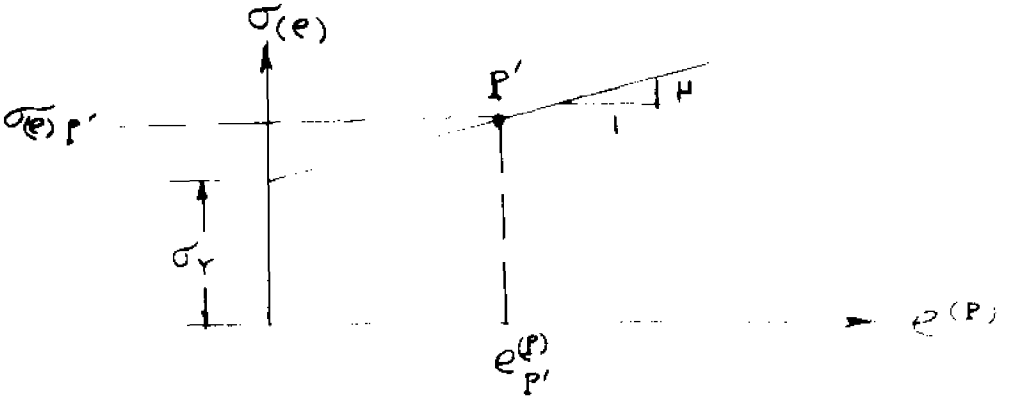

Figure E.1

(Effective stress vs. effective plastic strain)

This diagram is obtained by subtracting the elastic component of strain from the total strain as shown below for point P.

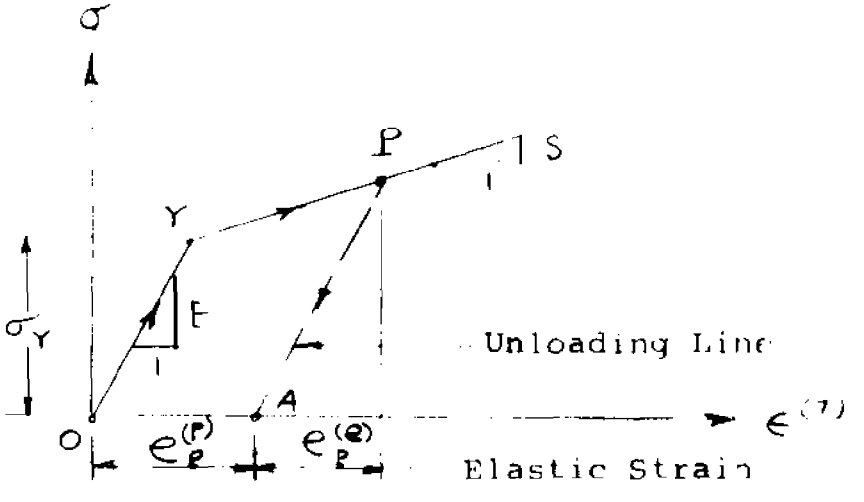

Figure E.2

Since unloading is assumed to occur elastically, it is merely necessary to fit a parallel curve to OY from P to A.

The area under the curve of Figure E.1 is the total plastic work done on the uniaxial specimen. Thus two possible relationships for σ_e may be inferred; i.e.

$$\sigma_e = G\ (W_p) \tag{E.1}$$

$$\sigma_e = H\ (e^{(P)}) \tag{E.2}$$

where $W_p = \int \tau_{ij} d\epsilon^{(P)}_{ij} = \int_0^{e^{(P)}} \sigma_e de^{(P)}$ (E.3)

is the plastic work.

But $$\sigma_e = \sqrt{3J_2} = \sqrt{3/2\ (\tau'_{ij}\ \tau'_{ij})} \tag{E.4}$$

Then in order to relate the diagram of Figure E.1 to a general three dimensional stress state, $e^{(P)}$ must be defined as [3];

$$e^{(P)} = \int_0^{e^{(P)}} de^{(P)}$$

$$de^{(P)} = \sqrt{\frac{2}{3}\ (d\epsilon^{(P)}_{ij}\ d\epsilon^{(P)}_{ij})} \tag{E.5}$$

For the particular case of linear strain hardening in which the uniaxial stress strain law is expressed as;

$$(\sigma - \sigma_y) = S(\epsilon - \epsilon_y) \qquad (E.6)$$

the line equation of Figure E.1 is;

$$\sigma_e = He^{(P)} + \sigma_y \qquad (E.7)$$

where $$H = (ES)/(E-S) \qquad (E.8)$$

APPENDIX F

Determination of the Integration Interval 'h'

The estimate of 'h' will be governed, at least at the beginning of the integration procedure, by the linearly elastic case in which dilitational wave velocities are maximum. The equations of motion for this case are written as;

$$[M]\{\ddot{\delta}\} + [K]\{\delta\} = \{F\} \qquad (F.1)$$

The matrix [K] above is an 'assembled stiffness' matrix obtained by summing up contributions of stiffness from elements to nodes having those elements in common. By referring to equation (6.), the element stiffness matrix is defined as;

$$[K']_n = \int_{V_o} [B_n^T \; L \; E \; B_n] \, J_n \, dV_o \qquad (F.2)$$

The matrix has dimension 6 x 6 or 8 x 8, depending on whether it represents a triangular or quadrilateral element. If it is triangular, then [K'] may be written in the partitioned form;

$$[K']_n = \begin{bmatrix} \underset{\sim}{K}_{ii} & \underset{\sim}{K}_{ij} & \underset{\sim}{K}_{iK} \\ \underset{\sim}{K}_{ji} & \underset{\sim}{K}_{jj} & \underset{\sim}{K}_{jK} \\ \underset{\sim}{K}_{Ki} & \underset{\sim}{K}_{Kj} & \underset{\sim}{K}_{KK} \end{bmatrix} \qquad (F.3)$$

where

$$\underset{\sim}{K}_{ij} = \begin{bmatrix} K_{ij}^{UU} & K_{ij}^{UV} \\ K_{ij}^{VU} & K_{ij}^{VV} \end{bmatrix}$$

k_{ij}^{uu} = the force at node i in the U direction due to a unit displacement at node j in the U direction

k_{ij}^{uv} = the force at node i in the U direction due to a unit displacement at node j in the V direction

etc.

and U and V are the displacements in the R and Z directions respectively.

The method of obtaining the assembled stiffness matrix is illustrated below. Figure (F.1) represents a typical element cluster with node 5 common to elements 1 through 4 inclusive.

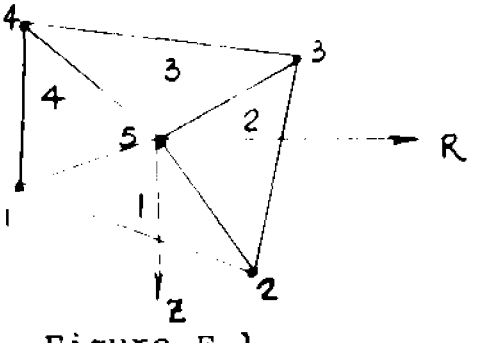

Figure F.1

Then the contributions of element stiffness to the stiffness of node 5 are;

$$[K]_{55} = [k_{55}]_{(1+2+3+4)}$$

$$[K]_{51} = [k_{51}]_{(1+4)}$$

$$[K]_{52} = [k_{52}]_{(1+2)}$$

etc.

For the linearly elastic case, the system of equations (F.1) has a discrete number of modal frequencies; one for each degree of freedom of the finite element system. These frequencies may be found by solving for the eigenvalues of ;

$$\left| \underset{\sim}{M}^{-1} \underset{\sim}{K} - \underset{\sim}{I} \lambda \right| = 0 \qquad (F.4)$$

The maximum circular frequency ω_{max} is related to the maximum eigenvalue λ_{max} by;

$$\omega^2_{max} = \lambda_{max} \qquad (F.5)$$

An approximate approach to finding ω_{max} follows from the observation that the diagonal terms of the diagonally banded stiffness matrix are generally much larger in magnitude than the off diagonal terms.

Hence a fair approximation to ω_{max} is;

$$\omega^2_{max} \approx (K_{ii}/M_i)_{max}$$

$$T_{min} \approx \frac{2\pi}{\sqrt{(K_{ii}/M_i)_{max}}}$$

and

$$h = \frac{T_{min}}{20} \qquad (F.6)$$

APPENDIX G

CYLINDRICAL BAR ANALYSIS

(Refer to Figures G 1,2,3,4)

For the constrained bar, assumed to be long compared to its radius, only ϵ_{ZZ} is considered non zero. Hence, in the elastic region

$$\tau_{ZZ} = (\lambda + 2\mu)\,\epsilon_{ZZ} = \frac{E\,(1-\nu)}{(1+\nu)\,(1-2\nu)}\,\epsilon_{ZZ}$$

$$\tau_{\theta\theta} = \tau_{RR} = \lambda\,\epsilon_{ZZ} = \frac{E\,\nu}{(1+\nu)\,(1-2\nu)}\,\epsilon_{ZZ}$$

$$\tau_{RR} = \tau_{\theta\theta} = \left(\frac{\nu}{1-\nu}\right)\tau_{ZZ}$$

then: $J_2 = \frac{1}{3}\,(\tau_{zz}^2 + \tau_{RR}^2 + \tau_{\theta\theta}^2 - (\tau_{RR}\tau_{\theta\theta} + \tau_{RR}\tau_{zz} + \tau_{\theta\theta}\tau_{zz}))$

or $$J_2 = \frac{\tau_{zz}^2}{3}\left(\frac{1-2\nu}{1-\nu}\right)^2 \qquad (G\ 1)$$

Hence, at yielding, we have;

$$\frac{\sigma_\theta^{\,2}}{3}\left(\frac{1-2\nu}{1-\nu}\right)^2 = \frac{\sigma_Y^{\,2}}{3}$$

or $$\sigma_o = \left(\frac{1-\nu}{1-2\nu}\right)\sigma_y \qquad (G.\ 1a)$$

At the instant of initial yielding, the following relationships hold.

$$\tau'_{ZZ} = \frac{2}{3}\left(\frac{1-2\nu}{1-\nu}\right)\tau_{ZZ} \qquad (G.2)$$

$$\tau'_{\theta\theta} = \tau'_{RR} = -\frac{1}{2}\tau'_{ZZ} \qquad (G.3)$$

$$(d\tau'_{\theta\theta} + d\tau'_{RR}) = -d\tau'_{ZZ} \qquad (G.4)$$

$$d\epsilon_{RR} = d\epsilon_{\theta\theta} = \epsilon_{RR} = \epsilon_{\theta\theta} = 0 \qquad (G.5)$$

$$\frac{1}{3}(d\tau_{RR} + d\tau_{\theta\theta} + d\tau_{ZZ}) + \frac{E}{3(1-2\nu)}\, d\epsilon_{ZZ} \qquad (G.6)$$

It is recalled that the expression for the increment in plastic strain is;

$$de^P_{ij} = \lambda \tau'_{ij} \qquad (G.7)$$

where $$\lambda = \frac{3\, de^P}{2\,\sigma_e} \qquad (G.8)$$

But from Figure G.2;

$$de^P = \frac{d\sigma_e}{H} \qquad (G.9)$$

and $$d\sigma_e = \frac{3\tau'_{ij}\, d\tau'_{ij}}{2\sigma_e} \qquad (G.10)$$

Hence $$\lambda = \frac{9\tau'_{ij}\, d\tau'_{ij}}{4H\,\sigma_e^2} \qquad (G.11)$$

Since $\sigma_e^2 = 3\,J_2$, we have from equation (G.1)

$$\sigma_e^2 = \tau_{ZZ}^2 \left(\frac{1-2\nu}{1-\nu}\right)^2 \qquad (G.12)$$

Then inserting expressions (G.2), (G.3) and (G.12) into (G.11) we obtain

$$\lambda = \frac{9\; d\tau'_{ZZ}}{4H\,\tau_{ZZ}\left(\frac{1-2\nu}{1-\nu}\right)} \qquad (G.13)$$

and from (G.7)

$$de^P_{ZZ} = \frac{3\; d\tau'_{ZZ}}{2H} \qquad (G.14)$$

Then the total stain increment is;

$$de^T_{ZZ} = \frac{2}{3}\, d\epsilon^T_{ZZ} = \left(\frac{1}{2G} + \frac{3}{2H}\right) d\tau'_{ZZ}$$

$$= \left(\frac{3E + 2H(1+\nu)}{2EH}\right)\left(d\tau_{ZZ} - \frac{E}{3(1-2\nu)}\, d\epsilon^T_{ZZ}\right)$$

(G.15)

Upon rearranging (G.15) we finally obtain

$$d\tau_{ZZ} = \left(\frac{\frac{E}{2(1-2\nu)} + \frac{H(1-\nu)}{(1-2\nu)}}{\frac{3}{2} + \frac{H(1+\nu)}{E}}\right) d\epsilon^T_{XX} \qquad (G.16)$$

Hence the slope S_1 in Figure G.3 is given by

$$S_1 = \frac{\frac{E}{2(1-2\nu)} + \frac{H(1-\nu)}{(1-2\nu)}}{\frac{3}{2} + \frac{H(1+\nu)}{E}} \qquad (G.17)$$

The D'Alembert solution to the one dimensional wave problem for a step pulse of $P > \sigma_o$ is:

$$U(Z,t) = \frac{\sigma_o}{E_o} (C_o t - Z) \qquad (G.18)$$

for $C_1 t \leq Z \leq C_o t$

and

$$U(Z,t) = \frac{\sigma_o}{E_o} (C_o t - Z) + \frac{\sigma - \sigma_o}{S_1} (C_1 t - Z) \qquad (G.19)$$

for $0 \leq Z \leq C_1 t$

where

$$C_o = \sqrt{E_o/\rho}$$

$$C_1 = \sqrt{S_1/\rho}$$

$$E_o = \frac{E(1-\nu)}{(1+\nu)(1-2\nu)}$$

ρ is the mass density

σ is the applied end stress

By differentiating equations (G.9a) and (G.9b) with respect to time, we obtain:

$$\frac{\dot{U}_o}{C_o} = \frac{\sigma_o}{E_o} \quad \text{for } C_1 t \leq Z \leq C_o t \qquad (G.20)$$

and

$$\dot{U}_1 = \frac{\sigma_o}{E_o} C_o + \frac{\sigma - \sigma_o}{S_1} C_1 \qquad (G.21)$$

for

$$0 \leq Z \leq C_1 t$$

For the material properties shown in Figure 7.4a at a time equal to 3.67×10^{-5} sec. after time zero, the elastic wave has traveled 8.65 inches and the plastic wave has traveled 7.42 inches along the bar. The particle velocities for the elastic and plastic waves respectively are 305 in./sec. and 492 in./sec. The maximum displacement of the end of the bar at $Z = 0$ is 18×10^{-3} in. The displacement occurring at $Z = 7.42$ inches is 1.58×10^{-3} in.

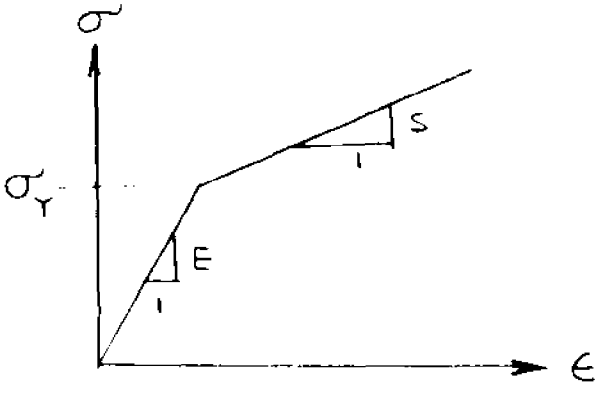

Figure G.1

Uniaxial
1-D Experimental Data

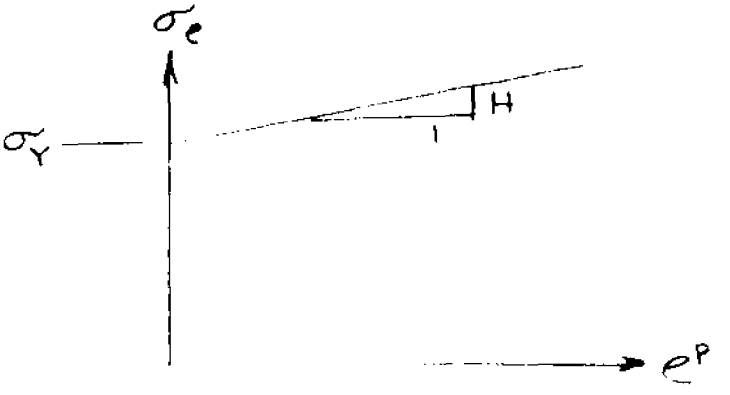

Figure G.2

Effective - Stress - Strain
Diagram

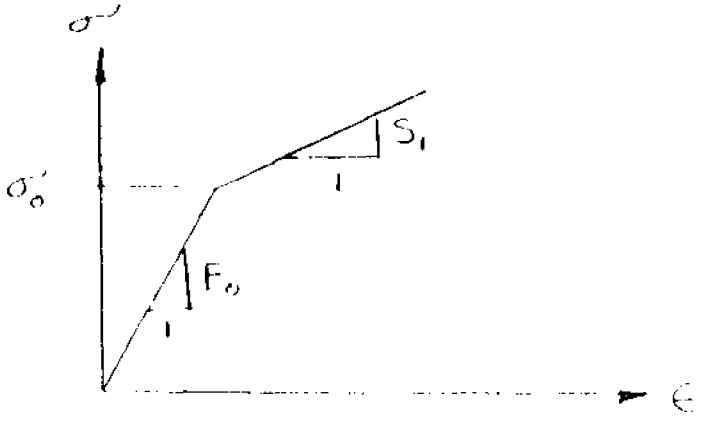

Figure G.3

Equivalent Stress-Strain Relationship
for Constrained Cylindrical Bar

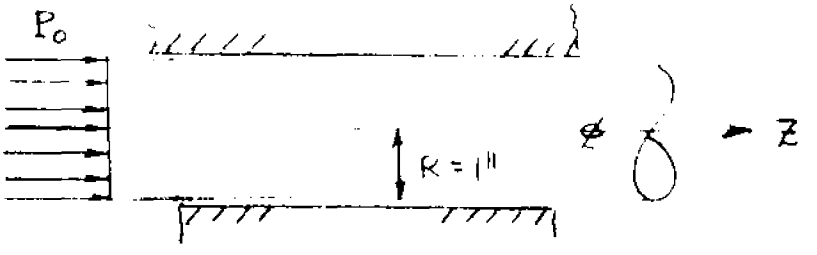

Figure G.4

Constrained Cylindrical Bar

BIBLIOGRAPHY

[1] Eringen, A.C., 'Nonlinear Theory of Continuous Media' McGraw Hill, 1962.

[2] Truesdell, 'The Elements of Continuum Mechanics' Springer Verlag, 1966.

[3] Hill, R. 'The Mathematic Theory of Plasticity' Oxford Univ. Press, 1950.

[4] Truesdell, C. 'The Simplest Rate Theory of Pure Elasticity' Comm. on Pure and Appl. Math., Vol. VIII, pp. 123-132, 1955.

[5] Prager, W. 'An Elementary Discussion of the Definitions of Stress Rate', Quart. App. Math. 18, pp. 403-407, 1961.

[6] Prager, W. 'A New Method of Analysing Stresses and Strains in Work Hardening Plastic Solids' J. Appl. Mech., Trans. ASME Vol. 17, no. 1, 1959.

[7] Hopkins, H.G. and Prager, W. 'The Load Carrying Capacity of Circular Plates' J. of Mech. and Phys. of Solids, Vol. 2, 1953, pp. 1-13.

[8] Goodier, J.N. and Hodge, P.G. Jr. 'Elasticity and Plasticity' John Wiley and Sons, 1958.

[9] Fung, T.C. 'Foundations of Solid Mechanics', Prentice Hall, 1965.

[10] Rice, M.H., Mcqueen, R.G. and Walsh, J.M. 'Compression of Solids by Strong Shock Waves' Solid State Physics-Advances in Research and Application-F. Seitz and Turnbull, Editors, Vol. 6 - Academic Press Inc. 1958.

[11] Thomas, T.Y. 'Combined Elastic and Prandtl-Reuss Stress-Strain Relations' Proc. Natl. Acad. Sci. Vol. 41, no. 10, pp 720-726, 1955.

[12] Lee, E.H. 'Thermo-Elastic Plastic Analysis at Finite Strain' Army Symp. on Solid Mech. 1967.

[13] Lee, E.H., Liu, D.T. 'Finite Strain Elastic-Plastic Theory with Application to Plane Wave Analysis' J. Appl. Phys., Vol. 38, no. 1 Jan. 1967.

[14] Lee, E.H. and Weirzbicki, T. 'Analysis of the Propagation of Plane Elastic Plastic Waves at Finite Strain' J. of Appl. Mech. pp. 931-936, Dec. 1967.

[15] Drucker, D.C. 'Some Implications of Work Hardening and Ideal Plasticity', Quart. Appl. Math. 7, pp. 411-418, 1950.

[16] Truesdell and Noll-Handbuch Der Phys. - Ph III/3-Flugge, Ed.

[17] Budiansky, B. 'A Reassessment of Deformation Theories of Plasticity,' J. of Appl. Mech. June, 1959, pp. 259-264.

[18] Havner, K.S. 'A Path Criterion for Deformation Plastic Theory', J. of Eng. Mech., Proc. ASME, pp. 747-761, Ju. 1969.

[19] Taylor, G.I. 'The Plastic Wave in a Wire Extended by an Impact Load' Civil Defense Res. Comm., Ministry of Home Sec. Gr. Br., 1942.

[20] Von Karman, Y. 'On the Propagation of Plastic Deformation in Solids' Nat'l. Defense Res. Comm. Report #a-29, 1942.

[21] Zienkiewicz, O.C. and Cheung, Y.K. 'The Finite Element Method in Structural and Continuum Mechanics' McGraw-Hill, 1967.

[22] Crandall, S.H. 'Engineering Analysis' McGraw Hill, 1956.

[23] Sheid, F. 'Theory and Problems of Numerical Analysis' Shaum's Outline Series, McGraw Hill, 1968.

[24] Melosh, R.J. 'Basis for the Derivation of Matrices for the Direct Stiffness Method' AIAA, Vol. 1, No. 7 July. 1963, pp. 1631-1637.

[25] Baker, W.E. 'The Elastic Plastic Reponse of Thin Spherical Shells to Internal Blast Loading', J. of Appl. Mech., Mar. 1960, pp. 139-144.

[26] Florence, A.L. 'Circular Plates Under Uniformly Distributed Impulses' Int. J. Solids Struct. 1966, Vol. 2, pp. 37-47.

[27] Sokolnikoff, 'Mathematical Theory of Elasticity' McGraw-Hill, 1956.

[28] Ralston, A. 'Numerical Integration Methods for the Solution of Ordinary Differential Equations' Mathematical Methods for Digitual Computers, Ralston, and Wilf, Editors, Wiley, 1959.

[29] Henrici, P. 'Discrete Variable Methods in Ordinary Differential Equations' J. Wiley and Sons, 1967.

[30] Newmark, N.M. 'A Method of Computation for Structural Dynamics' J. of The Eng. Mech. Div. Proc. ASCE, Jul. 1969, pp. 67-94.

[31] Turner, M.J., Clough, H.C., Martin, Topp, L.J. 'Stiffness and Deflection Analysis of Complex Structures' J. Aero. Sci. 23, pp. 805-823, 1956.

[32] Hudson, G.E. 'A Theory of the Dynamic Plastic Deformation of a Thin Diaphragm', J. of Appl. Phys., Vol. 22, no. 1, Jan. 1951.

[33] Masaki, S. 'Dynamic Plastic Deformation of Thin Cylindrical Shells Under Radial Impulsive Pressure' 2nd Int. Conf. of the Ctr. for High Energy Forming, Jun. 1969, Ester Pk, Col.

[34] Jones, N. 'Finite Deflections of a Simply Supported Rigid Plastic Annular Plate Loaded Dynamically' Int. J. Solids Struct., 1968, Vol. 4, pp. 593-603.

[35] Cristescu, N. 'Dynamic Plasticity' 1967, John Wiley and Sons.

[36] Munday and Newitt 'The Deformation of Transversely Loaded Discs Under Dynamic Loads' Phil. Trans. Roy. Soc. London, A256, pp. 130, (5.2), (5.4).

[37] Wang, A.J. 'The Permanent Deflection of a Plastic Plate Under Blast Loading' J. Appl. Mech. paper no. 55-APM-1.

[38] Leech, J., Emmett, A., Witmer and Pian 'Numerical Calculation Technique for Large Elastic Plastic Deformations of Thin Shells,' AIAA Journal, Vol. 6, no. 12, Dec. 1968.

[39] Maenchen, G. and Sack, S. 'The Tensor Code' 'Methods in Computational Physics' Alden, Fernbach, Rotenberg, Ed. Vol. 3, Academic Press, 1964, pp. 181-210.

[40] Wilkins, M.L. 'Calculation of Elastic-Plastic Flow' 'Methods in Computational Physics' Alden, Fernbach, Rotenberg, ed. Vol. 3 Academic Press, 1964, pp. 211-263.

[41] Oden and Sato 'Finite Strains and Displacements of Elastic Membranes by the Finite Element Method' Int. J. Solids Struct. 1967, Vol. 3, pp. 471-488.

[42] Becker, E.B. 'A Numerical Solution of a Class of Problems of Finite Elastic Deformations' PHD thesis, Univ, of Cal., Berkeley, Cal., 1966.

[43] Hibbitt, H.D. Marcal, P.V. and Rice, 'A Finite Element Formulation for Problems of Large Strain and Displacement' Int. J. Solids Struct., 1970, Vol. 6, pp. 1069-1086.

[44] Raftopoulos, D. and Davids, N. 'Elastic-Plastic Impast on Rigid Targets' AIAA J. Vol. 5, no. 12, Dec. 1967, pp. 2254-2260.

[45] Fu, C.C. 'A Method for the Numerical Integration of the Equations of Motion Arising from a Finite Element Analysis' J. Appl. Mech., Sept. 1970, pp. 599-605.

[46] Costantino, C.J. 'Finite Element Approach to Stress Wave Problems' J. Eng. Div. ASCE, Vol. 93, no. EM2, 1967, pp. 153-176.

[47] Costantino, C.J. 'Two Dimensional Wave Propagation through Nonlinear Media' J. Comp. Phys., Vol. 4, no. 2, Aug. 1969, pp. 147-170.

[48] Turner, M.J., Dill, E.H., Martin, H.C. and Melosh, R.J. 'Large Deflections of Structures Subjected to Heating and External Loads' J. Aero. Sci. Vol. 27, Feb. 1960.

[49] Martin, H.C. 'Derivation of Stiffness Matrices for the Analysis of Large Deflection and Stability Problems' Proc. 1st Conf. on Matrix Methods in Struct. Mech., pp. 607-715.

[50] Thomas, T.Y. 'On the Structure of the Stress-Stain Relations' Natl. Acad. Sci. Proc. Vol. 41, 1955, No. 10, pp. 716-720.

[51] Tong, P., Pian, T. 'A Variational Principal and the Convergence of the Finite Element Method Based on Assumed Stress Distributions' Int. J. Solids Struct. 1969, Vol. 5, pp. 463-472.

[52] Tong, P., Pian, T. 'The Convergence of the Finite Element Method in Solving Linear Elastic Problems', Int. J. Solids Struct., 1967, Vol. 3, pp. 865-879.

[53] Johnson, M.W., McLay, R.W., 'Convergence of the Finite Element Method in the Theory of Elasticity', J. Appl. Mech., Paper No. 68-APM-2.

[54] Visser, C., 'The Approximate Analysis of Thin Shells by the Finite Element Method', Ph.D. thesis, Ohio State Univ., Dept. of Eng. Mech. 1968.

[55] Jones, N., 'Impulsive Loading of a Simply Supported Circular Rigid Plate', J. Appl. Mech., Mar. 1968, pp. 59-65.

[56] Florence, A.C., 'Clamped Circular Rigid Plastic Plates Under Blast Loading', J. Appl. Mech., June, 1966, pp. 256-260.

[57] Zaid, M. and Paul, B., 'Mechanics of High Speed Projectile Perforation', J. Franklin Inst. Vol. 264, pp. 117-126 (1957).

[58] Boyd, D., 'Dynamic Deformations of Circular Membranes', J. Eng. Mech., Div., ASCE, June, 1966, pp. 1-136.

[59] Taylor, G. 'The Use of Flat-Ended Projectiles for Determining Dynamic Yield Strength I', Proc. Roy. Soc. (London), A194, 289 (1948).

[60] Whiffers, A.C. 'The Use of Flat-Ended Projectiles for Determing Dynamic Field Strength II; on Various Metallic Materials', Proc. Roy. Soc. (London) A194, 300 (1948).

[61] Reissner, E., 'On Finite Deflection of Circular Plates' Proc. Symp. of Appl. Math., Vol. 1, Amer. Math. Soc. N.Y. 1949; pp. 213-219.

[62] Thomas, T.Y. 'On the Structure of the Stress Strain Relations' - National Acad. Sci. Proc. Vol. 41, 1955, No. 10, pp. 716-720.

AUTOBIOGRAPHICAL STATEMENT

Joseph Heifetz is a graduate of CCNY (B.S. in C.E. 1958; M.S. in C.E. 1964). His eight years as senior research associate at the Foster Wheeler Corporation were spent as in-house consultant to engineering design staffs, director of development in explosive forming methods, and program developer for the stress analysis of pipes and shells. During this time several valuable patents in explosive forming methods were obtained.

His earlier experience was with the M.H. Treadwell Company and Singstad & Baillie as structural engineer and stress analyst. During his residency at CUNY he was a lecturer for the Civil Engineering and Computor Science departments. He is married and has three children.